USGS
science for a changing world

Geochemistry and Geochronology of Middle Tertiary Volcanic Rocks of the Central Chiricahua Mountains, Southeast Arizona

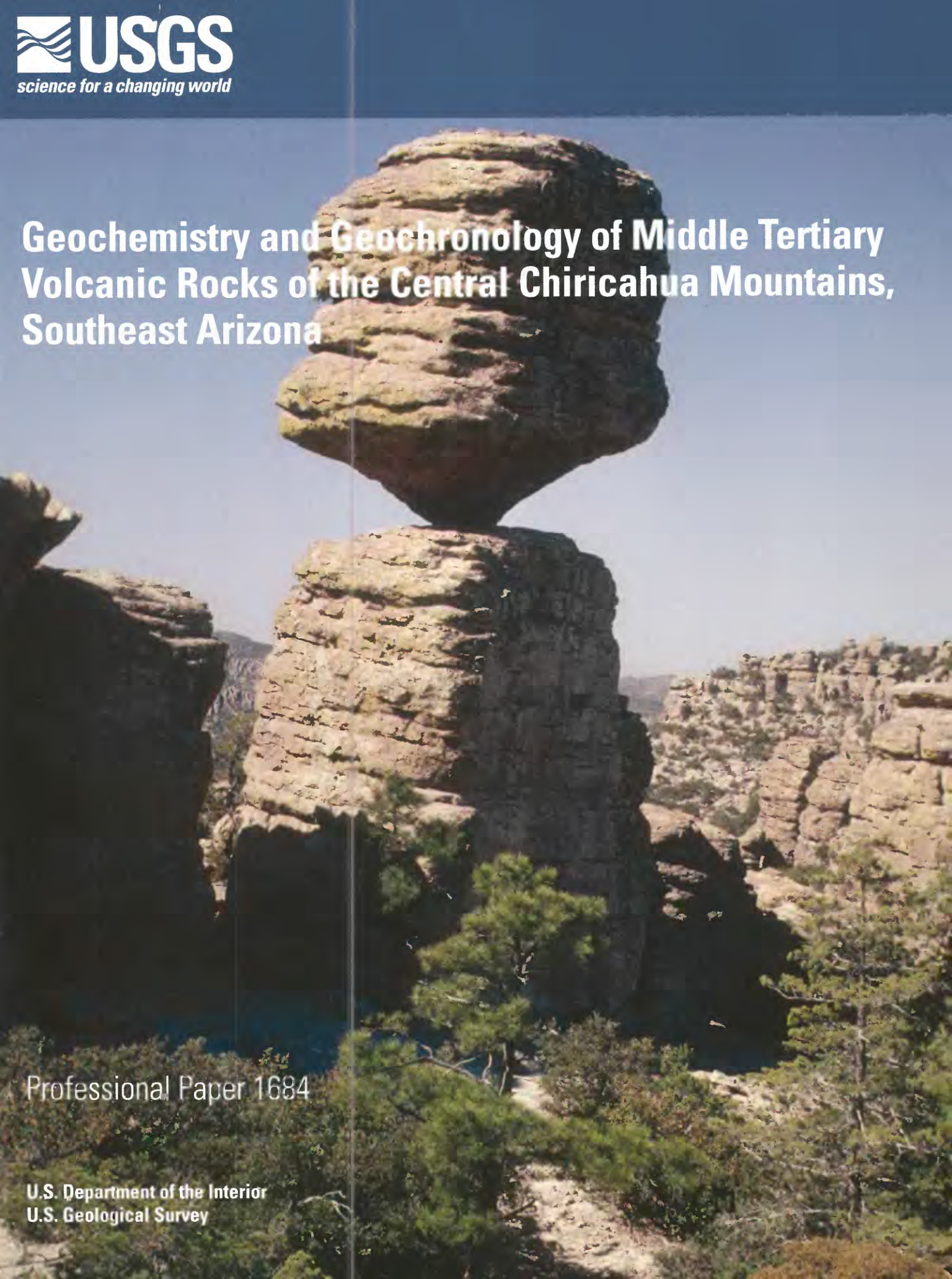

Professional Paper 1684

U.S. Department of the Interior
U.S. Geological Survey

Front cover. Balanced Rock in Chiricahua National Monument, composed of outflow facies Rhyolite Canyon Tuff.

Back cover. The feature known as The Fingers is located on the north side of Cave Creek and is composed of aphyric, high-silica rhyolite lava.

Geochemistry and Geochronology of Middle Tertiary Volcanic Rocks of the Central Chiricahua Mountains, Southeast Arizona

By Edward A. du Bray, Lawrence W. Snee, and John S. Pallister

Professional Paper 1684

U.S. Department of the Interior
U.S. Geological Survey

U.S. Department of the Interior
Gale A. Norton, Secretary

U.S. Geological Survey
Charles G. Groat, Director

U.S. Geological Survey, Reston, Virginia: 2004

Version 1.0

For sale by U.S. Geological Survey, Information Services
Box 25286, Denver Federal Center
Denver, CO 80225

For more information about the USGS and its products:
Telephone: 1-888-ASK-USGS
World Wide Web: http://www.usgs.gov/

Suggested citation:
du Bray, E.A., Snee, L.W., and Pallister, J.S., 2004, Geochemistry and geochronology of middle Tertiary volcanic rocks of the central Chiricahua Mountains, southeast Arizona: U.S. Geological Survey Professional Paper 1684, 57 p.

ISBN 0-607-95559-7

Contents

Abstract 1
Introduction 2
Acknowledgments 2
Sampling and Analytic Methods 2
Petrographic and Stratigraphic Characteristics 7
    Pre-Turkey Creek Caldera Rocks 7
    Rocks Associated with the Turkey Creek Caldera 11
    Post-Turkey Creek Caldera Rocks 12
Geochemistry 13
    Classification 13
    Within-Unit Geochemical Variation 15
        Pre-Turkey Creek Caldera Rocks 18
        Rocks Associated with the Turkey Creek Caldera 18
        Post-Turkey Creek Caldera Rocks 19
    Geochemistry- and Petrography-Based Stratigraphic Distinctions 19
        Lavas 19
        Ash-Flow Tuffs and Other Pyroclastic Flow Deposits 22
    Petrogenetic Implications 23
    Petrogenetic Evolution of the Turkey Creek Caldera Magmatic System 27
Geochronology 31
    Miscellaneous Units 31
    Pre-Turkey Creek Caldera Rocks 40
    Rocks Associated with the Turkey Creek Caldera 50
    Post-Turkey Creek Caldera Rocks 51
Concluding Remarks 51
References Cited 54

Figures

1. Index map showing location of central Chiricahua Mountains, Ariz. 3
2. Simplified correlation chart of map units and identification of studied volcanic rock units 10
3. Total alkali-silica variation diagram showing compositions of volcanic rocks 13
4. Abundance diagrams of selected major oxides and trace elements 14
5. Chondrite-normalized extended trace-element diagrams 15
6. Diagrams showing stratigraphic versus compositional variation among volcanic rocks 20
7. Trace-element–tectonic setting discrimination variation diagrams showing average compositions 24
8. Chondrite-normalized extended trace-element diagram showing average compositions 26
9. Ternary variation diagram showing average relative proportions of rubidium, potassium, and strontium 27
10. Chondrite-normalized rare earth element diagrams showing average compositions 28
11. Diagrams of $^{40}Ar/^{39}Ar$ age spectra 32

Tables

1. Compositions of volcanic rocks of the central Chiricahua Mountains 5
2. Summary of $^{40}Ar/^{39}Ar$ age-spectrum results from the central Chiricahua Mountains 8
3. $^{40}Ar/^{39}Ar$ data for volcanic rocks of the central Chiricahua Mountains 42
4. Diagnostic age, petrographic, and geochemical features of middle Tertiary volcanic rocks of the central Chiricahua Mountains 52

Geochemistry and Geochronology of Middle Tertiary Volcanic Rocks of the Central Chiricahua Mountains, Southeast Arizona

By Edward A. du Bray, Lawrence W. Snee, and John S. Pallister

Abstract

Middle Tertiary volcanic rocks of the central Chiricahua Mountains in southeast Arizona are the westernmost constituents of the Eocene-Oligocene Boot Heel volcanic field of southwestern New Mexico and southeastern Arizona. About two dozen volumetrically and stratigraphically significant volcanic units are present in this area. These include large-volume, regionally distributed ash-flow tuffs and smaller volume, locally distributed lava flows. The most voluminous of these units is the Rhyolite Canyon Tuff, which erupted 26.9 million years ago from the Turkey Creek caldera in the central Chiricahua Mountains. The Rhyolite Canyon Tuff consists of 500–1,000 cubic kilometers of rhyolite that was erupted from a normally zoned reservoir. The tuff represents sequential eruptions, which became systematically less geochemically evolved with time, from progressively deeper levels of the source reservoir. Like the Rhyolite Canyon Tuff, other ash-flow tuffs preserved in the central Chiricahua Mountains have equivalents in nearby, though isolated mountain ranges. However, correlation of these other tuffs, from range to range, has been hindered by stratigraphic discontinuity, structural complexity, and various lithologic similarities and ambiguities. New geochemical and geochronologic data presented here enable correlation of these units between their occurrences in the central Chiricahua Mountains and the remainder of the Boot Heel volcanic field.

Volcanic rocks in the central Chiricahua Mountains are composed dominantly of weakly peraluminous, high-silica rhyolite welded tuff and rhyolite lavas of the high-potassium and shoshonitic series. Trace-element, and to a lesser extent, major-oxide abundances are distinct for most of the units studied. Geochemical and geochronologic data depict a time and spatial transgression from subduction to within-plate and extensional tectonic settings. Compositions of the lavas tend to be relatively homogeneous within particular units. In contrast, compositions of the ash-flow tuffs, including the Rhyolite Canyon Tuff, vary significantly owing to eruption from compositionally zoned reservoirs. Reservoir zonation is consistent with fractional crystallization of observed phenocryst phases and resulting residual liquid compositional evolution. Rhyolite lavas preserved in the moat of the Turkey Creek caldera depict compositional zonation that is the reverse of that expected of magma extraction from progressively deeper parts of a normally zoned reservoir. Presuming that the source reservoir was sequentially tapped from its top downward, development of reverse zonation in the rhyolite lava sequence may indicate that later erupted, more evolved magma contains systematically less wallrock contamination derived from the geochemically primitive margins of its incompletely mixed reservoir.

New $^{40}Ar/^{39}Ar$ geochronology data indicate that the principal middle Tertiary volcanic rocks in the central Chiricahua Mountains were erupted between about 34.2 and 26.2 Ma, and that the 5.2 m.y. period between 33.3 and 28.1 Ma was amagmatic. The initial phase of eruptive activity in the central Chiricahua Mountains, between 34.2 and 33.3 Ma, was associated with a regional tectonic regime dominated by subduction along the west edge of North America. We infer that the magmatic hiatus, nearly simultaneous with a hiatus of similar duration in parts of the Boot Heel volcanic field east of the central Chiricahua Mountains, is related to a period of more rapid convergence and therefore shallower subduction that may have displaced subduction-related magmatic activity to a position east of the present-day Boot Heel volcanic field. The hiatus also coincides with a major plate tectonic reorganization along the west edge of North America that resulted in cessation of subduction and initiation of transform faulting along the San Andreas fault. The final period of magmatism in the central Chiricahua Mountains, between 28.1 and 23.2 Ma, appears to be coincident with rapid westward retreat of the subducting slab hinge line and consequent redevelopment of an asthenospheric mantle wedge, probably associated with foundering of the Farallon plate beneath western North America. Shortly thereafter, magmatism ceased in the central Chiricahua Mountains as the position of extension-related magmatism rapidly shifted westward to the Great Basin.

Introduction

This study is an outgrowth of investigations of the Turkey Creek caldera (du Bray and Pallister, 1991; Pallister and du Bray, 1997; du Bray and others, 1997), the principal volcanic edifice of the central Chiricahua Mountains east-southeast of Tucson, Ariz. (fig. 1). The Turkey Creek caldera is an Oligocene volcanic center that formed during eruption of the 26.9-Ma Rhyolite Canyon Tuff and partial evacuation of an underlying rhyolitic to dacitic magma chamber (Marjaniemi, 1969; du Bray and Pallister, 1991). Caldera evolution involved three distinct phases that concluded in a span of no more than 200,000 years: (1) eruption of 500–1,000 km^3 of Rhyolite Canyon Tuff and attendant caldera collapse, (2) resurgent intrusion of dacite porphyry and eruption of consanguineous dacite porphyry lava flows, (3) renewed eruption of high-silica rhyolite as lava flows. The majority of the rocks that form the topographic margin of the caldera are older, middle Tertiary volcanic rocks, and are principally rhyolite ash-flow tuffs. The Turkey Creek caldera is the westernmost and youngest source of regionally distributed ash-flow tuff sheets that are part of the Boot Heel volcanic field described by McIntosh and Bryan (2000).

During geologic mapping of the Turkey Creek caldera and its eruptive products, du Bray and others (1997) defined numerous pre-caldera volcanic rock units and mapped their distributions. Earlier attempts to define stratigraphic relations in isolated parts of the central Chiricahua Mountains (Raydon, 1952; Enlows, 1951, 1955; Fernandez and Enlows, 1966; Drewes, 1982; Bryan, 1988; Drewes and Brooks, 1988) had resulted in significant stratigraphic uncertainty and volcanologic ambiguity. Because none of the characteristics of these older units had been synthesized, we collected stratigraphic, petrographic, geochemical, and geochronological data for the older rocks; these data provide a framework for our own studies as well as provide data essential in correlating these rocks with their equivalents throughout southeastern Arizona and southwestern New Mexico.

In this report, we synthesize all available petrographic and stratigraphic data for volcanic rocks of the central Chiricahua Mountains. In addition, we present and discuss geochemical data for about two dozen volcano-stratigraphic rock units along with geochronologic data for 14 of these units. These units have significant implications for middle Tertiary volcanic stratigraphy in southeastern Arizona and adjacent southwestern New Mexico. Many of the units are ash-flow tuff. Because of their emplacement mode, the ash-flow tuffs are considerably more widely distributed than the lava flow units present in our study area. The distribution of the lava flow units is probably limited to the central Chiricahua Mountains; their utility in stratigraphic correlation is probably similarly restricted.

In order to construct a comprehensible framework for the volcanic rocks under study, we divided them into three groups. Because the Turkey Creek caldera dominates the geology of the area, we defined the first group as "rocks associated with the Turkey Creek caldera." The two other logically identifiable groups are therefore referred to as "pre-Turkey Creek caldera rocks" and "post-Turkey Creek caldera rocks." In the discussions that follow, rocks are assigned to one of the three groups, as appropriate, and data and interpretations ordered accordingly.

In this report, we present a broad array of geologic data to refine knowledge of the central Chiricahua Mountains in particular and the Boot Heel volcanic field in general. First, we present basic stratigraphic setting and petrographic data acquired from the literature and from our own geologic investigations of the mountain range. Subsequently, in the geochemistry section, we present geochemical data, apply classification schemes, evaluate within-unit compositional variation, and establish diagnostic, between-unit compositional characteristics. The geochemistry section concludes with an analysis of the geochemical evolution of the Turkey Creek caldera and its magmatic components. Next, new geochronologic data are presented in order to refine complex stratigraphy-age relations among middle Tertiary volcanic rocks of the central Chiricahua Mountains. In the report's concluding section, we synthesize all the data in order to constrain the large-scale magmatic-tectonic environment in which the middle Tertiary volcanic rocks of the area were erupted, and evaluate how this regime evolved through the middle Tertiary time frame.

Acknowledgments

Our field work was facilitated by the cooperation and assistance of the Southwestern Research Station (SWRS) of the American Museum of Natural History, Chiricahua National Monument, and the University of Arizona. We especially thank Wade and Emily Sherbrooke, Pam Limberger, and Christina Schwartz of SWRS for assistance and for providing a stimulating research environment. Dick Armstrong, Carol Kruse, Chuck Milliken, David Moore, and Alan Whalon provided accommodations and assistance during our work in the national monument. We thank Joe Austin, Carol Hudson, Billie and Jean Riggs, Jim Riggs, and Robin Riggs for providing access to their land. We thank D.B. Yager for preparing geochronology mineral separates and for conducting most of the trace-element analyses. R.A.Yeoman ably conducted argon analyses. Reviews by W.C. Shanks, C.A. Nutt, and D.A. John improved this study.

Sampling and Analytic Methods

Petrographic and stratigraphic relations presented in the next section of this report are expanded versions of map

Figure 1 (facing page). Location of central Chiricahua Mountains, Ariz. Letters show collection sites for samples whose ages were determined by the $^{40}Ar/^{39}Ar$ method (tables 2 and 3).

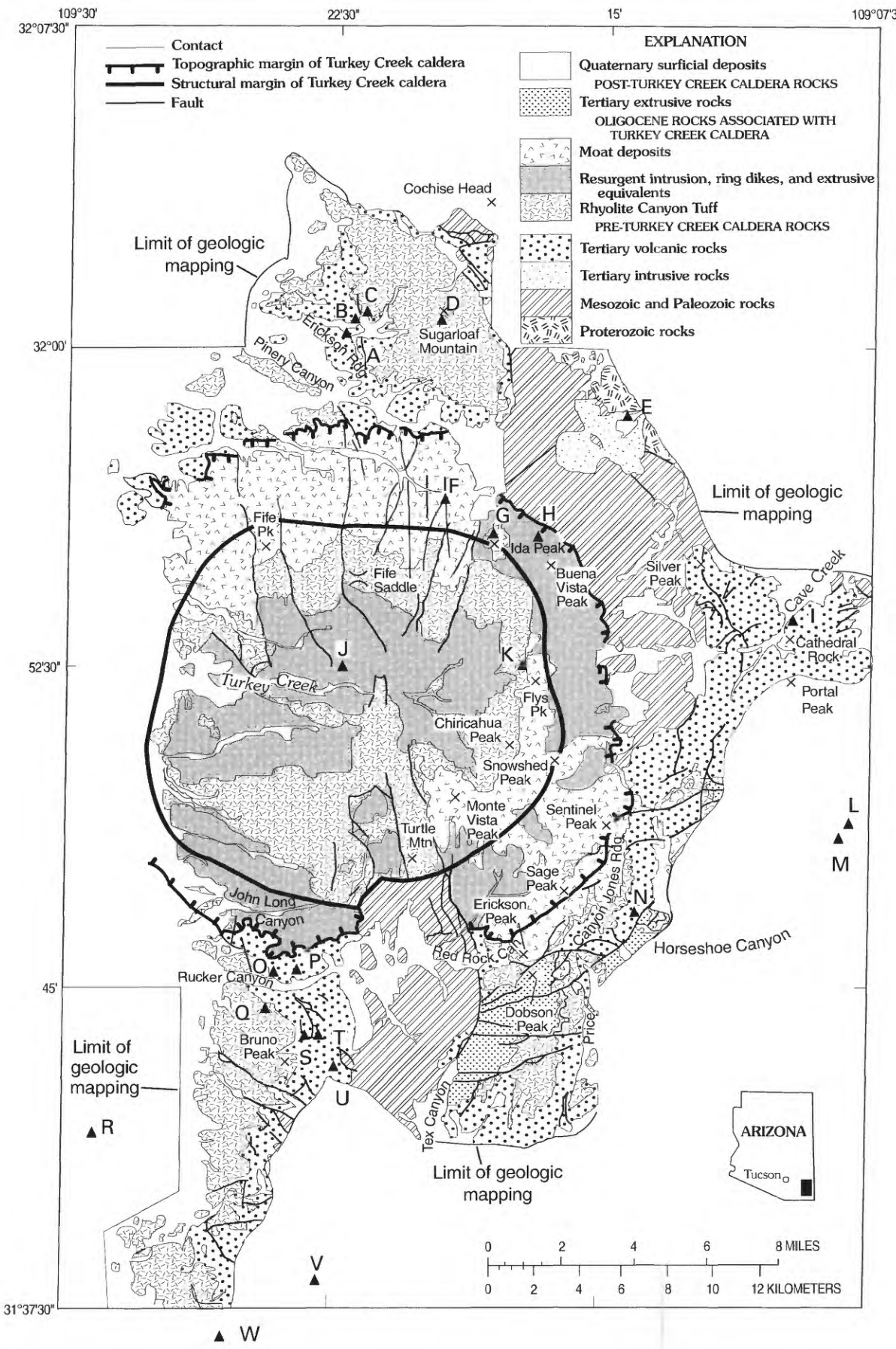

A = P475
B = 201769
C = 201771
D = 201765
E = 201570
F = 201996
G = 201580
H = P3
I = P272C
J = 201587
K = 201538
L = 202156
M = 202154
N = 202151
O = P652
P = P650A
Q = DY91-36
R = DY92-54
S = 202064
T = DY91-11
U = 202057
V = DY91-77
W = P5

unit descriptions included on the geologic map of the central Chiricahua Mountains (du Bray and others, 1997) and contain more detailed petrographic information than that included in the map unit descriptions. Standard thin sections of selected samples were prepared and examined using a petrographic microscope. Multiple samples of each stratigraphic unit were examined; the resulting observations were synthesized and petrographic descriptions developed accordingly.

Numerous samples of each ash-flow tuff stratigraphic unit were collected and chemically analyzed in order to establish their compositional ranges. This procedure is essential in sampling of ash-flow tuffs derived from zoned magma reservoirs (Hildreth, 1979; 1981). Establishing the full range of compositional zonation within each of the ash-flow tuff units of the study area is required if composition is to be employed as a tool of stratigraphic correlation. Most ash-flow tuff samples were collected without our having specifically determined their relative stratigraphic position within the sampled unit. Although we consider our sampling to have been reasonably comprehensive, it is possible that our data do not define the full nature and extent of vertically oriented geochemical variation within some of the studied units because the unit's complete stratigraphic extent may not be represented by the collected samples. In contrast, we were able to systematically sample complete sections of outflow facies Rhyolite Canyon Tuff and tuff of Horseshoe Canyon. Their resulting sample suites are well referenced to relative stratigraphic position, and their chemistry fully defines compositional variation within these units.

The geochemistry presented pertains to samples collected at more than 500 sites. A map showing collection sites for these samples appears in du Bray and others (1997). Complete analytical results for these samples are contained in a series of reports by du Bray and others (1992a; 1992b; 1993) and du Bray and Pallister (1994; 1995). Samples collected throughout the study area provide representative areal coverage of all the units whose compositions are considered. Each sample was crushed coarsely at the outcrop and all obvious xenolithic clasts were removed. Abundances of rubidium, strontium, yttrium, zirconium, niobium, and barium were determined for all of these samples by energy dispersive X-ray fluorescence spectrometry. Major-oxide abundances were determined for more than 230 samples, and additional trace-element abundances in almost 100 of these samples were determined by instrumental neutron activation analysis. The number of samples for which the various types of geochemical data were obtained is listed, by stratigraphic unit, in table 1.

Compositional studies of ash-flow tuffs (Boden, 1989; Fridrich and Mahood, 1987) have relied on analysis of cognate pumice inclusions because these are considered to represent quenched magma. Because most of the middle Tertiary tuffs of the central Chiricahua Mountains are indurated and moderately to densely welded, pumices are flattened to the extent that they are inseparable from enclosing tuff matrix. Therefore, to collect pumice fragments for this compositional study was not routinely possible. Lipman (1965) demonstrated that the compositions of middle Tertiary ash-flow tuff vitrophyre (including pumice) are in some cases considerably modified during postmagmatic processes, including devitrification. Consequently, devitrified pumice blocks such as those contained in the tuffs of our study area are of uncertain utility in compositional studies. The compositional study of ash-flow tuffs by du Bray (1995) demonstrated that data obtained from whole-rock samples are highly reliable and of considerable utility in characterization and correlation of lithic-poor, large-volume, high-silica ash-flow tuff stratigraphic units.

We are aware that the types of whole-rock samples we collected and analyzed are subject to physical sorting that has known potential for affecting chemical compositions. However, we did not determine the magnitude of potential compositional variation resulting from glass shard elutriation and sorting or winnowing during ash-flow emplacement that may affect phenocryst, ash, and pumice distributions. Consequently, although the bulk compositions presented here are believed to broadly reflect magmatic values, some of the observed compositional variation must also result from emplacement dynamics. The coherence of compositional data for volcanic rocks of the mountain range suggests that data presented here represent magma compositions reasonably well. Regardless of the origin of intra-ash-flow chemical variation, distinctive compositions for individual ash-flow tuff units have proven to be of great value for regional correlation. Finally, the effects of sectoral compositional variation, as indicated by compositional overlap between samples from throughout the area, seem to be minor. To further evaluate the potential effects of sectoral variation, compositions of volcanic rocks could be more completely established from samples collected throughout their distributions in other isolated mountain ranges of this region.

All chemical compositions were determined in analytical laboratories of the U.S. Geological Survey in Denver, Colo. Major-oxide abundances were determined by X-ray fluorescence techniques (Taggart and others, 1987) (analysts, J.E. Taggart, A.J. Bartel, D.F. Siems, E.C. Robb, and K.C. Stewart). FeO:FeO*(total iron as FeO) ratios were adjusted to 0.8, and major-oxide abundances were recalculated to 100 percent volatile free. Energy-dispersive X-ray fluorescence spectroscopy, using ^{109}Cd and ^{241}Am radioisotope excitation sources (Elsass and du Bray, 1982), was used to determine abundances of Rb, Sr, Y, Zr, Nb, and Ba (analysts, D.B. Yager and E.A. du Bray); the precision and accuracy of these data are discussed by Sawyer and Sargent (1989) and Yager and Quick (1992). The abundances of Co, Ni, Cr, Cs, Hf, Sb, Ta, Th, U, Zn, Sc, La, Ce, Nd, Sm, Eu, Gd, Tb, Tm, Yb, and Lu were determined by instrumental neutron activation analysis (Baedecker and McKown, 1987) (analysts, R.J. Knight, J.R. Budahn, and R.B. Vaughn).

Thirty mineral separates (21 sanidines, 8 biotites, and 1 hornblende) from twenty-three samples representing 20 stratigraphic units of the region (fig. 1; table 2) were analyzed by the $^{40}Ar/^{39}Ar$ incremental heating technique. Two splits

Table 1. Compositions of volcanic rocks of the central Chiricahua Mountains.

[Major-oxide data in weight percent (normalized to 100%, anhydrous). Trace-element data in parts per million. Ferrous iron/total iron as FeO adjusted to 0.8. ND, not detected at the indicated abundance. Averages and standard deviations given for *n* analyses. NA, not analyzed]

	Pre-Turkey Creek caldera rocks							
	Tim	Thl	Tjg	Tkr	Tc	Tfre	Thcl	Thcu
n=	16	6	10	0	5	6	9	12
SiO_2	62.58±2.19	76.97±2.03	73.02±1.17	NA	77.28±0.66	73.27±0.53	75.94±1.30	69.75±1.94
Al_2O_3	17.06±0.51	12.61±0.86	14.59±0.81	NA	12.20±0.37	14.91±0.25	12.49±0.69	15.64±0.90
Fe_2O_3	1.21±0.17	0.25±0.05	0.49±0.05	NA	0.20±0.05	0.26±0.02	0.28±0.06	0.47±0.12
FeO	4.37±0.60	0.89±0.20	1.77±0.19	NA	0.72±0.17	0.94±0.07	1.02±0.23	1.87±0.16
MgO	2.22±0.78	0.36±0.13	0.43±0.13	NA	0.12±0.07	0.38±0.24	0.15±0.03	0.42±0.13
CaO	3.89±1.08	0.93±0.85	0.56±0.32	NA	0.27±0.19	1.20±0.23	0.21±0.13	0.91±0.69
Na_2O	3.64±0.57	1.32±0.43	2.60±0.72	NA	2.54±1.51	4.01±0.25	2.14±0.98	3.34±0.79
K_2O	3.83±1.52	6.48±1.41	6.10±1.27	NA	6.46±2.45	4.80±0.10	7.50±1.36	6.85±1.25
TiO_2	0.80±0.15	0.15±0.02	0.32±0.04	NA	0.17±0.04	0.19±0.01	0.25±0.09	0.58±0.10
P_2O_5	0.27±0.05	ND(0.01)	0.08±0.03	NA	ND(0.01)	ND(0.01)	0.01±0.02	0.12±0.03
MnO	0.08±0.03	0.03±0.02	0.03±0.01	NA	0.04±0.03	0.04±0.02	0.02±0.03	0.05±0.01
n=	24	15	13	3	11	6	23	25
Rb	152±81	314±102	312±106	419±25	459±147	172±11	486±118	251±73
Sr	489±109	177±147	122±32	26±6	30±17	249±22	40±18	143±82
Y	30±7	40±14	35±12	43±1	51±11	29±6	51±10	55±14
Zr	189±20	107±8	174±32	144±9	181±24	163±4	247±88	640±182
Nb	11±3	17±2	14±4	27±5	32±3	15±2	32±7	23±5
Ba	840±220	517±290	818±163	54±11	35±15	829±53	197±162	1496±651
n=	3	0	0	0	3	2	1	2
Co	15.0±1.5	NA	NA	NA	0.166±0.07	0.910±0.14	0.211	2.20±0.39
Ni	13.9±3.49	NA	NA	NA	4.00±6.93	8.30±5.23	ND(0.5)	17.2±3.0
Cr	18.1±4.9	NA	NA	NA	0.567±0.98	1.04±0.27	1.65	1.08±1.86
Cs	7.69±4.18	NA	NA	NA	55.7±78.5	6.52±2.28	14.9	5.84±3.45
Hf	5.31±0.35	NA	NA	NA	7.60±0.59	5.35±0.33	7.44	17.3±1.1
Sb	3.39±5.29	NA	NA	NA	1.54±2.35	0.133±0.02	2.74	0.277±0.12
Ta	0.96±0.17	NA	NA	NA	2.70±0.21	1.24±0.06	2.56	1.40±0.09
Th	14.5±4.1	NA	NA	NA	29.6±1.3	17.2±0.9	29.0	15.6±1.0
U	3.58±0.84	NA	NA	NA	7.31±0.55	3.88±0.29	8.12	2.72±0.21
Zn	59.1±4.4	NA	NA	NA	60.4±7.9	36.6±0.9	87.5	66.6±10.6
Sc	10.2±1.6	NA	NA	NA	2.78±0.57	2.95±0.13	2.41	6.19±0.48
La	36.9±2.4	NA	NA	NA	45.5±8.8	46.8±2.9	40.2	67.1±4.2
Ce	74.3±4.1	NA	NA	NA	99.9±23.1	91.5±9.2	82.0	140±16
Nd	33.3±4.1	NA	NA	NA	38.8±12.9	32.6±3.5	28.8	58.3±2.9
Sm	6.38±.82	NA	NA	NA	8.44±3.11	5.39±0.52	5.65	11.0±0.7
Eu	1.34±0.22	NA	NA	NA	0.393±0.24	0.767±0.05	0.393	3.18±0.29
Gd	5.44±0.39	NA	NA	NA	8.82±-	4.31±0.91	5.31	8.91±-
Tb	0.77±0.10	NA	NA	NA	1.20±0.32	0.609±0.05	0.801	1.31±0.09
Tm	0.41±0.03	NA	NA	NA	0.874±-	0.407±0.02	0.748	0.696±-
Yb	2.59±0.15	NA	NA	NA	5.35±0.07	2.56±0.13	4.79	4.40±0.13
Lu	0.39±0.02	NA	NA	NA	0.777±0.02	0.368±0.04	0.719	0.646±0.02
Ba/Nb	76.4	30.6	56.4	2.00	1.09	56.6	6.13	64.9
Ba/Ta	840	NA	NA	NA	12.9	670	77.0	1066
La/Nb	3.3	NA	NA	NA	1.43	3.19	1.25	2.91

from each of two of the sanidine separates (fig. 1; 201765 and 201769) were analyzed in order to evaluate analytical reproducibility for samples analyzed during the several years that geochronologic investigations were conducted. Mineral separates were prepared, after crushing, grinding, and sieving, by magnetic separator, mica-table, and heavy liquid methods; grains ranged in size between 60 and 120 mesh (250–125 μm). Separates were handpicked to greater than 99 percent purity. Individual samples were cleaned with reagent-grade acetone, alcohol, and deionized water in an ultrasonic bath, air-dried, wrapped in aluminum capsules and sealed in silica vials along with monitor minerals before irradiation. Samples were irradiated in two irradiation packages, one in 1995 and an earlier one in 1988, at two separate TRIGA research reactor facilities. After irradiation, the samples were progressively degassed in a double-vacuum resistance furnace in a series of 11 to 16

Table 1. Compositions of volcanic rocks of the central Chiricahua Mountains.—Continued

	Pre-caldera rocks	Rocks associated with the Turkey Creek caldera						
	Tjj	Trcb	Trcl	Trcm	Trcu	Trci	Trcf	Tdpl
n=	6	6	20	17	9	39	7	24
SiO_2	77.57±0.21	77.08±0.44	77.21±0.39	77.50±0.26	76.09±0.68	76.59±1.16	76.65±1.36	65.42±1.39
Al_2O_3	12.40±0.20	11.98±0.50	12.08±0.16	12.10±0.12	12.50±0.26	12.32±0.59	11.99±0.67	15.54±0.42
Fe_2O_3	0.22±0.04	0.35±0.03	0.34±0.03	0.31±0.03	0.40±0.08	0.42±0.05	0.41±0.06	0.97±0.08
FeO	0.78±0.14	1.26±0.11	1.21±0.11	1.10±0.10	1.55±0.11	1.49±0.18	1.48±0.23	3.49±0.28
MgO	0.31±0.08	0.02±0.04	0.16±0.10	0.09±0.09	0.24±0.14	0.16±0.13	0.11±0.08	1.38±0.40
CaO	0.37±0.12	0.07±0.06	0.29±0.17	0.23±0.07	0.34±0.13	0.23±0.14	0.06±0.04	2.84±0.74
Na_2O	3.07±0.62	2.25±0.40	3.55±0.27	3.47±0.20	3.32±0.72	3.10±0.71	2.12±1.33	3.77±0.49
K_2O	5.08±0.49	6.84±0.50	4.96±0.12	5.02±0.33	5.25±0.27	5.43±0.71	6.95±1.61	5.26±1.07
TiO_2	0.15±0.03	0.10±0.00	0.12±0.02	0.12±0.02	0.22±0.01	0.21±0.05	0.21±0.04	0.92±0.09
P_2O_5	ND(0.01)	ND(0.01)	ND(0.01)	ND(0.01)	0.01±0.03	ND(0.01)	ND(0.01)	0.34±0.03
MnO	0.05±0.02	0.05±0.01	0.07±0.01	0.06±0.02	0.06±0.02	0.03±0.03	0.03±0.03	0.09±0.02
n=	8	18	33	47	15	67	15	60
Rb	304±8	553±55	423±25	394±24	285±23	332±100	397±122	208±66
Sr	26±7	24±4	22±6	22±8	42±13	38±14	34±7	227±54
Y	41±5	78±11	75±27	74±18	65±7	59±11	64±8	48±8
Zr	175±25	283±14	289±16	278±10	366±31	383±68	395±59	490±89
Nb	34±3	59±3	61±5	57±4	42±5	43±7	42±4	26±3
Ba	33±41	43±14	20±12	24±18	77±29	77±38	94±88	794±117
n	5	0	6	13	4	12	3	10
Co	0.287±0.09	NA	0.297±0.23	0.426±0.32	0.870±0.27	0.573±0.71	0.248±0.03	8.84±1.35
Ni	2.08±3.81	NA	2.69±4.33	2.50±2.71	1.20±2.40	2.83±3.69	ND(0.5)	22.3±3.6
Cr	1.35±0.80	NA	0.403±0.50	0.693±0.78	1.28±0.89	1.15±1.48	0.693±0.60	16.5±6.2
Cs	8.43±1.68	NA	9.20±1.67	6.38±0.57	4.70±0.54	6.25±3.74	7.52±1.43	11.7±22.0
Hf	7.16±0.26	NA	11.5±0.7	11.0±0.7	12.1±0.9	13.2±1.2	11.1±0.5	11.6±1.7
Sb	0.530±0.46	NA	0.248±0.06	0.225±0.07	0.228±0.07	0.905±0.77	1.06±0.27	0.244±0.14
Ta	2.88±0.13	NA	5.40±0.32	4.88±0.48	3.73±0.14	3.79±1.20	3.70±0.54	1.92±0.25
Th	34.0±1.7	NA	48.3±4.3	48.1±2.9	41.7±1.5	42.8±6.4	40.2±2.8	22.5±3.01
U	6.69±0.83	NA	11.2±1.1	9.29±1.41	8.49±0.69	7.89±2.44	8.20±0.30	4.59±0.94
Zn	56.2±15.6	NA	79.4±13.2	63.5±13.8	61.7±11.1	70.4±14.3	61.9±11.3	77.9±7.3
Sc	2.31±0.12	NA	1.95±0.08	2.09±0.34	3.50±0.25	3.85±1.08	2.80±0.03	9.50±0.60
La	39.2±6.7	NA	51.3±15.3	63.5±16.6	96.5±11.4	100±38	87.8±7.4	80.1±11.1
Ce	74.2±7.9	NA	132±30	146±20	224±27	220±80	180±18	175±27
Nd	26.3±4.2	NA	44.6±15.9	58.9±18.6	83.8±8.8	82.5±28.7	67.3±3.7	72.3±10.7
Sm	5.54±1.13	NA	10.3±4.1	13.3±4.4	15.2±2.1	13.7±3.9	13.2±0.5	12.0±1.8
Eu	0.156±0.02	NA	0.103±0.04	0.146±0.05	0.264±0.04	0.334±0.24	0.212±0.03	2.00±0.22
Gd	5.18±0.78	NA	9.97±3.96	13.4±4.3	12.7±1.3	11.3±2.6	10.4±0.3	10.1±1.4
Tb	0.83 ±0.08	NA	1.78±0.72	2.17±0.72	1.95±0.18	1.66±0.41	1.63±0.06	1.42±0.15
Tm	0.809±0.06	NA	1.32±0.43	1.53±0.39	1.17±0.15	1.08±0.09	1.08±0.07	0.740±0.08
Yb	5.27±0.37	NA	8.42±2.70	9.53±2.34	7.38±0.44	6.74±0.62	6.95±0.67	4.59±0.47
Lu	0.770±0.04	NA	1.23±0.36	1.33±0.30	1.06±0.07	0.969±0.10	0.987±0.09	0.669±0.08
Ba/Nb	0.98	0.72	0.33	0.42	1.84	1.76	2.27	31.1
Ba/Ta	11.5	NA	3.66	4.95	20.5	20.1	25.5	412
La/Nb	1.16	NA	0.84	1.11	2.32	2.30	2.11	3.14

individual, 20-minute-long temperature steps to a maximum temperature of 1,650°C. All analyses were done in the Argon Laboratory, U.S. Geological Survey, Denver, Colo. Decay constants are those of Steiger and Jäger (1977). The standard used in these age determinations was hornblende MMhb-1 with a K-Ar age of 520.4 Ma (Samson and Alexander, 1987). Apparent ages were calculated using decay constants recommended by Steiger and Jäger (1977). The determination of whether the individual apparent ages yielded a "plateau" was made using the critical value test of Dalrymple and Lanphere (1969) following the plateau definition of Fleck and others (1977). Plateaus that pertain to more than 50 percent of the gas produced during heating were achieved for all but seven of the mineral separates. Plateau dates were calculated using a weighted mean, where weighting is by the inverse of the analytical variance (Taylor, 1982).

Table 1. Compositions of volcanic rocks of the central Chiricahua Mountains.—Continued

	Rocks associated with the Turkey Creek caldera						Post-caldera rocks	
	Tdpi	Ttp	Tmrb	Tmr1	Tmr2	Tmr3	Ts	Trdp
n=	16	2	6	12	9	3	4	4
SiO_2	65.88±2.73	64.00±5.00	73.73±0.62	76.55±0.47	77.32±0.55	77.45±0.09	77.64±0.35	76.79±0.40
Al_2O_3	15.29±0.57	15.99±0.72	14.01±0.41	12.81±0.26	12.62±0.33	12.31±0.16	12.09±0.33	12.73±0.20
Fe_2O_3	0.97±0.20	1.02±0.37	0.39±0.01	0.27±0.02	0.22±0.01	0.24±0.01	0.25±0.10	0.22±0.07
FeO	3.51±0.74	3.68±1.34	1.41±0.03	0.98±0.07	0.78±0.04	0.86±0.05	1.04±0.15	0.95±0.08
MgO	1.40±0.48	1.66±0.72	0.46±0.08	0.17±0.02	0.08±0.06	0.11±0.01	0.09±0.07	ND(0.10)
CaO	2.59±0.88	2.46±2.16	1.46±0.30	0.55±0.24	0.19±0.17	0.15±0.07	0.41±0.16	0.34±0.10
Na_2O	3.80±0.32	4.43±0.07	3.41±0.47	3.84±0.52	3.65±0.48	3.57±0.03	3.05±0.27	3.98±0.05
K_2O	5.20±0.56	5.38±0.91	4.76±0.77	4.59±0.88	4.93±0.79	5.12±0.09	5.24±0.41	4.81±0.09
TiO_2	0.94±0.21	0.99±0.30	0.28±0.02	0.18±0.01	0.15±0.03	0.15±0.01	0.15±0.01	0.11±0.01
P_2O_5	0.33±0.09	0.32±0.18	0.07±0.04	ND(0.01)	0.01±0.03	ND(0.01)	ND(0.01)	ND(0.01)
MnO	0.09±0.03	0.08±0.05	0.03±0.02	0.06±0.01	0.06±0.02	0.03±0.01	0.05±0.01	0.07±0.02
n=	25	4	17	64	27	6	10	12
Rb	204±62	206±29	265±57	351±70	413±55	391±14	407±44	555±65
Sr	206±48	152±117	162±66	34±14	18±7	20±4	34±20	17±3
Y	47±8	63±4	39±6	59±14	48±12	38±12	58±14	69±30
Zr	474±81	839±120	175±25	220±39	93±7	196±6	161±31	150±13
Nb	24±4	34±4	15±3	40±8	53±7	51±2	42±6	64±16
Ba	763±96	266±182	667±109	81±18	14±9	12±5	90±106	20±14
n=	9	0	6	7	7	2	0	0
Co	9.35±2.83	NA	2.31±0.24	0.395±0.05	0.370±0.42	0.223±0.01	NA	NA
Ni	13.2±9.3	NA	8.23±3.00	5.18±2.51	11.2±22.0	2.40±0.00	NA	NA
Cr	9.46±3.63	NA	2.26±0.83	0.398±0.44	0.587±0.65	8.91±1.29	NA	NA
Cs	5.02±2.34	NA	4.91±2.87	22.2±19.4	11.1±0.7	7.10±1.13	NA	NA
Hf	11.8±0.6	NA	5.68±0.39	8.00±0.41	8.62±1.21	8.20±0.21	NA	NA
Sb	0.268±0.02	NA	0.098±0.02	0.222±0.07	0.242±0.06	0.176±0.02	NA	NA
Ta	2.10±0.18	NA	1.45±0.13	3.65±0.18	4.81±0.80	4.54±0.16	NA	NA
Th	25.7±5.7	NA	27.8±2.5	38.9±2.9	51.4±12.8	44.9±0.6	NA	NA
U	4.53±0.74	NA	3.72±0.48	8.95±1.29	11.2±2.5	8.11±1.95	NA	NA
Zn	77.1±7.9	NA	39.6±6.5	69.9±24.2	57.8±11.8	64.3±26.3	NA	NA
Sc	9.45±1.84	NA	3.79±0.29	2.53±0.22	2.29±0.43	2.04±0.01	NA	NA
La	83.8±10.6	NA	52.2±5.8	70.5±9.3	36.5±7.3	25.0±0.9	NA	NA
Ce	178±14	NA	114±15	158±18	92.1±24.9	56.8±14.0	NA	NA
Nd	72.3±7.4	NA	46.3±7.4	61.8±5.5	24.2±7.6	15.8±3.0	NA	NA
Sm	12.1±1.3	NA	8.44±1.33	11.4±0.9	5.02±1.88	3.34±0.75	NA	NA
Eu	1.92±0.23	NA	1.01±0.08	0.487±0.03	0.189±0.05	0.176±0.02	NA	NA
Gd	10.2±0.9	NA	7.50±1.17	10.7±0.7	4.91±2.82	3.37±0.28	NA	NA
Tb	1.47±0.14	NA	1.09±0.16	1.73±0.13	0.880±0.33	0.598±0.11	NA	NA
Tm	0.779±0.09	NA	0.606±0.08	1.18±0.04	0.853±0.33	0.652±0.08	NA	NA
Yb	4.87±0.53	NA	3.69±0.50	7.46±0.22	6.61±1.37	4.53±0.23	NA	NA
Lu	0.721±0.08	NA	0.524±0.07	1.07±0.05	0.996±0.22	0.694±0.02	NA	NA
Ba/Nb	31.6	7.74	45.4	2.01	0.27	0.23	2.14	0.31
Ba/Ta	363	NA	460	22.1	2.96	2.57	NA	NA
La/Nb	3.47	NA	3.55	1.76	0.68	0.49	NA	NA

Petrographic and Stratigraphic Characteristics

In the descriptions that follow, a three- to four-letter map unit code is identified for each of the stratigraphic units in order to aid their identification in the tables and figures. Map unit symbols designated by du Bray and others (1997) on the geologic map of the Turkey Creek caldera match those used here. The first letter in each of these map unit symbols, T, denotes their Tertiary age. A simplified correlation of map units and a set of abbreviated rock unit identifiers are provided in order to define stratigraphic relations among the various volcanic rock units that were studied (fig. 2).

Pre-Turkey Creek Caldera Rocks

Basement rocks on which middle Tertiary volcanic rocks were deposited include interlayered Mesozoic sedimentary

Table 2. Summary of $^{40}Ar/^{39}Ar$ age-spectrum results from the central Chiricahua Mountains.

[Preferred ages in bold; % data in Type of apparent age column indicates percentage of total gas included in plateau steps; --, apparent age, isochron, initial 40/36, not calculated]

Sample No.; unit symbol	Unit	Mineral	Apparent age (Ma)	Type of apparent age	Isochron age	Initial 40/36
			Pre-Turkey Creek caldera rocks			
DY91-77	Dacitic rocks of Half-moon Valley, intrusion.	Biotite	73.23±0.11	Excess argon Saddle-low	**74.6±0.6**	276±19
202057 Thl	Rhyolite tuff of High Lonesome Canyon.	Sanidine	**34.16±0.17**	Plateau (76.5%)	--	--
DY91-11 Tjg	Lower member of the rhyolite of Joe Glenn Ranch.	Biotite	**33.81±0.08**	Plateau (91.1%)	--	--
P650A	Pyroclastic rocks of Rucker Canyon, rhyolite lava.	Biotite	**33.32±0.07**	Plateau (83.5%)	--	--
202064	Pyroclastic rocks of Rucker Canyon.	Biotite	**33.21±0.09**	Plateau (68.9%)	--	--
202064	Pyroclastic rocks of Rucker Canyon.	Sanidine	33.04±0.04	Weight average	**33.04±0.04**	310±7
201570	Granodiorite of Mackey Canyon.	Hornblende	32.08±0.20	Plateau (50.8%) excess Ar	**31.42±0.30**	309±6
201570	Granodiorite of Mackey Canyon.	Biotite	**30.62±0.15**	Plateau (59.1%)	--	--
P272C Tc	Rhyolite lava of Cave Creek.	Sanidine	**28.10±0.12**	Plateau (89.3%)	--	--
P475 Tfre	Rhyolite of Erickson Ridge.	Sanidine	**27.89±0.09**	Plateau (78.5%)	--	--
P475 Tfre	Rhyolite of Erickson Ridge.	Biotite	28.24±0.08	Plateau (65.5%)	--	--
P652 Tjj	Jesse James Canyon Tuff.	Sanidine	**27.52±0.06**	Plateau (61.3%)	--	--
201771 Tjj	Jesse James Canyon Tuff.	Sanidine	**27.59±0.06**	Plateau (55.8%)	27.71±0.02	270±10
202156 Thcl	Lower member of the tuff of Horseshoe Canyon.	Biotite	**27.62±0.10**	Plateau (88.8%)	--	--
202156 Thcl	Lower member of the tuff of Horseshoe Canyon.	Sanidine	--	No plateau	25.42±0.10	297±4
202154	Latite of Darnell Peak	Sanidine	**27.58±0.08**	Plateau (77.9%)	--	--

and volcanic rocks. These Mesozoic rocks are underlain by Paleozoic marine sedimentary rocks that were deposited on a basement composed of Proterozoic granitoid rocks. These Mesozoic, Paleozoic, and Proterozoic rocks are not discussed further in this report.

In many parts of the central Chiricahua Mountains, the Tertiary volcanic rocks described herein are directly underlain by intermediate-composition lava flows, flow breccias, and near-source pyroclastic rocks (Tim) that probably were erupted from a field of coalescing composite volcanoes. These dacitic to andesitic rocks, which denote the onset of middle Tertiary volcanism in this area, are dark greenish gray to greenish black and maroon where oxidized and form massive, locally densely jointed and fractured outcrops. These rocks are aphyric to sparsely porphyritic; glassy flow margins are preserved in some places. Phenocrysts form trachytic or

Table 2. Summary of $^{40}Ar/^{39}Ar$ age-spectrum results from the central Chiricahua Mountains.—Continued

Sample No.; unit symbol	Unit	Mineral	Apparent age (Ma)	Type of apparent age	Isochron age	Initial 40/36
Rocks associated with the Turkey Creek caldera						
201769 Trcl	Lower member of the Rhyolite Canyon Tuff.	Sanidine	**26.97±0.09**	Plateau (60.8%)	27.09±0.04	309±2
201769 Trcl	Lower member of the Rhyolite Canyon Tuff.	Sanidine	**26.93±0.12**	Plateau (90.8%)	--	--
DY91-36 Trcm	Middle member of the Rhyolite Canyon Tuff.	Sanidine	**27.03±0.11**	Plateau (75.0%)	27.14±0.03	297±2
201765 Trcu	Upper member of the Rhyolite Canyon Tuff.	Sanidine	--	No plateau	**26.98±0.04**	309±2
201765 Trcu	Upper member of the Rhyolite Canyon Tuff.	Sanidine	**26.94±0.12**	Plateau (91.3%)	--	--
201587 Tdpi	Dacite porphyry, intrusion.	Sanidine	26.84±0.17	Weight average	**26.90±0.04**	296±2
P3 Tdpl	Dacite porphyry, lava flow.	Sanidine	**26.97±0.13**	Minimum age step	27.44±0.15	303±2
201996 Tmrb	Turkey Creek caldera moat lava, biotite rhyolite lava.	Biotite	27.11±0.06	Plateau (67.8%)	**26.63±0.04**	366±15
201996 Tmrb	Turkey Creek caldera moat lava, biotite rhyolite lava.	Sanidine	**26.74±0.05**	Plateau (65.6%)	--	--
201538 Tmrl	Turkey Creek caldera moat lava, unit 1 rhyolite lava.	Sanidine	26.93±0.17	Weight average	**26.89±0.05**	298±1
201580 Tmrl	Turkey Creek caldera moat lava, unit 1 rhyolite lava.	Sanidine	**26.64±0.13**	Plateau (94.3%)	--	--
Post-Turkey Creek caldera rocks						
DY92-54	Rhyolite lava	Sanidine	**26.35±0.08**	Plateau (65.9%)	--	--
202151 Trdp	Rhyolite lava of Dobson Peak.	Sanidine	**26.20± 0.07**	Plateau (62.8%)	--	--
P5	Rhyolite of Packsaddle Mountain.	Sanidine	**23.23± 0.06**	Plateau (65.0 %)	--	--

intergranular intergrowths of plagioclase, pyroxene, hornblende, and biotite in a devitrified or aphanitic groundmass; accessory phases include Fe-Ti oxide minerals and apatite. The groundmass is variably altered to clay minerals, Fe-Ti oxide minerals, zeolites, and calcite.

Intermediate-composition volcanic rocks are only present at the base of the Tertiary section in the map area; rocks of this type are not interstratified with younger, voluminous rhyolitic volcanic rocks. The onset of rhyolitic volcanism denotes the development of large, low-density magma reservoirs in the shallow crust. Once established, these reservoirs likely inhibited the buoyant ascent and eruption of additional intermediate-composition magma. Consequently, solidified masses representing unerupted parts of the rhyolitic reservoirs are probably underplated by a considerable volume of solidified, intermediate-composition magma petrologically similar

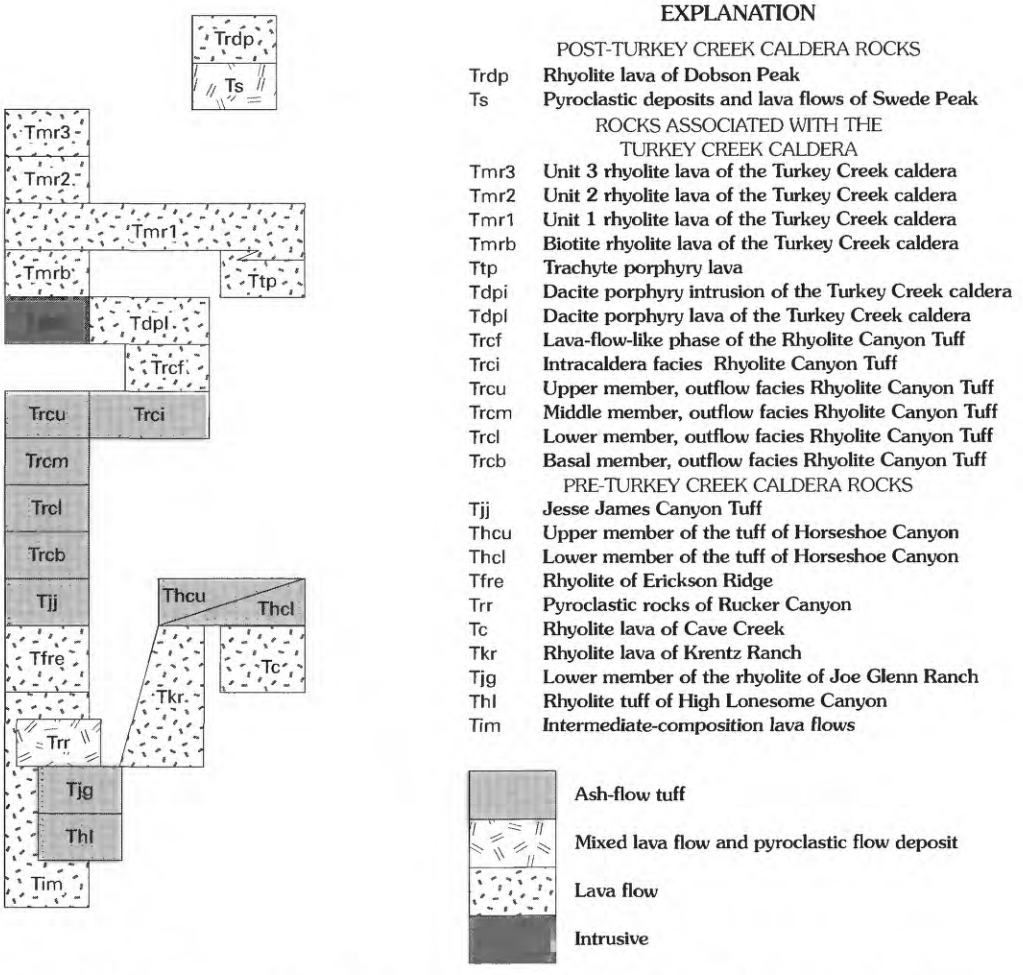

Figure 2. Simplified correlation of map units and identification of studied volcanic rock units.

to the intermediate-composition volcanic rocks preserved at the base of the Tertiary section in the map area.

The oldest regionally extensive ash-flow tuff in the central Chiricahua Mountains was erupted from an unknown source; it is the pale-orange to yellowish-gray rhyolite tuff of High Lonesome Canyon (Thl). This ash-flow tuff, first described by Drewes and Brooks (1988), is crystal poor (contains about 5 percent crystals), pumice and lithic rich, and weakly to moderately welded. Phenocrysts include approximately equal amounts of partly resorbed and embayed quartz and subhedral to anhedral sanidine, lesser amounts of anhedral albite and Fe-Ti oxide minerals, and trace amounts of oxidized biotite, all in a devitrified ash- and shard-rich matrix. In exposures near the mouth of Rucker Canyon, the tuff consists of two cooling units separated by a 1-m-thick volcanic sandstone. Andesitic lithic fragments are common. In the study area, the tuff is restricted to a small area south of the Turkey Creek caldera.

The lower member of the rhyolite of Joe Glenn Ranch (Tjg) is grayish-orange-pink to pale-red-purple ash-flow tuff erupted from an unknown source. Only the lower member of the rhyolite of Joe Glenn Ranch, first described by Drewes and Brooks (1988), is present in the area studied by du Bray and others (1997). The tuff, which overlies the rhyolite tuff of High Lonesome Canyon, is crystal rich (20–40 percent), pumice and lithic poor, and weakly to moderately welded. Crystals are resorbed quartz, subhedral sanidine, subhedral albite, and anhedral oxidized biotite, and include trace amounts of anhedral Fe-Ti oxide minerals and zircon in a devitrified ash matrix. This unit may be correlative with Faraway Ranch Formation member 3 of Fernandez and Enlows (1966). In the central Chiricahua Mountains, the tuff is restricted to small areas north and south of the Turkey Creek caldera.

The rhyolite lava of Krentz Ranch (Tkr), defined by Drewes and Brooks (1988), is composed of light-gray to pale-orange-gray, nearly aphyric, massive to flow-laminated, high-silica rhyolite lava that contains interbedded, cogenetic pyroclastic flow deposits. These lava flows, vitrophyric in some places, probably represent a field of coalesced rhyolite domes. Sparse phenocrysts, which are in a massive, variably devitrified groundmass, include subhedral sanidine, resorbed quartz, and trace amounts, especially in vitrophyre, of zircon, Fe-Ti oxide minerals, and hornblende. The rhyolite lava of Krentz Ranch underlies an area of less than 10 km^2 about 160 km southeast of the center of the Turkey Creek caldera.

The rhyolite lava of Cave Creek (Tcc), defined by Raydon (1952), is light gray to pale orange gray and reddish orange, crystal-poor to aphyric, and massive to flow-laminated. Phenocrysts are mostly sanidine and quartz, but trace amounts of hornblende, biotite, magnetite, and titanite are preserved, especially in glassy rocks. The groundmass of the rhyolite is a devitrified intergrowth of quartz and feldspar that is spherulitic or granophyric in some places. The rhyolite of Cave Creek, which overlies andesite to dacite lava flows in the east part of the study area, forms numerous flow domes and contains interbedded, cogenetic pyroclastic flow deposits. These rocks probably overlie the small vents from which they were erupted. Bryan (1988) identified and mapped lower, middle, and upper members of the rhyolite in the Cave Creek watershed.

The rhyolite of Erickson Ridge (Tfre), as described by Pallister and others (1994), is light-gray (devitrified) to black (glassy) biotite rhyolite. It contains phenocrysts of oscillatory-zoned, subhedral oligoclase-albite (3–7 percent) and biotite (1–2 percent). Accessory to trace titanite forms euhedral phenocrysts. The rhyolite forms small lava domes and lobate flow-layered lava flows having black glassy carapace breccias and minor interbedded, cogenetic pyroclastic flow deposits. The rhyolite overlies andesite lava flows and forms extensive overlapping flow domes that probably overlie and conceal their small vents. The lava flows are probably correlative with Faraway Ranch Formation member 7 of Fernandez and Enlows (1966), whereas interbedded pyroclastic flow deposits are probably correlative at least in part with Faraway Ranch Formation member 6 of Fernandez and Enlows (1966). The rhyolitic lava flows of the Faraway Ranch Formation, which underlie an area of about 5 km^2 about 5 km west of Sugarloaf Mountain and north of the Turkey Creek caldera, probably represent a field of coalesced rhyolite domes.

The tuff of Horseshoe Canyon (Bryan, 1988) crops out extensively east and southeast of the Turkey Creek caldera and consists of upper (Thcu) and lower (Thcl) members separated by a plagioclase-sanidine porphyry sill known as the latite of Darnell Peak (Bryan, 1988). This tuff, erupted from the Portal caldera (Bryan, 1988), is gray- to orange-weathering, densely welded, and strongly zoned. The lower member is zoned from a thin basal unit composed of high-silica rhyolite tuff with moderate crystal content (10–15 percent) to crystal-rich (20–35 percent) trachyte tuff containing phenocrysts of sanidine, quartz, plagioclase, biotite, clinopyroxene, titanite, and Fe-Ti oxide minerals. The upper member has moderate crystal content (10–20 percent) and is composed of low-silica rhyolite tuff that contains phenocrysts of sericitized sanidine, quartz, and accessory or trace biotite. The tuff of Horseshoe Canyon is correlative with tuff of Price Canyon (Drewes and Brooks, 1988) and the Eagle Cliffs member of the rhyolite of Cave Creek (Raydon, 1952).

The Jesse James Canyon Tuff (Tjj), as described by Pallister and others (1994), erupted from an unknown source; it is light-gray or pinkish-gray, typically lithic poor, moderately crystal rich (approximately 10 percent), biotite-bearing quartz-sanidine rhyolite ash-flow tuff. This unit is similar to middle and lower members of Rhyolite Canyon Tuff but is distinguished by trace amounts of biotite and titanite, an absence of clinopyroxene, a higher ratio of sanidine to quartz, less evolved chemistry, and stratigraphic position. The Jesse James Canyon Tuff is correlative, in part, with the welded tuff of Rucker Canyon (Drewes and Brooks, 1988). In the study area, the tuff is restricted to small areas north and south of the Turkey Creek caldera.

Rocks Associated with the Turkey Creek Caldera

The Rhyolite Canyon Tuff, as redefined by Pallister and others (1994), consists of intracaldera and outflow facies. Drewes (1982) provided a synopsis for the correlation between the Rhyolite Canyon Formation, parts of which were redefined to the Rhyolite Canyon Tuff, and earlier nomenclature established for these rocks by Enlows (1955) and Fernandez and Enlows (1966). The tuff, whose eruption caused collapse of the Turkey Creek caldera, is the volumetrically dominant eruptive product of the caldera (du Bray and Pallister, 1991). The outflow facies rocks have been divided into basal (Trcb), lower (Trcl), middle (Trcm), and upper (Trcu) members. The intracaldera facies (Trci) is dominated by a thick accumulation of homogeneous tuff but also includes a lava-flow-like phase (Trcf). All parts of the Rhyolite Canyon Tuff are petrographically similar, with the exceptions noted following. The unit is light-gray to reddish-brown, high-silica rhyolite ash-flow tuff that contains 7–35 percent phenocrysts; phenocrysts are almost entirely quartz and sanidine. Sanidine forms lath-shaped crystals typically 1–4 mm long but locally as long as 1 cm in the upper member of the Rhyolite Canyon Tuff. Quartz typically is rounded and embayed, and grains are 1–3 mm in diameter. The tuff also contains accessory Fe-Ti oxide minerals and trace augite, hornblende, zircon, apatite, and allanite. The lava-flow-like phase in the uppermost exposures of intracaldera tuff is distinguished by large (0.5–1 cm), mostly lath shaped crystals of perthitic sanidine, large subhedral or partly resorbed quartz phenocrysts, an apparent absence of eutaxitic structure, and a few lithic inclusions. The intracaldera facies is reddish brown, red, pink, orange, or gray and lithic-poor to lithic-rich (<5–20 percent). The Rhyolite Canyon Tuff is correlative with the tuff of Shake Gulch and the tuff of Bruno Peak (Drewes and Brooks, 1988).

Dacite porphyry was emplaced as a resurgent intrusion (Tdpi) in the center of the collapsed Turkey Creek caldera. Its extrusive equivalent, dacite porphyry lava flows (Tdpl), was erupted onto the floor of the evolving moat of the Turkey Creek caldera shortly after eruption of the Rhyolite Canyon Tuff. Dacite porphyry that forms lava flows is petrographically and compositionally similar to dacite porphyry of the resurgent intrusion, except that clinopyroxene is its predominant mafic mineral and its groundmass is much finer grained. Glassy margins, brecciated in places, are exposed locally

between flows at shallow stratigraphic levels. The dacite porphyry is gray to tan, massive, and highly jointed. Its groundmass grades from coarse cuneiform granophyre, most common at the lowest exposed levels of the resurgent intrusion, through medium- to fine-grained granophyre higher in the intrusion. The dacite porphyry contains megacrysts (5 mm to >3 cm across) of alkali feldspar and plagioclase, and small (typically 1 cm across) hornfels inclusions. Alkali feldspar, commonly zoned, forms overgrowths on plagioclase, and is exsolved variably to microperthite; cores of some alkali feldspar phenocrysts are resorbed. Plagioclase phenocrysts (1–3 mm) are zoned from albite rims to andesine cores. The dacite porphyry also contains glomerocrysts of albite-andesine and phenocrysts or microphenocrysts of sanidine, quartz, biotite, hornblende, clinopyroxene, and Fe-Ti oxide minerals, and trace amounts of apatite, zircon, and titanite; phenocryst assemblages are highly variable. Phenocrysts of partly resorbed quartz are present locally, and groundmass quartz is abundant in granophyre.

Trachyte porphyry lava (Ttp) crops out locally at the base of the volcanic section preserved in the moat of the Turkey Creek caldera. The unit consists of red to reddish-brown or orange trachyte lava with intersertal to granophyric groundmass textures. The lava contains large phenocrysts (2 mm to >1 cm) of sanidine that have dusty reaction rims. Phenocrysts also include small crystals composed of Fe-Ti oxide minerals, oxyhornblende, clinopyroxene, and plagioclase. Strained quartz xenocrysts are present in some samples. The trachyte porphyry forms very restricted outcrops in the southeastern part of the Turkey Creek caldera.

A sequence of rhyolite lava flows and minor associated pyroclastic flow deposits, the Fife Canyon Volcanics of Latta (1983), are stratigraphically above dacite and trachyte porphyry lava flows in the moat of the Turkey Creek caldera. These rocks, with a total preserved volume of about 60 km^3, probably were erupted from vents along the buried ring fracture collapse system of the Turkey Creek caldera. The presence of biotite in the basal rhyolite of this sequence is distinctive. The upper three rhyolite lava flows, units 1 through 3, from oldest to youngest, are petrographically indistinguishable, nearly aphyric, high-silica rhyolite lava flows separated by thin pyroclastic flow deposits.

The biotite rhyolite (Tmrb) forms flows and domes on the north flank of the Turkey Creek caldera. The lava is gray to brownish- or yellowish-gray (devitrified) or black (glassy), moderately phenocryst rich (5–20 percent) rhyolite that contains plagioclase, sanidine, quartz, biotite, Fe-Ti oxide minerals, and trace amounts of zircon and monazite. Plagioclase also forms small (<1 mm), oscillatory-zoned (andesine cores) crystals; a xenocrystic origin is suggested by resorption, wormy glass inclusions, and its occurrence in small crystal clots, commonly with biotite. Perlite, locally preserved at the basal contact, is spherulitic in some outcrops. Flow interiors are devitrified and locally granophyric.

Unit 1 lava (Tmr1) consists of light-gray to reddish-gray or brown rock, most of which is flow layered and intricately flow folded—although some exposures are massive. The lava is devitrified, except at its base, where perlitic glass locally contains spherulitic zones and geodes. It is typically aphyric or crystal poor (<5 percent) and contains sanidine, quartz, and Fe-Ti oxide minerals, along with trace amounts of plagioclase, hornblende, and clinopyroxene. Carapace breccia is exposed locally at margins of lava flows. Flow interiors are recrystallized to granophyre and contain vapor-phase quartz and feldspar in amygdules.

Unit 2 lava (Tmr2) is light-gray to reddish-gray, phenocryst-poor rhyolite lava that is flow layered and intricately flow folded, locally massive, and aphyric or sparsely (0–2 percent) porphyritic. It contains phenocrysts (<1 mm) of sanidine, quartz, and Fe-Ti oxide minerals; accessory biotite and zircon are present in some samples. The lava is devitrified, except at its base, where black or green glassy breccia or flow-layered perlite is locally exposed; spherulitic and axiolitic (with respect to flow layers) devitrification and granophyric recrystallization are common.

Unit 3 lava (Tmr3) is light-gray to reddish-gray, typically aphyric, flow-layered and folded rhyolite. It contains trace amounts of sanidine phenocrysts and biotite microphenocrysts. Spherulitic and axiolitic (with respect to flow layers) devitrification and granophyric recrystallization are common features of this unit.

Post-Turkey Creek Caldera Rocks

Pyroclastic deposits and lava flows of Swede Peak (Ts), as defined by Drewes and Brooks (1988), consist of white to tan high-silica rhyolite. The rhyolite is commonly crystal rich (>20 percent); phenocrysts are sanidine, quartz, albite, and oxidized biotite and trace amounts of Fe-Ti oxide minerals, titanite, and zircon. Vitroclastic groundmass in unwelded pyroclastic deposits is composed of variably devitrified ash, glass shards, and crystal and lithic fragments. Abundances of pumice and glass shards are variable within and between individual pyroclastic flows. Abundance of lithic fragments also is widely variable. The great thickness of these areally restricted deposits near Swede Peak and decreasing thicknesses in surrounding areas suggest vent(s) near this feature southeast of the Turkey Creek caldera.

The rhyolite lava of Dobson Peak (Trdp) is light-gray to reddish-gray, flow-layered and intricately flow folded, high-silica rhyolite lava that is crystal poor (1–4 percent); phenocrysts are resorbed quartz, sanidine, and subordinate albite and trace amounts of Fe-Ti oxide minerals and biotite. Its groundmass commonly is devitrified and recrystallized to an aggregate of microscopic spherulites and granophyre. Thickness relations are similar to those of pyroclastic deposits and lava flows of Swede Peak, which, together with compositional and temporal similarities, imply cogenesis and eruption from associated conduits. The rhyolite underlies an area of about 5 km^2 about 15 km southeast of the center of the Turkey Creek caldera.

Geochemistry

Classification

The International Union of Geological Sciences (IUGS) classification of volcanic rocks (Le Bas and others, 1986) was applied to the compositions of volcanic rocks of the central Chiricahua Mountains (table 1); most of the units studied are rhyolite (fig. 3). Because the resurgent intrusion in the Turkey Creek caldera, its associated moat-filling lava flows, and the immediately overlying lava flows contain less than 20 percent normative quartz and greater than 9 percent Na_2O+K_2O and 64–66 percent SiO_2, they are alkaline and can be classified as trachyte using the criteria of Le Bas and others (1986). However, in the case of the resurgent intrusion and its associated lava flows, we have chosen to apply the name dacite, the subalkaline variant of trachyte, because their compositions are transitional between alkaline and subalkaline compositions as defined by Irvine and Baragar (1971) and Le Bas and others (1986), and to emphasize their consanguinity with the other subalkaline products of the Turkey Creek caldera. That this igneous system is not intrinsically alkaline is another reason that we have elected not to use the name trachyte; our choice of dacite is in accord with the absence of alkali-rich minerals, such as aegirine and alkali amphiboles, that are characteristic of alkaline series rocks. Because the trachyte porphyry lava flows (Ttp) that immediately overlie the dacite porphyry flows have compositions (fig. 3) that are alkaline, even by the definition of Irvine and Baragar (1971), we do apply the name trachyte to these rocks. However, all of the rhyolites are subalkaline, as defined by Irvine and Baragar (1971), and all but the upper member of the tuff of Horseshoe Canyon, the rhyolite of Erickson Ridge, the lower member of the rhyolite of Joe Glenn Ranch, and the biotite rhyolite lava of the Turkey Creek caldera moat sequence contain >76 percent SiO_2, and are therefore high-silica rhyolite. Most volcanic rocks in the central Chiricahua Mountains are weakly peraluminous (alumina saturation indices range from 1.03 to 1.11); the exception is the dacite and trachyte porphyries, which are metaluminous (alumina saturation indices 0.91–0.92). The peraluminous tendencies may reflect minor, posteruptive alkali loss relative to alumina rather than primary magmatic characteristics. The lower member of the rhyolite of Joe Glenn Ranch and the rhyolite tuff of High Lonesome Canyon are distinctly more strongly peraluminous (alumina saturation indices 1.23 and 1.16, respectively).

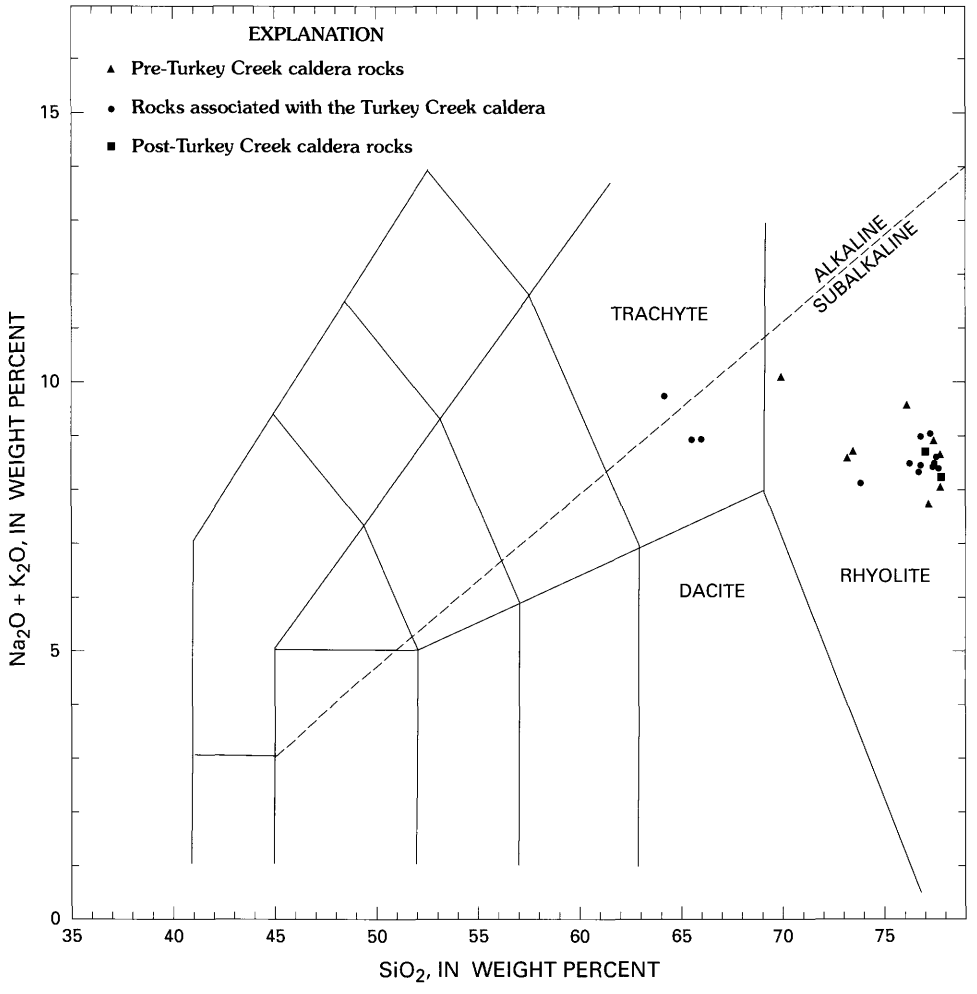

Figure 3. Average (table 1) total alkali-silica variation diagram showing compositions of volcanic rocks in the central Chiricahua Mountains, Ariz. International Union of Geological Sciences classification grid (Le Bas and others, 1986) is also shown.

As is typical for most calc-alkaline rocks, abundances of Al_2O_3, total iron, MgO, CaO, P_2O_5, and TiO_2 decrease with increasing SiO_2 in volcanic rocks of these mountains, whereas abundances of Na_2O, K_2O, and MnO show no clear relationship with SiO_2 (fig. 4). Variation patterns for Na_2O, K_2O, and MnO are poorly developed, largely because most of the volcanic rock units studied are composed of high-silica rhyolite; variation within this narrowly defined SiO_2 compositional range is relatively limited. Exceptions to this generalization relate to the abundances of Na_2O and K_2O. Within the group of high-silica rhyolites, those units with 76–77.6 percent SiO_2, Na_2O abundances vary from about 1.3 to 4.0 weight percent, whereas K_2O abundances vary from about 4.6 to 7.5 weight percent. A significant geochemical trait of volcanic rocks of the area is their elevated K_2O abundances (fig. 4); all of the units are members of either the high-potassium calc-alkaline or the shoshonitic series of Ewart (1982). The K_2O/Na_2O ratio for all of the studied units is >1.0, which indicates that all of these units are potassic as defined by Le Bas and others (1986).

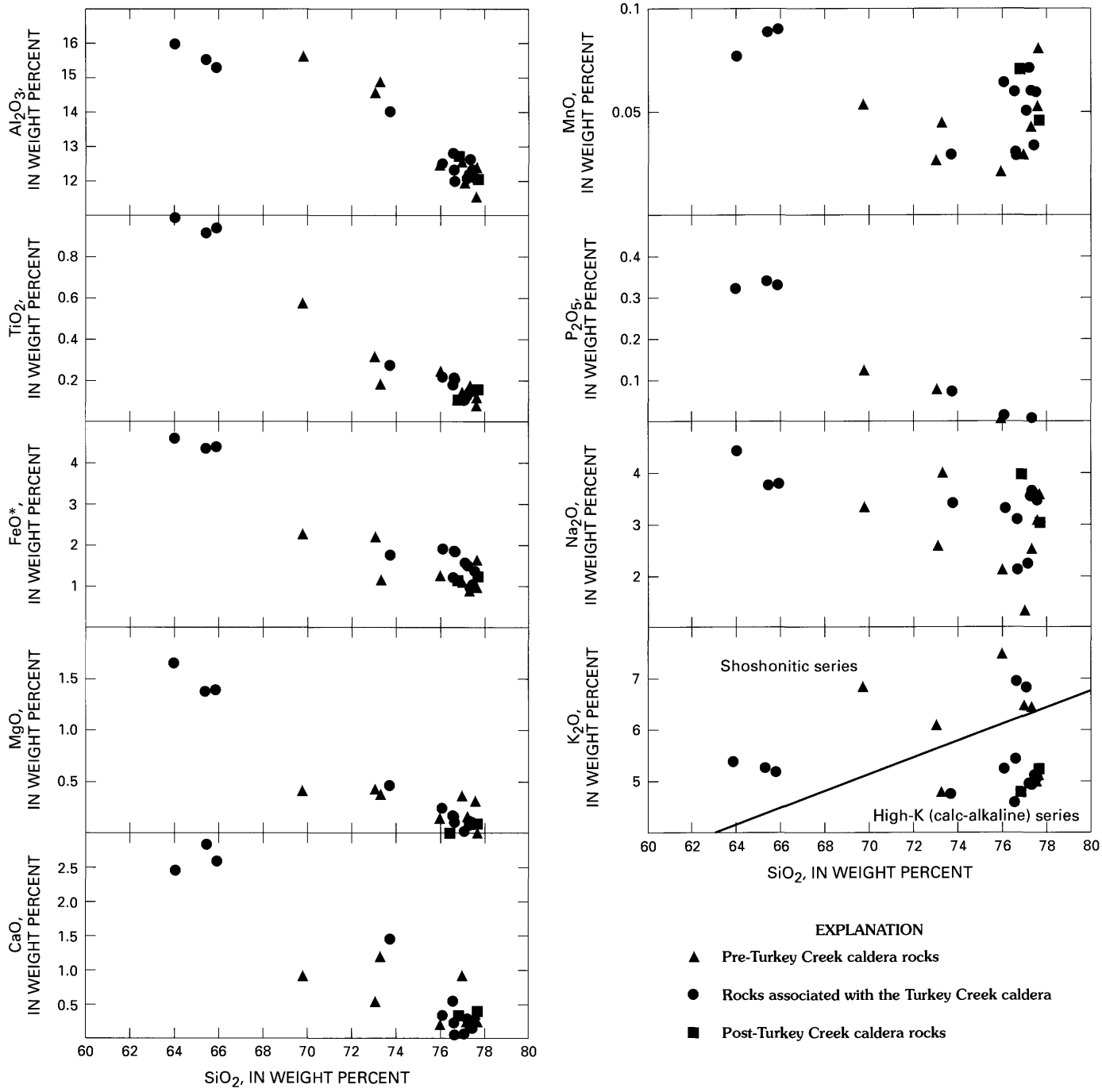

Figure 4. Abundances (table 1) of selected major oxides and trace elements of volcanic rocks in the central Chiricahua Mountains, Ariz.

Within-Unit Geochemical Variation

In order to better define the volcanic units, we used several analytical methods to study the character and extent of within-unit compositional variation, as portrayed by all available geochemical data (du Bray and others, 1992a; 1992b; 1993; du Bray and Pallister, 1994; 1995). We first created a series of extended trace-element diagrams (Thompson and others, 1983) to evaluate within-unit compositional variation; for each volcanic unit a separate diagram (fig. 5) displays

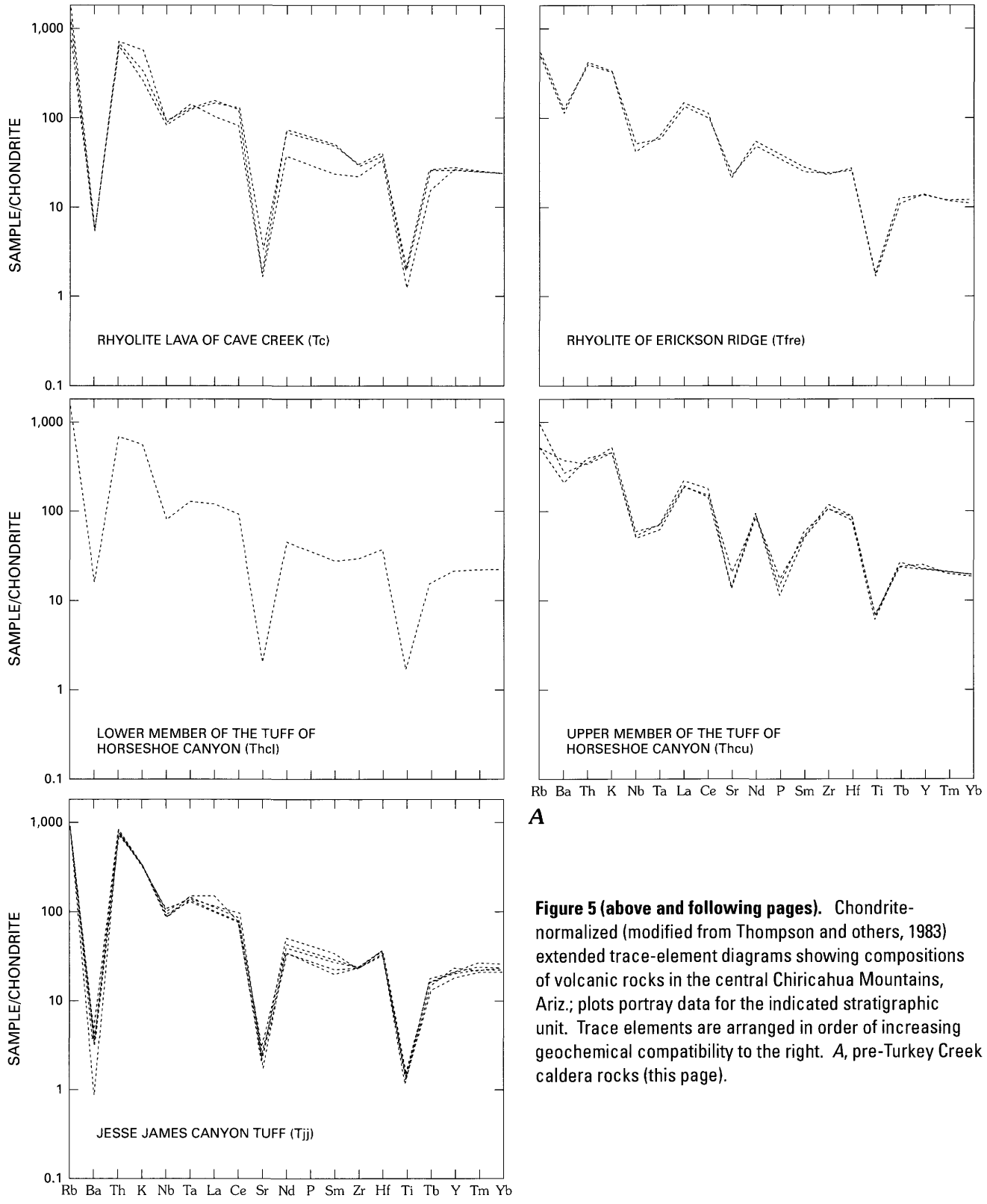

Figure 5 (above and following pages). Chondrite-normalized (modified from Thompson and others, 1983) extended trace-element diagrams showing compositions of volcanic rocks in the central Chiricahua Mountains, Ariz.; plots portray data for the indicated stratigraphic unit. Trace elements are arranged in order of increasing geochemical compatibility to the right. *A*, pre-Turkey Creek caldera rocks (this page).

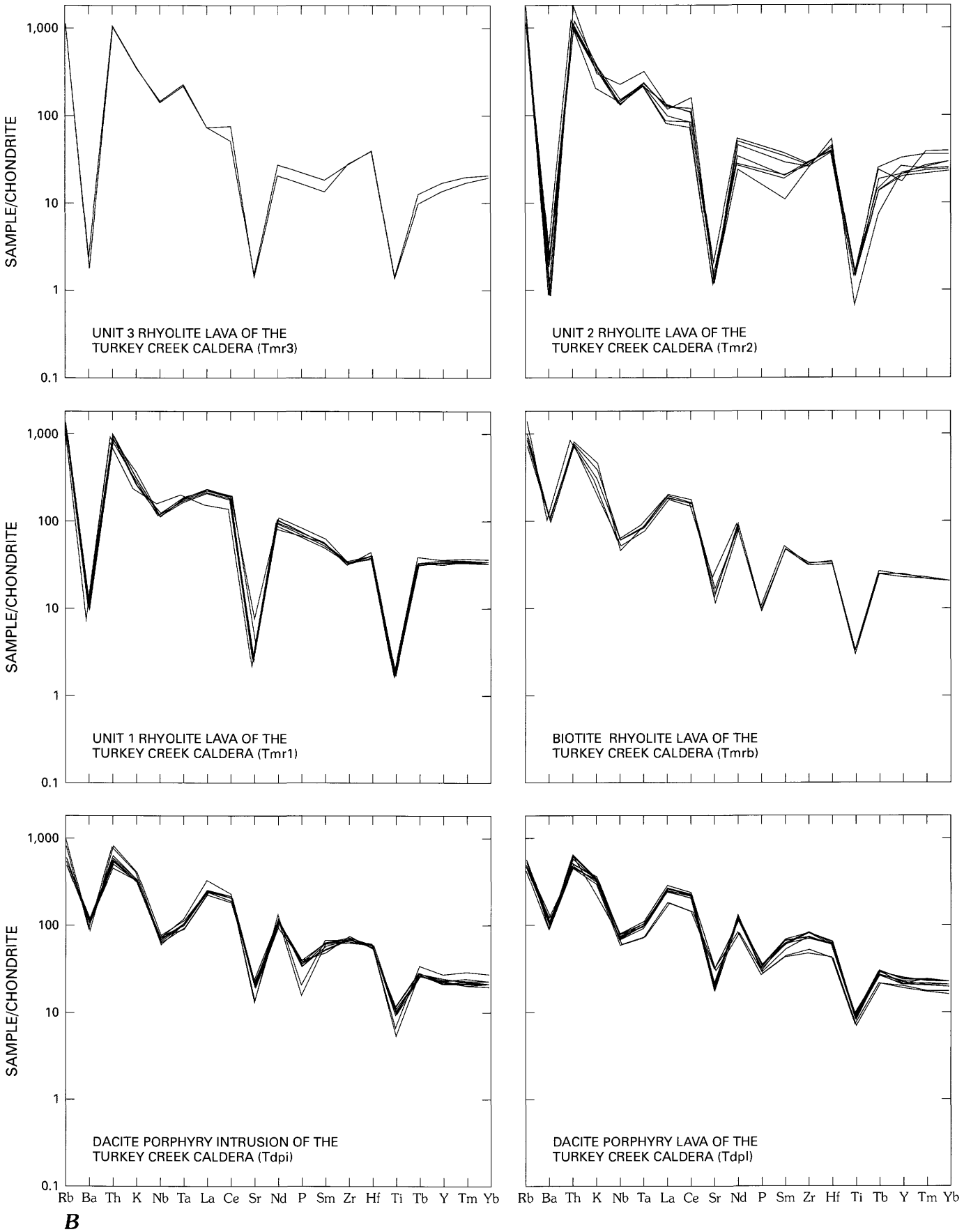
SAMPLE/CHONDRITE
1,000
100
10
1
0.1
UNIT 3 RHYOLITE LAVA OF THE TURKEY CREEK CALDERA (Tmr3)
UNIT 2 RHYOLITE LAVA OF THE TURKEY CREEK CALDERA (Tmr2)
UNIT 1 RHYOLITE LAVA OF THE TURKEY CREEK CALDERA (Tmr1)
BIOTITE RHYOLITE LAVA OF THE TURKEY CREEK CALDERA (Tmrb)
DACITE PORPHYRY INTRUSION OF THE TURKEY CREEK CALDERA (Tdpi)
DACITE PORPHYRY LAVA OF THE TURKEY CREEK CALDERA (Tdpl)
Rb Ba Th K Nb Ta La Ce Sr Nd P Sm Zr Hf Ti Tb Y Tm Yb

B

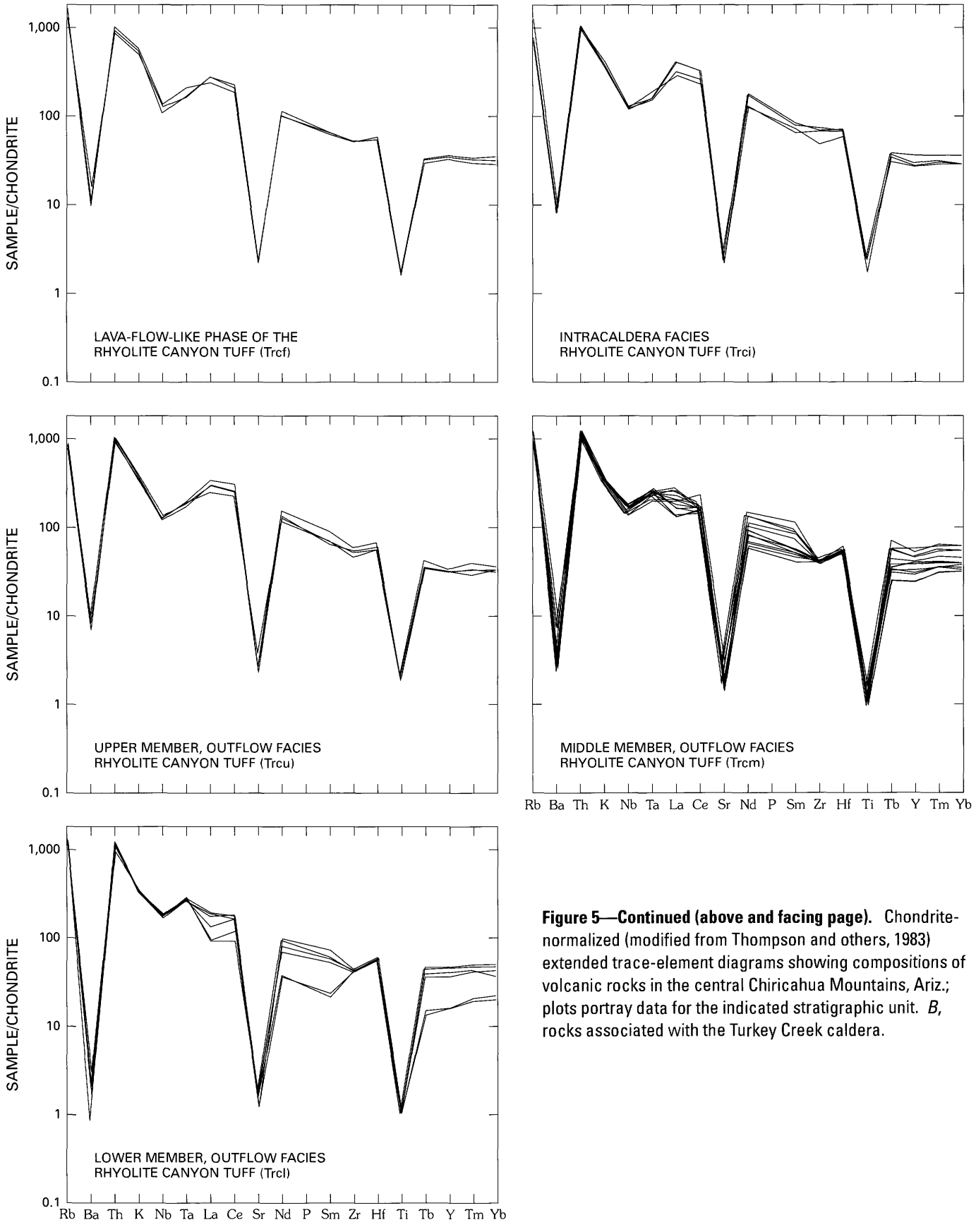

Figure 5—Continued (above and facing page). Chondrite-normalized (modified from Thompson and others, 1983) extended trace-element diagrams showing compositions of volcanic rocks in the central Chiricahua Mountains, Ariz.; plots portray data for the indicated stratigraphic unit. *B*, rocks associated with the Turkey Creek caldera.

trace-element abundances for all samples analyzed by instrumental neutron activation analysis. Additional graphical portrayal of within-unit compositional variation, for a significantly greater number of samples (those for which trace-element abundances were determined by energy-dispersive X-ray fluorescence spectroscopy), appears in figure 6. Finally, the magnitude of calculated standard deviations relative to mean abundances (table 1) for each unit was considered. These data evaluations indicate that individual volcanic rock stratigraphic units of the central Chiricahua Mountains, especially units composed of lava flows, are relatively homogeneous. However, some of the ash-flow tuff units are characterized by considerable within-unit compositional variation. Moderate, systematic compositional variation characteristic of these units is consistent with eruption from normally zoned reservoirs (Hildreth, 1981). These observations suggest that neither flow sorting, elutriation, incorporation of exotic material, nor other factors significantly skewed the whole-rock composition of these samples from magmatic values.

Pre-Turkey Creek Caldera Rocks

Volcanic rocks erupted prior to Turkey Creek caldera formation display variable amounts of within-unit compositional inhomogeneity. The rhyolite tuff of High Lonesome Canyon has considerable variation especially with respect to abundances of SiO_2, K_2O, Ba, Sr, and Rb; given the preferential partitioning of these components into feldspars (Hanson, 1978), these variations probably indicate varying amounts of feldspar fractionation. Similarly, because of preferential partitioning of Sr and Ba into feldspar (Hanson, 1978), the considerable variation of Sr and Ba abundances in samples of the lower member of the rhyolite of Joe Glenn Ranch probably results from variable amounts of feldspar fractionation.

The rhyolite lavas of Cave Creek, Krentz Ranch, and Erickson Ridge, and the Jesse James Canyon Tuff display limited within-unit compositional variation. Of these, the rhyolite lava of Cave Creek displays the most significant variation; moderate variation in Na_2O, K_2O, and Rb abundances may result from non-isochemical devitrification processes. Lipman (1965) showed that post-magmatic effects can significantly modify primary compositions of glassy volcanic rocks; alkali element abundances are most strongly affected. As glassy rocks interact with ground water, they become hydrated and alkali elements are susceptible to leaching. Light REE (rare earth element) abundances in samples of the Jesse James Canyon Tuff are moderately variable, although the tuff is otherwise quite homogeneous.

Samples collected without specific regard for vertical position in both members of the tuff of Horseshoe Canyon indicate considerable compositional inhomogeneity (table 1). Samples of the lower member of the tuff of Horseshoe Canyon contain variable abundances of SiO_2, Na_2O, K_2O, Rb, and Ba, which again may reflect varying amounts of alkali feldspar fractionation. In contrast, samples of the upper member of the tuff of Horseshoe Canyon contain variable abundances of SiO_2, CaO, Na_2O, K_2O, Rb, Sr, Zr, and Ba; these variations probably reflect control by plagioclase, biotite, and zircon, the principal residences of these components (Hanson, 1978). A reconnaissance evaluation of the nature and extent of vertical zonation within these two units was conducted by a systematic sampling of a continuous vertical section through these units along a ridge west of Dripping Spring, on the south side of Sulphur Draw in the Portal Peak 7.5' quadrangle. The thick section of the lower member of the tuff of Horseshoe Canyon along the ridge seems to be intact, complete, and representative of the unit, whereas the upper member of the tuff of Horseshoe Canyon section is relatively thin here and may be incomplete. Geochemical abundances in a suite of samples from the lower member of the tuff of Horseshoe Canyon vary up section as follows: SiO_2 decreases from 75.3 to 74.5 weight percent, Na_2O increases from 1.25 to 2.98 weight percent, K_2O decreases from 8.97 to 7.31 weight percent, Rb decreases from 571 to 362 ppm, Sr increases from 54 to 99 ppm, Zr increases from 262 to 467 ppm, and Ba increases from 210 to 647 ppm. Geochemical abundances in a suite of samples from the upper member of the tuff of Horseshoe Canyon vary up section as follows: SiO_2 decreases from 73.4 to 71.8 weight percent, Na_2O increases from 3.79 to 3.92 weight percent, K_2O decreases from 5.80 to 5.66 weight percent, Rb decreases from 270 to 142 ppm, Sr increases from 73 to 104 ppm, Zr increases from 411 to 609 ppm, and Ba increases from 714 to 1,243 ppm. Geochemical variation depicted by these two suites of samples has the same polarity, is essentially overlapping and continuous, and is consistent with the tuff having originated as a series of eruptions from progressively deeper levels of a single, normally zoned reservoir.

Rocks Associated with the Turkey Creek Caldera

Volcanic units associated with the Turkey Creek caldera display limited inter- and intra-unit compositional inhomogeneity and zonation. Intracaldera facies Rhyolite Canyon Tuff is characterized by moderate compositional variation. Compositional variation within the intracaldera facies probably reflects physical incorporation of relatively large and variable amounts of exotic lithic fragments from the caldera's topographic wall during collapse. The lava-flow-like phase of intracaldera facies tuff is characterized by restricted compositional variation. In the lower and middle members of outflow facies Rhyolite Canyon Tuff, compositional variation, especially of REE abundances, is moderate, whereas that within the basal and upper members is relatively limited. Compositional variation among the four outflow facies members of the Rhyolite Canyon Tuff is continuous and systematic; as a group, the four members exhibit a trend of decreasing geochemical evolution with time. In particular, the upper member is characterized by lower abundances of SiO_2, Rb, Y, Nb, Ta, Th, and U, and higher abundances of total iron, MgO, CaO, TiO_2, Sr, Zr, Ba, and Eu.

Compositional data for a large number of dacite porphyry samples collected from widely distributed sites indicate that

this unit is relatively homogeneous. Trachyte porphyry lava flows in the moat of the Turkey Creek caldera generally display even less within-unit compositional variability, although SiO_2, CaO, Sr, and Ba abundances are highly variable and may reflect varying degrees of feldspar fractionation.

Of the rhyolite lavas in the moat of the Turkey Creek caldera, those in unit 2 lava display the greatest amount of within-unit compositional variation; in particular, REE abundances vary considerably within this unit (table 1). Compositional variation among the caldera's four rhyolite lava units indicates that the upper three units are very distinct relative to the basal biotite-bearing rhyolite lava, are considerably more evolved, and depict a trend toward increasing evolution with time. In particular, the basal lava is a low-silica rhyolite, whereas the upper three are all high-silica rhyolites. In addition, the basal biotite rhyolite is characterized by higher abundances of total iron, MgO, CaO, TiO_2, Sr, and Ba, and lower abundances of Rb, Y, Zr, Nb, Th, and U than the three high-silica rhyolites. The compositions of the two youngest high-silica rhyolites, lavas of units 2 and 3, are indistinguishable. However, these two rhyolites are compositionally distinct relative to the underlying unit 1 lava. The most diagnostic distinction pertains to barium abundances. Lavas of units 2 and 3 contain 10–20 ppm Ba, whereas unit 1 lava contains 60–100 ppm Ba. Other distinctions include higher SiO_2 and lower MgO, CaO, and REE abundances in lavas of units 2 and 3 relative to unit 1 lava.

Post-Turkey Creek Caldera Rocks

Volcanic rocks erupted following Turkey Creek caldera formation display limited within-unit compositional inhomogeneity. The most pronounced compositional variation in samples of the pyroclastic deposits and lava flows of Swede Peak is that of yttrium, whose abundances range from 37 to 90 ppm. Abundances of Ba and Sr are also somewhat variable in this unit, which suggests that these samples may have experienced varying amounts of feldspar fractionation. In samples of the rhyolite lava of Dobson Peak, Y, Nb, and Ba abundances vary considerably. Abundances of Y and Nb are probably controlled by accessory minerals, whereas Ba abundance variations suggest that magma represented by these samples may have experienced differing amounts of biotite and feldspar fractionation.

Geochemistry- and Petrography-Based Stratigraphic Distinctions

As demonstrated by Hildreth and Mahood (1985), various combinations or subsets of field, petrographic, paleomagnetic, or geochronologic data considered along with major-oxide and trace-element abundance data may facilitate stratigraphic identification and correlation. Compositional ranges of major oxides and trace elements in samples of central Chiricahua Mountains volcanic rocks (fig. 6) were used to aid stratigraphic determinations when other data were either insufficient or ambiguous. This approach is especially useful for instances in which sparse exposure or structural dismemberment resulted in limited stratigraphic context. Because macroscopic features are sufficient to distinguish lava flows from tuffs, in most cases, compositional and petrographic comparisons presented herein are made separately for lava flows and tuffs; data for lava flows are compared only to data for other lava flow units, whereas data for tuffs were compared only to data for other tuff units.

Lavas

The aphyric character of the high-silica rhyolite lava of Krentz Ranch distinguishes it from crystal-bearing lavas of the study area. Relative to most other aphyric high-silica rhyolite lavas in the area, the rhyolite lava of Krentz Ranch (abbreviated as KR in fig. 6) is compositionally indistinct, as indicated by limited available geochemical data. Low niobium abundances for the rhyolite lava of Krentz Ranch relative to those of aphyric rhyolite lavas exposed in the moat of the Turkey

Figure 6 (following pages). Stratigraphic versus compositional variation among volcanic rocks in the central Chiricahua Mountains, Ariz. Analytical uncertainty for oxide or element is shown by error bar in bottom right corner of each plot. Units arranged from youngest (top) to oldest (bottom) in each plot. Triangle, pre-Turkey Creek caldera rocks; dot, rocks associated with the Turkey Creek caldera; square, post-Turkey Creek caldera rocks. Unit designations are abbreviated here as follows:
DP, rhyolite lava of Dobson Peak
SW, pyroclastic deposits and lava flows of Swede Peak
R3, unit 3 rhyolite lava of the Turkey Creek caldera
R2, unit 2 rhyolite lava of the Turkey Creek caldera
R1, unit 1 rhyolite lava of the Turkey Creek caldera
RB, biotite rhyolite lava of the Turkey Creek caldera
TP, trachyte porphyry lava
PI, dacite porphyry intrusion of the Turkey Creek caldera
PL, dacite porphyry lava of the Turkey Creek caldera
RF, lava-flow-like phase of the Rhyolite Canyon Tuff
RI, intracaldera facies Rhyolite Canyon Tuff
RU, upper member, outflow facies Rhyolite Canyon Tuff
RM, middle member, outflow facies Rhyolite Canyon Tuff
RL, lower member, outflow facies Rhyolite Canyon Tuff
RO, basal member, outflow facies Rhyolite Canyon Tuff
JJ, Jesse James Canyon Tuff
HU, upper member of the tuff of Horseshoe Canyon
HL, lower member of the tuff of Horseshoe Canyon
RE, rhyolite of Erickson Ridge
CC, rhyolite lava of Cave Creek
KR, rhyolite lava of Krentz Ranch
JG, lower member of the rhyolite of Joe Glenn Ranch
HI, rhyolite tuff of High Lonesone Canyon

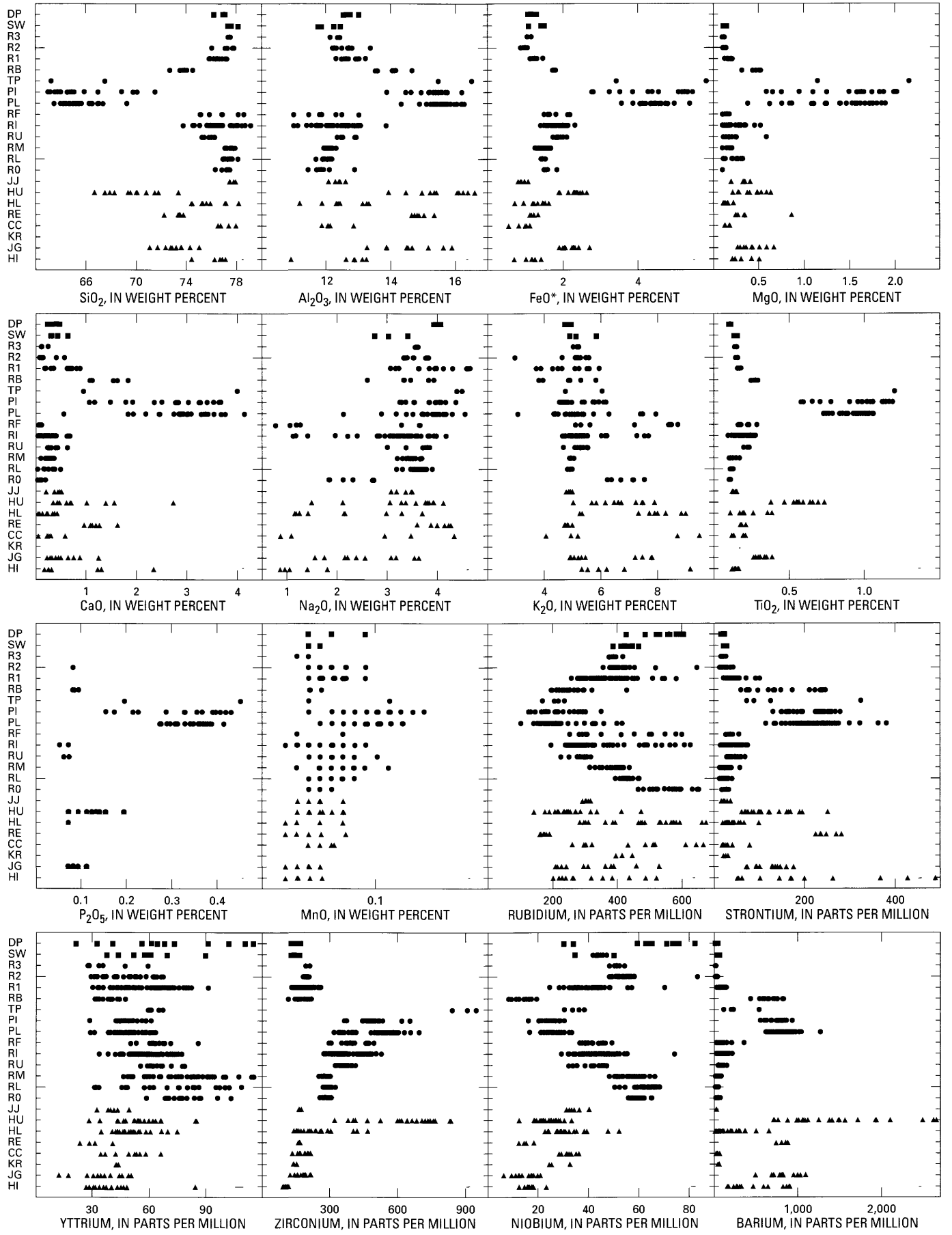
DP
SW
R3
R2
R1
RB
TP
PI
PL
RF
RI
RU
RM
RL
R0
JJ
HU
HL
RE
CC
KR
JG
HI
66 70 74 78
SiO2, IN WEIGHT PERCENT
12 14 16
Al2O3, IN WEIGHT PERCENT
2 4
FeO*, IN WEIGHT PERCENT
0.5 1.0 1.5 2.0
MgO, IN WEIGHT PERCENT
1 2 3 4
CaO, IN WEIGHT PERCENT
1 2 3 4
Na2O, IN WEIGHT PERCENT
4 6 8
K2O, IN WEIGHT PERCENT
0.5 1.0
TiO2, IN WEIGHT PERCENT
0.1 0.2 0.3 0.4
P2O5, IN WEIGHT PERCENT
0.1
MnO, IN WEIGHT PERCENT
200 400 600
RUBIDIUM, IN PARTS PER MILLION
200 400
STRONTIUM, IN PARTS PER MILLION
30 60 90
YTTRIUM, IN PARTS PER MILLION
300 600 900
ZIRCONIUM, IN PARTS PER MILLION
20 40 60 80
NIOBIUM, IN PARTS PER MILLION
1,000 2,000
BARIUM, IN PARTS PER MILLION

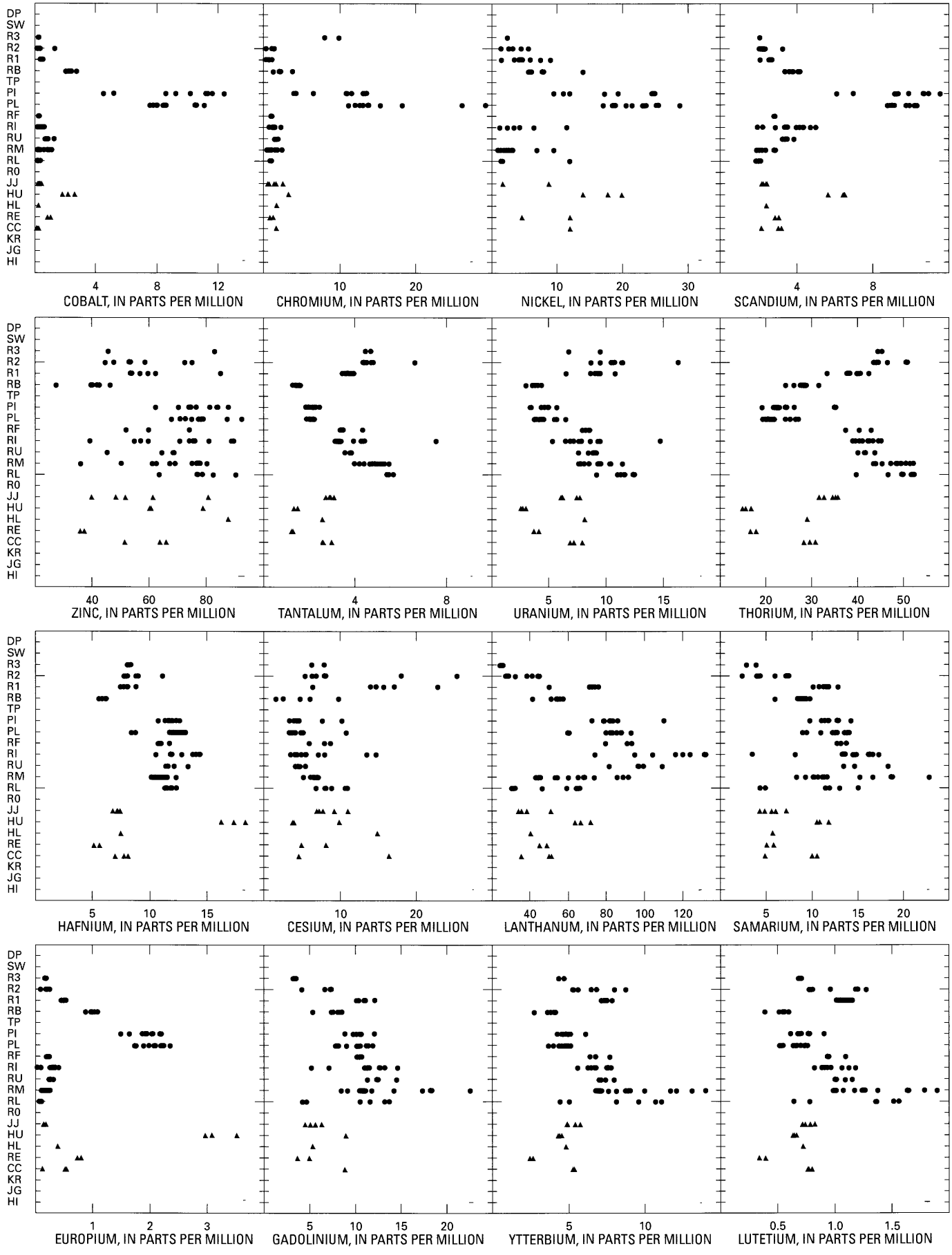
DP
SW
R3
R2
R1
RB
TP
PI
PL
RF
RI
RU
RM
RL
R0
JJ
HU
HL
RE
CC
KR
JG
HI
4 8 12
COBALT, IN PARTS PER MILLION
10 20
CHROMIUM, IN PARTS PER MILLION
10 20 30
NICKEL, IN PARTS PER MILLION
4 8
SCANDIUM, IN PARTS PER MILLION
40 60 80
ZINC, IN PARTS PER MILLION
4 8
TANTALUM, IN PARTS PER MILLION
5 10 15
URANIUM, IN PARTS PER MILLION
20 30 40 50
THORIUM, IN PARTS PER MILLION
5 10 15
HAFNIUM, IN PARTS PER MILLION
10 20
CESIUM, IN PARTS PER MILLION
40 60 80 100 120
LANTHANUM, IN PARTS PER MILLION
5 10 15 20
SAMARIUM, IN PARTS PER MILLION
1 2 3
EUROPIUM, IN PARTS PER MILLION
5 10 15 20
GADOLINIUM, IN PARTS PER MILLION
5 10
YTTERBIUM, IN PARTS PER MILLION
0.5 1.0 1.5
LUTETIUM, IN PARTS PER MILLION

Creek caldera and the rhyolite lava of Dobson Peak (DP in fig. 6) are the most diagnostic geochemical feature of this unit. In contrast, neither petrographic nor compositional data for the rhyolite lava of Krentz Ranch are distinguishable from those of the rhyolite lava of Cave Creek (CC in fig. 6). Given the stratigraphic settings of the rhyolite lava of Krentz Ranch and the rhyolite lava of Cave Creek, exposed beneath the tuff of Horseshoe Canyon, these two map units, which are spatially separated by about 15 km, may be parts of a single stratigraphic and magmatic unit. The rhyolite lava of Krentz Ranch may represent a distal part of the rhyolite dome field that also includes the rhyolite lava of Cave Creek.

By extension of the preceding observations, the aphyric character of the high-silica rhyolite lava of Cave Creek distinguishes it from porphyritic lavas of the study area; however, the petrographic characteristics and composition of this rhyolite are essentially indistinguishable from those of other aphyric, high-silica rhyolite lavas exposed in the area. The sole exception to this generalization may be the low niobium content of the rhyolite lava of Cave Creek relative to that of the other aphyric rhyolite lavas. As described in the preceding paragraph, this characteristic is common to the rhyolite lava of Cave Creek and the rhyolite lava of Krentz Ranch and hints at a possible common source. Lacking stratigraphic context, with the exception of diagnostic niobium abundances, distinguishing the rhyolite lava of Cave Creek from the other aphyric high-silica lavas is difficult.

Relative to the high-silica rhyolite lavas in the area, the composition and petrography of the rhyolite of Erickson Ridge (RE in fig. 6) are quite distinctive. The phenocryst content of the rhyolite of Erickson Ridge is distinctly greater than that of any other rhyolite exposed in the central Chiricahua Mountains, and the presence of 1–2 percent biotite is diagnostic. In contrast to most other rhyolite lavas in the area, the rhyolite of Erickson Ridge has low silica abundances that are similar to those of the biotite rhyolite of the Turkey Creek caldera. The rhyolite of Erickson Ridge is further distinguished by higher FeO*, CaO, Sr, Ba, and Eu abundances and lower Rb, Ta, Th, and U abundances. The rhyolite of Erickson Ridge is most easily distinguished from the biotite rhyolite lava of the Turkey Creek caldera (RB in fig. 6) by a Rb/Sr ratio less than 1, higher Ba abundances, and lower Th abundances.

Dacite porphyry of the Turkey Creek caldera has petrographic and compositional features that distinguish it from all other volcanic rocks in the study area. Dacite that forms lava flows (PL in fig. 6) and the resurgent intrusion (PI in fig. 6) in the caldera is greenish gray to tan and contains distinctive alkali feldspar megacrysts. The most distinctive geochemical characteristics of the dacite porphyry include FeO*, MgO, CaO, TiO_2, P_2O_5, Ba, Co, Cr, Ni, Sc, and Eu abundances that are elevated relative to abundances in the majority of the central Chiricahua Mountains volcanic rocks, which are considerably more evolved and contain significantly lower abundances of these components.

Trachyte porphyry (TP in fig. 6) forms an areally restricted set of outcrops characterized by distinctive sanidine phenocrysts. The trachyte porphyry is distinguished from the dacite porphyry by its distinctive reddish-brown color and finer grained groundmass. The composition of the trachyte porphyry is similar to that of the dacite porphyry and so is similarly chemically distinct relative to all other volcanic rocks of the central Chiricahua Mountains. Elevated abundances of Na_2O, Y, Zr, and Nb and lower abundances of Sr and Ba in the trachyte porphyry distinguish the trachyte porphyry from the dacite porphyry.

Of the four rhyolite lavas present in the moat of the Turkey Creek caldera, only the oldest of these, the biotite rhyolite lava (RB in fig. 6), is petrographically distinct. The biotite rhyolite contains phenocrysts of biotite, feldspar, and quartz that distinguish it from all other central Chiricahua Mountains rhyolite lavas, except the rhyolite of Erickson Ridge. The other three moat rhyolite lavas are virtually aphyric and macroscopically indistinguishable from one another and similarly cannot be distinguished petrographically from the aphyric rhyolite lavas of Krentz Ranch, Cave Creek, and Dobson Peak. The composition of the biotite rhyolite in the moat of the Turkey Creek caldera is distinguished from that of other rhyolites, except the rhyolite of Erickson Ridge, by lower SiO_2, Rb, Nb, Ta, U, Th, Hf, and heavy REE abundances and by higher FeO*, MgO, CaO, TiO_2, Sr, Ba, Co, Sc, and Eu abundances. The biotite rhyolite in the moat of the Turkey Creek caldera is distinguished from rhyolite of Erickson Ridge by a Rb/Sr ratio greater than 1, lower Ba abundances, and higher Th abundances. Compositions of the three aphyric moat rhyolites are almost indistinguishable from those of other aphyric rhyolites in the central Chiricahua Mountains, except that the moat lavas have higher Nb abundances than the rhyolite lavas of Cave Creek and Krentz Ranch, and lower Rb and Nb abundances than the rhyolite of Dobson Peak. Compositions of the youngest two rhyolite lavas (R2 and R3 in fig. 6) in the moat of the Turkey Creek caldera (lavas of units 2 and 3) are indistinguishable. They can only be differentiated in a stratigraphic context relative to the thin tuff that separates them. The composition of unit 1 lava (R1 in fig. 6) is distinct from that of units 2 and 3 lavas; unit 1 lava is distinguished by lower SiO_2, Nb, Ta, and Th abundances and higher CaO, Ba, light REE, and Eu abundances.

The rhyolite of Dobson Peak (DP in fig. 6) is an aphyric rhyolite that is macroscopically indistinguishable from other aphyric rhyolites in the map area. Its aphyric character distinguishes the rhyolite lava of Dobson Peak from rhyolite of Erickson Ridge and biotite rhyolite lava in the moat of the Turkey Creek caldera. Elevated Rb and Nb abundances distinguish the rhyolite lava of Dobson Peak from all other rhyolites of the area.

Ash-Flow Tuffs and Other Pyroclastic Flow Deposits

The low phenocryst content and presence of trace amounts of oxidized biotite distinguish the rhyolite tuff of High Lonesome Canyon (HI in fig. 6), the oldest of the

regionally exposed ash-flow tuffs, from most other tuffs of the central Chiricahua Mountains. In addition, the rhyolite tuff of High Lonesome Canyon is characterized by unusually low zirconium and Na_2O abundances relative to other high-silica rhyolite ash-flow tuffs of the study area. Although the composition of the rhyolite tuff of High Lonesome Canyon is otherwise nondistinct, these features are probably sufficient to be diagnostic.

Several features of the lower member of the rhyolite of Joe Glenn Ranch (JG in fig. 6) help to distinguish this tuff from others exposed in the central Chiricahua Mountains. It is characterized by a relatively high crystal content (from 20 to 40 percent) and distinctive, 1–3 mm wide, pseudohexagonal biotite crystals. The lower member of the rhyolite of Joe Glenn Ranch also is characterized by higher FeO*, TiO_2, and Ba abundances, and lower Nb abundances than other central Chiricahua Mountains tuffs.

The relatively crystal rich lower member of the tuff of Horseshoe Canyon (HL in fig. 6) contains diagnostic biotite phenocrysts in addition to quartz and sanidine. Geochemical characteristics diagnostic of the lower member of the tuff of Horseshoe Canyon include elevated K_2O, Ba, and Eu abundances and low Zr, Nb, and Th abundances, relative to other central Chiricahua Mountains high-silica rhyolite tuffs. In contrast, the relatively crystal poor upper member of the tuff of Horseshoe Canyon (HU in fig. 6) also is characterized by biotite phenocrysts as well as by relatively elevated Al_2O_3, FeO*, TiO_2, P_2O_5, Sr, Zr, Ba, Co, Ni, Cr, Sc, Hf, and Eu abundances, and low SiO_2, Nb, Ta, U, and Th abundances; another characteristic of the upper member of the tuff of Horseshoe Canyon is its dramatic within-unit compositional variation. As such, the upper member of the tuff of Horseshoe Canyon is probably the most geochemically distinct ash-flow tuff exposed in the study area. Its most distinguishing features relative to the lower member of the tuff of Horseshoe Canyon are its higher Al_2O_3, FeO*, TiO_2, Ba, and Eu abundances, and lower SiO_2, U, and Th abundances.

The Jesse James Canyon Tuff (JJ in fig. 6) is macroscopically almost indistinguishable from the Rhyolite Canyon Tuff. Its only diagnostic petrographic characteristic is the presence of trace amounts of biotite. The composition of the Jesse James Canyon Tuff is distinguished from those of other ash-flow tuffs of the central Chiricahua Mountains, including the Rhyolite Canyon Tuff, by its slightly lower FeO*, Zr, Ta, Th, and Hf abundances, none of which distinguish it from the lower member of the tuff of Horseshoe Canyon. Slightly lower K_2O, Rb, Ba, and Eu abundances of the Jesse James Canyon Tuff may distinguish it from the lower member of the tuff of Horseshoe Canyon.

The Rhyolite Canyon Tuff, the youngest regionally extensive ash-flow tuff in the central Chiricahua Mountains, is a high-silica rhyolite tuff that has been subdivided into six geologic map units. All these units contain diagnostic quartz and sanidine phenocrysts and, in contrast to most of the other ash-flow tuffs present in the study area, only rarely contain macroscopically identifiable mafic silicate minerals. The four outflow facies members are macroscopically indistinguishable. The intracaldera facies member is distinguished from the outflow facies members by its reddish-brown color and considerably greater lithic fragment content. The lava-flow-like phase is similar in appearance to intracaldera facies tuff, but it includes unbroken 0.5–1 cm sanidine phenocrysts, lacks eutaxitic structure, and contains very few lithic fragments. The basal (R0 in fig. 6), lower (RL in fig. 6), and middle (RM in fig. 6) members of the Rhyolite Canyon Tuff form a geochemically distinct subset of the Rhyolite Canyon Tuff, whereas the upper (RU in fig. 6), intracaldera (RI in fig. 6), and lava-flow-like phase (RF in fig. 6) form another. Elevated Zr and Nb abundances distinguish all parts of the Rhyolite Canyon Tuff from almost all other tuffs in the area. Zirconium abundances of 280–400 ppm in the Rhyolite Canyon Tuff are unusually elevated for subalkaline rhyolites and are distinctive relative to abundances of similar volcanic rocks exposed in the western United States. Although Zr abundances for the Rhyolite Canyon Tuff slightly overlap those of both members of the tuff of Horseshoe Canyon, Nb abundances of the former distinguish it from the latter two units. Similarly, elevated abundances of Ta, U, Th, Hf, and the heavy REE distinguish the Rhyolite Canyon Tuff from other study area tuffs. As a group, the basal, lower, and middle members of the Rhyolite Canyon Tuff are distinguished by higher SiO_2, Rb, Nb, and Ta abundances and lower TiO_2, Zr, Ba, and La abundances relative to the upper member, intracaldera facies, and lava-flow-like phase of the Rhyolite Canyon Tuff. The lower and middle members of the Rhyolite Canyon Tuff are essentially indistinguishable (a distinctive parting, and in some places a distinctive white ash deposit at the top of the lower member of the outflow facies tuff can be used to mark the boundary between these units), whereas the basal member of the Rhyolite Canyon Tuff is distinguished by higher K_2O and Rb abundances. The upper member of the Rhyolite Canyon Tuff and the intracaldera facies are indistinguishable, but the lava-flow-like phase is distinguished by its higher K_2O and Rb abundances.

The pyroclastic deposits and lava flows of Swede Peak (SW in fig. 6) are present in a relatively limited area in the southeast part of the central Chiricahua Mountains. Distinctive *macroscopic* characteristics of this unit include the fact that thick sections are composed of numerous separate pyroclastic flow deposits that (1) are essentially unwelded, (2) contain variable and frequently abundant lithic fragments, (3) are crystal rich (including phenocrysts of quartz, sanidine, albite, and biotite), and (4) are interbedded with volcanic sandstone, as well as cogenetic high-silica rhyolite lava flows. Fortunately, these features are diagnostic; *compositional* characteristics of the pyroclastic deposits and lava flows of Swede Peak are not diagnostic.

Petrogenetic Implications

Pearce and others (1984) recognized that granitoid rocks generated in various tectonic settings have distinctive

geochemical signatures. Trace-element abundance variations in coeval volcanic and plutonic rocks generated in a given terrane should be similar. Consequently, compositions of volcanic rocks from the central Chiricahua Mountains can be compared to the trace-element–tectonic setting diagrams developed by Pearce and others (1984). Trace-element data for most of these rock units plot in the within-plate field, near its boundary with the volcanic arc field (fig. 7). These trace-element characteristics indicate that genesis of magmas represented by this region's volcanic rocks involved a significant crustal component and processes different than those that result in trace-element characteristics diagnostic of subduction-related processes. Compositions plotting in or near the volcanic arc field may indicate that the associated magmas had somewhat distinct sources and (or) evolved by different genetic processes.

Gill (1981) determined that Ba/Nb, Ba/Ta, and La/Nb ratios of modern arc rocks are >26, >450, and 2–7 respectively, whereas Pearce and others (1984) indicated that values of these ratios are generally <<(much less than) 26, <<450, and <3, respectively, for within-plate granites. For example, Ba/Nb and La/Nb ratios for subduction-related Tertiary volcanic rocks of the Bolivian Altiplano are about 30 and 3, respectively (du Bray and others, 1995), whereas Ba/Nb, Ba/Ta, and La/Nb ratios for Late Proterozoic within-plate granites of the Arabian Shield are about 2, 5, and, 1 respectively (du Bray and others, 1988). Most, but not all, of central Chiricahua Mountains volcanic rock units (table 1) have values of Ba/Nb, Ba/Ta, and La/Nb that are <3, <50, and <2, respectively; these values are more like those of within-plate rocks than subduction-related arc rocks. However, the biotite rhyolite lava in the moat of the Turkey Creek caldera, dacite porphyry, upper member of the tuff of Horseshoe Canyon, rhyolite of Erickson Ridge, lower member of the rhyolite of Joe Glenn Ranch, and rhyolite tuff of High Lonesome Canyon consistently yield arc-like values for these ratios.

Average chondrite-normalized extended trace-element patterns (fig. 8) for volcanic units of the study area are gently negatively sloping, and have superposed, well-developed negative Ba, Sr, P, and Ti anomalies; these patterns also include weakly developed, negative Nb-Ta anomalies. A striking feature of trace-element patterns for volcanic rocks of the area is their parallelism and relatively limited compositional range. The greatest amounts of compositional variation are among phosphorus, titanium, barium, and strontium, which probably reflect simple fractionation of varying amounts of apatite (P), iron-titanium oxide minerals (Ti), and plagioclase (Ba and Sr). The shape, slope, and abundance levels of chondrite-normalized extended trace-element patterns for volcanic rocks of the area are somewhat distinct from those characteristic of

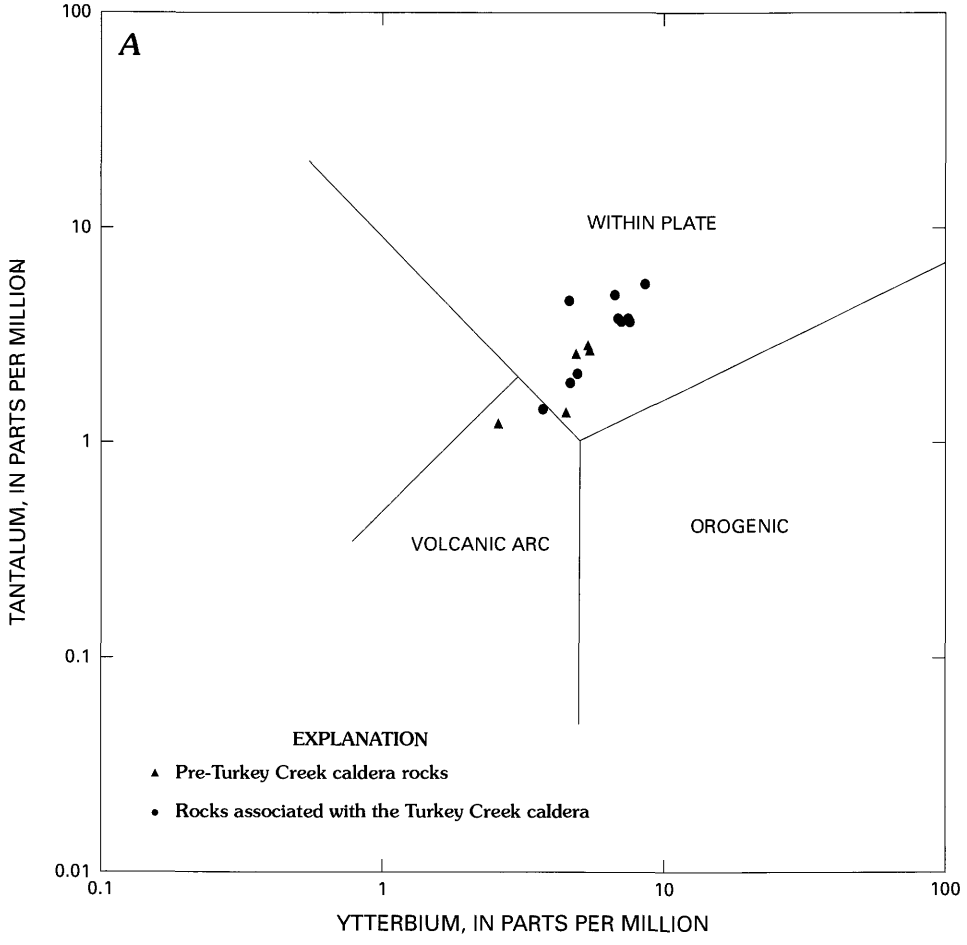

Figure 7 (alongside and facing page). Trace-element–tectonic setting discrimination variation diagrams showing average compositions of volcanic rocks of the central Chiricahua Mountains, Ariz. Tectonic setting–composition boundaries from Pearce and others (1984); compositions from table 1. *A*, tantalum versus ytterbium. *B*, niobium versus yttrium.

subduction-related arc volcanic rocks. In particular, for the rocks under study, the magnitudes of negative Ba, Sr, P, and Ti anomalies are greater, negative Nb-Ta anomalies are smaller, and, as indicated by heavy REE abundances that are greater than those of subduction-related arc rocks (fig. 8), the patterns are less steeply sloping. Negative Nb-Ta anomalies are considered (Wood and others, 1979; Gill, 1981; Pearce and others, 1984) a hallmark of subduction-related, arc volcanic rocks. The weakly developed nature of Nb-Ta anomalies in the central Chiricahua Mountains rocks (fig. 8) further emphasizes the transition from subduction-related magmatism, characteristic of the oldest volcanic rocks in the area, to within-plate magmatism epitomized by younger volcanic rocks in this area. A measure of the magnitude of the negative Nb-Ta anomaly derives from the chondrite-normalized K/Nb ratio, $(K/Nb)_{CN}$. The average value of $(K/Nb)_{CN}$ for 18 middle Tertiary, demonstrably subduction-related ash-flow tuffs of southeastern Nevada is 8.0±1.4 (du Bray, 1995), whereas values of this ratio are <4 for most of the volcanic rocks of the study area. Rocks with $(K/Nb)_{CN}$ values >4 are the biotite rhyolite lava in the moat of the Turkey Creek caldera (7.8), dacite porphyry (4.5), both members of the tuff of Horseshoe Canyon (7.1 and 5.6), rhyolite of Erickson Ridge (7.9) and rhyolite lava of Cave Creek (4.9), the lower member of the rhyolite of Joe Glenn Ranch (10.1), and the rhyolite tuff of High Lonesome Canyon (9.3); this ratio increases among progressively older rocks. All these compositional features suggest that volcanic rocks of the study area are principally of the within-plate type, but record the transition from an older subduction-related setting to a younger, within-plate setting. Furthermore, compositions of most volcanic rocks in the area are remarkably similar to the average obsidian composition for igneous systems situated in continental interior settings (Macdonald and others, 1992).

Zirconium abundances for most of the study area volcanic rocks are commensurate with the experimentally determined zirconium saturation threshold of 100–200 ppm for subalkaline compositions at typical magmatic temperatures (Watson and Harrison, 1983). Thus, magmas represented by these rocks did not equilibrate with peralkaline liquids, nor did they equilibrate at a temperature greater than about 860°C. Zirconium abundances in rocks derived from the Turkey Creek caldera and both members of the tuff of Horseshoe Canyon are variably elevated and imply final pre-eruption equilibration at greater than about 860°C and (or) an association with magma having an alkaline affinity (Watson and Harrison, 1983). Of these units with elevated zirconium abundances, rhyolite lava flows in the moat of the Turkey Creek caldera have the lowest zirconium abundances (175–220 ppm) and appear to have been least affected by the processes that caused pronounced zirconium enrichments in the other caldera-related

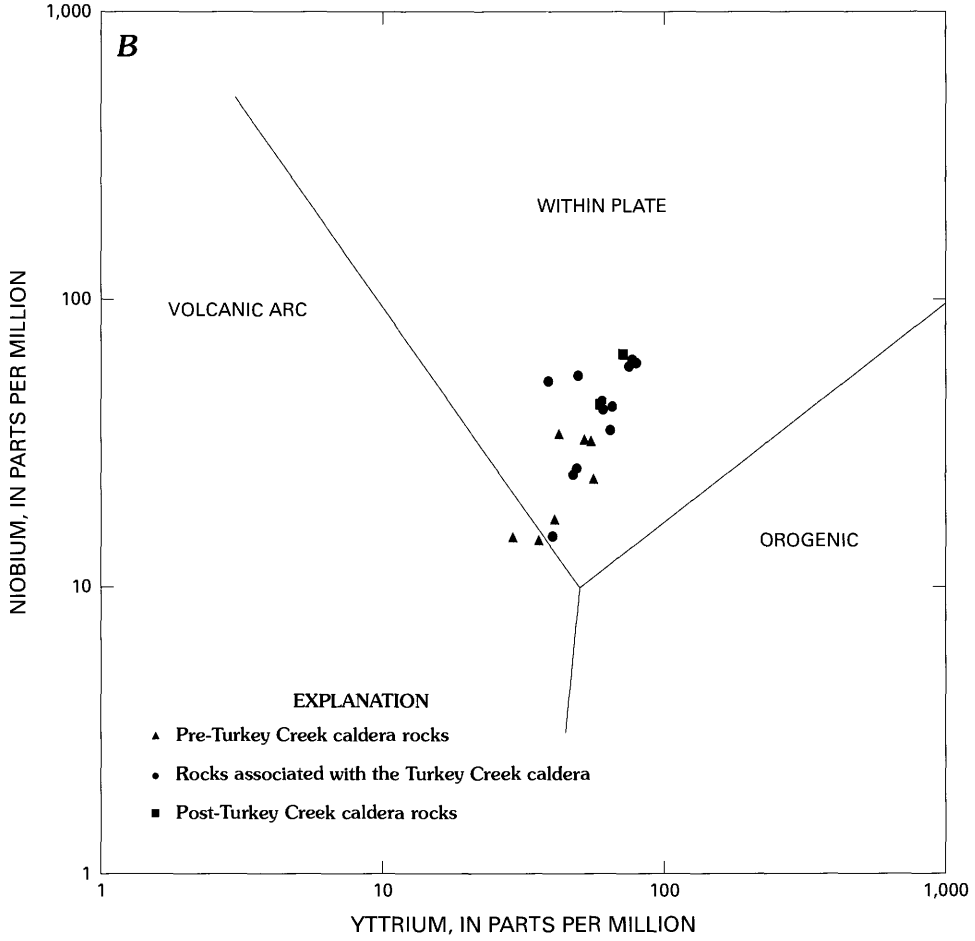

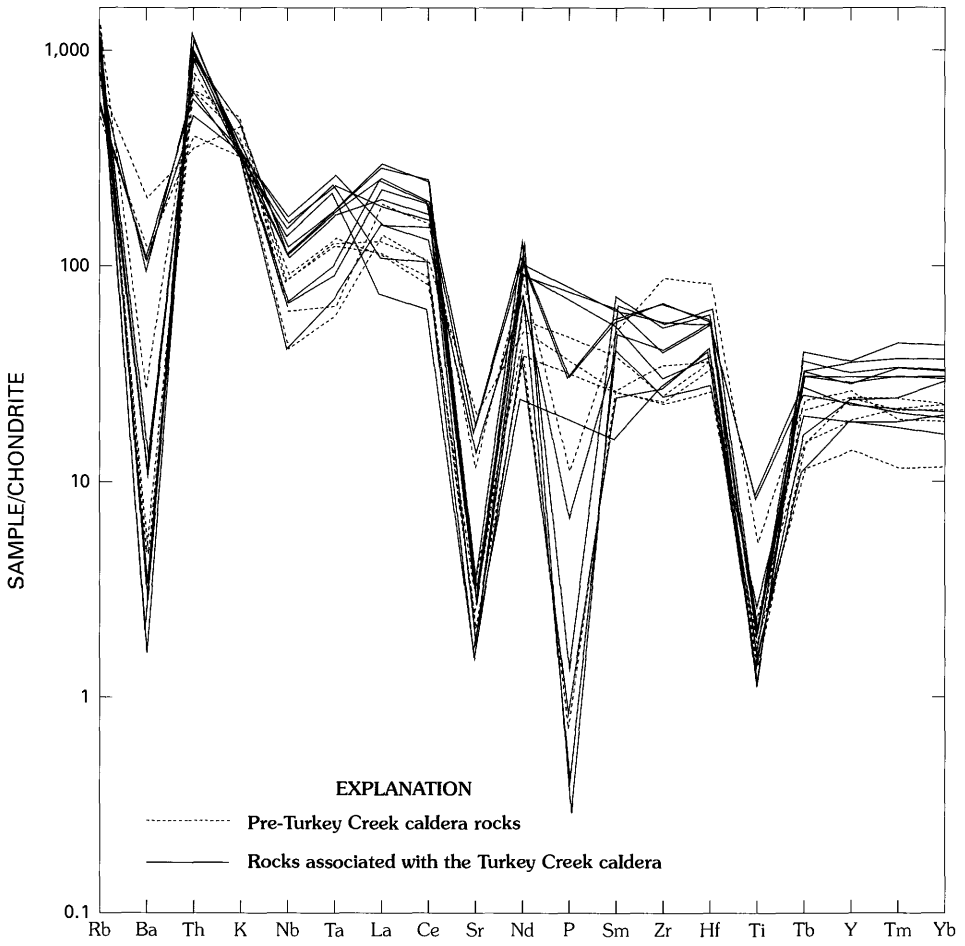

Figure 8. Chondrite-normalized extended trace-element diagram showing average compositions of volcanic rocks in the central Chiricahua Mountains, Ariz. Trace elements are arranged in order of increasing geochemical compatibility to the right. Modified from Thompson and others (1983).

rocks. The remaining rock units that have unusually high zirconium abundances are also characterized by elevated Na_2O and especially K_2O abundances and were previously identified (fig. 4) as members of the shoshonite series defined by Ewart (1982). These elevated zirconium abundances may be related to elevated alkali abundances in magmas represented by the associated volcanic units, because elevated alkali abundances stabilize zircono-alkali silicate complexes (Watson and Harrison, 1983), which inhibit zircon nucleation, fractionation, and zirconium concentrations from reaching maximum thresholds in silicate liquids.

Feldspar-melt distribution coefficients for strontium, potassium, and rubidium (Hanson, 1978) are such that feldspar fractionation preferentially removes strontium and then potassium from the melt phase, relative to rubidium, causing residual liquids to become progressively enriched in rubidium relative to potassium and strontium. In volcanic rocks of the central Chiricahua Mountains, rubidium abundances increase systematically relative to those of strontium and potassium (fig. 9). Rubidium enrichment in most of these units is significantly better developed than in subduction-related volcanic arc rocks, including, for example, ash-flow tuffs of southeastern Nevada (du Bray, 1995), and is strikingly similar to that characteristic of highly evolved, within-plate granites of the Arabian Shield (du Bray and others, 1988). Rb/Sr ratios range from a low of 0.69 in the rhyolite of Erickson Ridge to a highly evolved value of 32 in the rhyolite lava of Dobson Peak; the average Rb/Sr ratio for the 23 volcanic units is 11. These ratios contrast dramatically with those for subduction-related dacite to rhyolite ash-flow tuffs of southeastern Nevada, whose average Rb/Sr ratio is 0.68 (du Bray, 1995).

Average chondrite-normalized REE patterns for volcanic rock units of the study area (fig. 10*A*) mimic relations portrayed by chondrite-normalized extended trace-element patterns, in that the REE patterns are remarkably parallel and define a relatively narrow compositional range. The light REE parts of the patterns are moderately negatively sloping, whereas the heavy REE parts are essentially flat; the patterns include small to moderately well developed negative europium anomalies that probably indicate modest to considerable amounts of feldspar fractionation (Hanson, 1978). Chondrite-normalized La/Lu ratios range from 3.73 to 13.2 and average 8.1±3.3; units with geochemical characteristics most like those of subduction-related arc volcanic rocks have the steepest patterns. Total REE contents range from 110 to 444 (average 276±103) ppm.

Petrogenetic Evolution of the Turkey Creek Caldera Magmatic System

Hildreth (1979, fig. 13) documented systematic compositional variation within the Quaternary Bishop Tuff (associated with the Long Valley caldera of east-central California), one of the first ash-flow tuffs for which systematic compositional variation was well characterized. In particular, cooler, earlier erupted parts of Bishop Tuff, extracted from the top of the magma reservoir, have lower light REE abundances and higher heavy REE abundances than hotter, later erupted material extracted from deeper within the reservoir. In addition, each sequentially erupted fraction of Bishop Tuff magma is characterized by a progressively smaller negative europium anomaly. These abundance variations for sequential eruptions from a zoned reservoir yield a clockwise rotation of chondrite normalized REE patterns and smaller negative europium anomalies. Hildreth (1981) also demonstrated that a broad suite of additional incompatible trace elements is more abundant in earlier erupted parts of the Bishop Tuff, whereas compatible trace-element abundances are greatest in its latest erupted parts. This same type of compositional variation is preserved among outflow facies members of the Rhyolite Canyon Tuff.

Sanidine, clinopyroxene, and zircon are the principal phenocrysts in the Rhyolite Canyon Tuff and thus are most likely to have controlled trace-element abundance variations in the evolving liquid represented by the tuff. Mineral-melt distribution coefficients (K_D's) for these minerals in rhyolitic melts are as follows (Hanson, 1978, 1980):

Sanidine: light REE K_D's (0.02–0.04) are greater than heavy REE K_D's (0.006); except Eu (1–2). Values for K_D's of Sr, Ba, and Rb are about 4, 6, and 0.7, respectively. Sanidine fractionation causes counterclockwise REE pattern rotation (light REE depletion), results in negative europium anomaly development, increases overall REE and Rb abundances, and decreases Sr and Ba abundances in the residual liquid.

Clinopyroxene: heavy REE K_D's (1–2) are slightly greater than light REE K_D's (0.5–1). Values for K_D's of Sr, Ba, and Rb are less than 1. Clinopyroxene fractionation causes slight clockwise REE pattern rotation (heavy REE depletion), results in overall REE depletion, and increases Sr, Ba, and Rb abundances in the residual liquid.

Zircon: heavy REE K_D's (as high as 300) are significantly greater than light REE K_D's (about 1). Values for K_D's of Sr, Ba, and Rb are less than 1. Zircon fractionation causes dramatic clockwise REE pattern rotation (heavy REE

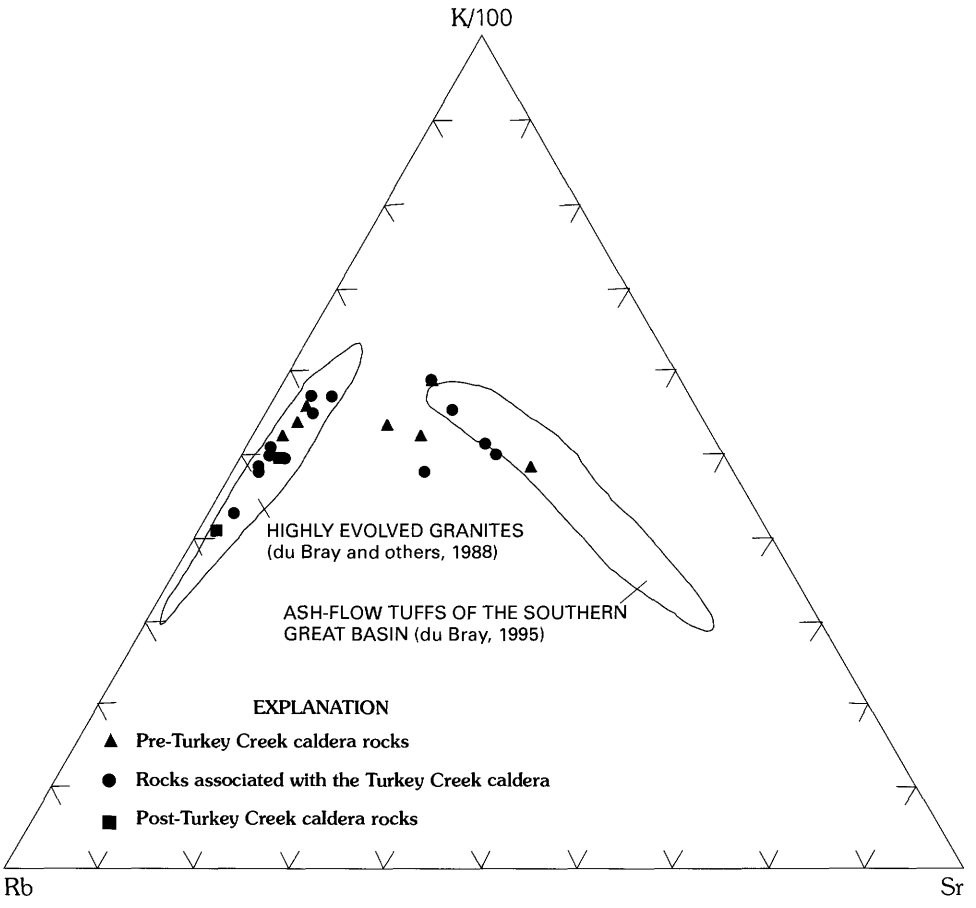

Figure 9. Ternary variation diagram showing average relative proportions of rubidium, potassium, and strontium in volcanic rocks of the central Chiricahua Mountains, Ariz.

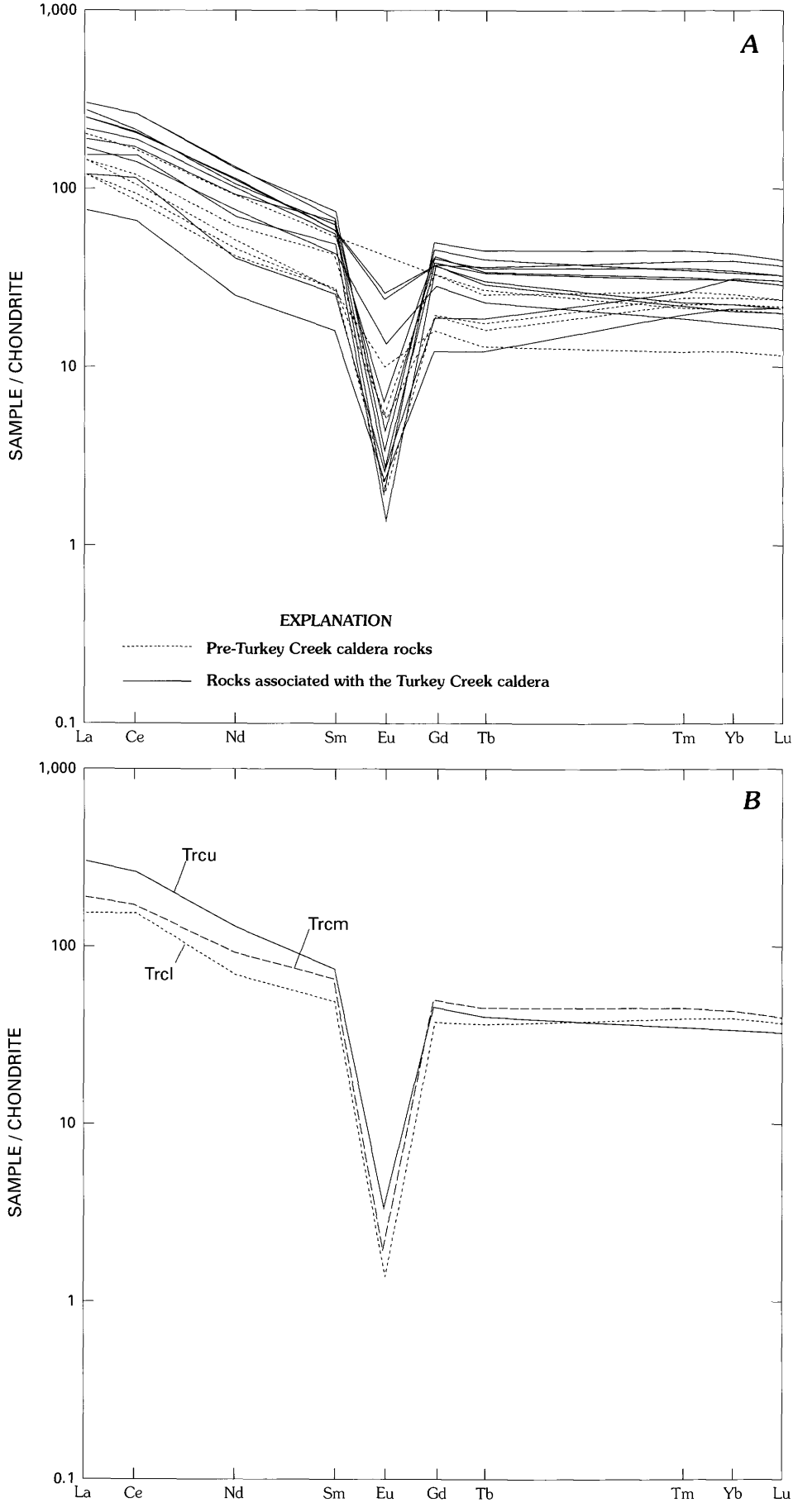

Figure 10 (alongside and facing page). Chondrite-normalized (modified from Anders and Ebihara, 1982) rare earth element diagrams. *A*, average compositions of volcanic rocks in the central Chiricahua Mountains, Ariz. *B*, compositions of the lower (Trcl), middle (Trcm), and upper (Trcu) members of outflow facies Rhyolite Canyon Tuff. *C*, compositions of the biotite rhyolite (Tmrb) and units 1 (Tmr1), 2 (Tmr2), and 3 (Tmr3) of rhyolite lava preserved in moat of Turkey Creek caldera.

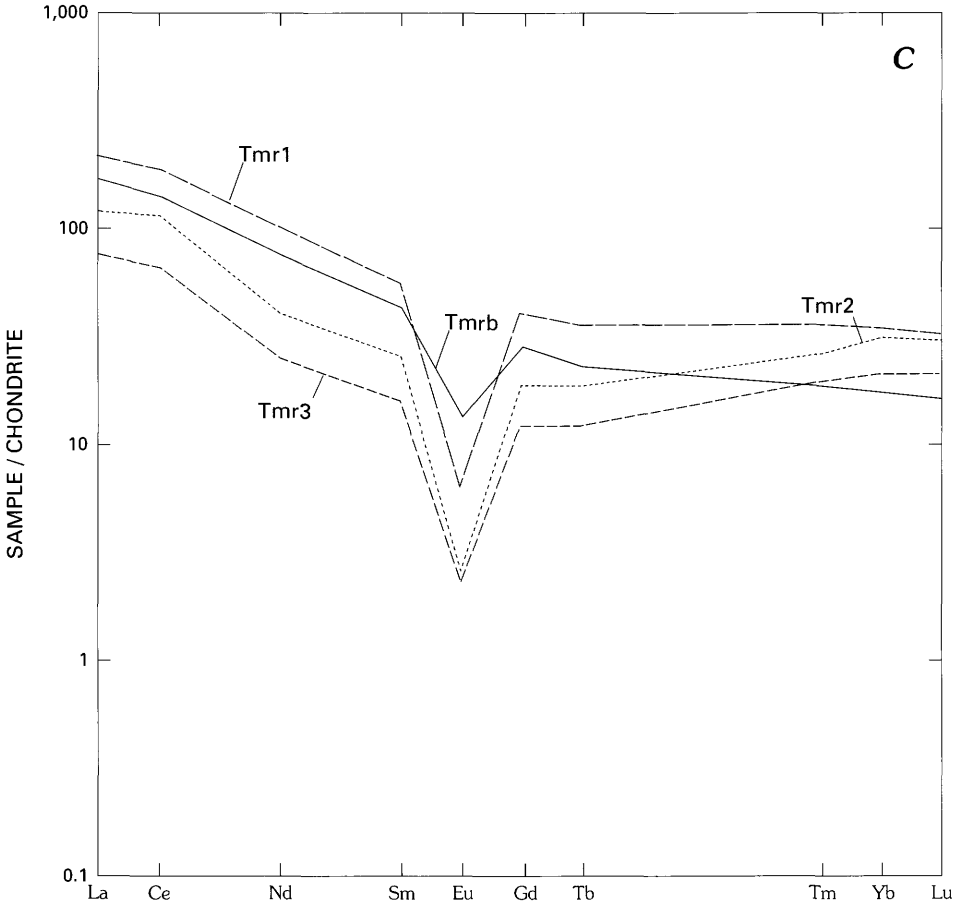

depletion), results in overall REE depletion, and increases Sr, Ba, and Rb abundances in the residual liquid.

REE abundance variations within outflow facies members of the Rhyolite Canyon Tuff (fig. 10*B*; table 1) are similar to those of the Bishop Tuff as well as those of many other high-silica rhyolite systems. The upper member of outflow facies Rhyolite Canyon Tuff is the least geochemically evolved of the three members, and it therefore is considered to represent a composition similar to that from which the other two members could have evolved. REE patterns for sequentially erupted members of outflow facies Rhyolite Canyon Tuff rotate in a clockwise sense, have progressively smaller negative europium anomalies, and depict compositional evolution of earlier erupted members from later erupted members. Abundances of other trace elements also vary consistently relative to stratigraphic position within the Rhyolite Canyon Tuff. In particular, early erupted Rhyolite Canyon Tuff, represented by stratigraphically lower deposits, contain higher abundances of Rb, Y, Nb, Ta, Th, and U, and lower abundances of Sr, Zr, and Ba. Consequently, evolution of trace-element abundance variations within the reservoir represented by outflow facies Rhyolite Canyon Tuff is qualitatively consistent with fractionation of the phenocryst phases contained therein. Sanidine crystallization and fractionation from the least evolved, parental magma, represented by the upper member of the Rhyolite Canyon Tuff, caused the residual liquid to contain lower light REE abundances relative to heavy REE abundances, lower Sr, Eu, and Ba abundances, and higher Rb abundances. Clinopyroxene crystallization and fractionation caused the residual liquid to contain slightly lower REE abundances overall. Zircon crystallization and fractionation caused the residual liquid to contain lower Zr abundances and partially counteracted heavy REE enrichment caused by sanidine fractionation. These mineral-melt distribution relations and crystal fractionation processes caused the residual liquid to differentiate to more evolved compositions and more evolved liquids accumulated at the top of the reservoir prior to eruption. Subsequent top-down eruptions from the normally zoned reservoir represented by the Turkey Creek caldera and its eruptive products depict compositional gradients that developed in the reservoir as a consequence of these crystal liquid equilibria.

The four rhyolite moat lava units (units 1, 2, and 3 and the biotite rhyolite), considered together, are zoned from less evolved (biotite rhyolite) to more evolved (unit 3) compositions, which is the reverse of that which results from progressive, top-down magma extraction from a normally zoned reservoir. Each subsequently erupted unit is more evolved than the previously erupted unit. For example, the abundances of compatible elements, such as Ti, Ba, and Sr, are greater in the biotite rhyolite relative to those in the three successively erupted rhyolite lavas of units 1, 2, and 3, in which their abundances are progressively lower. In contrast, abundances of

incompatible elements, such as Rb, Th, and Nb, are lowest in the first erupted rhyolite lava and progressively higher in subsequently erupted moat rhyolite lavas (table 1). As described by Duffield and Ruiz (1992) for the Oligocene Taylor Creek Rhyolite of New Mexico, this type of zoning is a logical consequence of a reservoir's being progressively contaminated by incorporation of variable amounts of geochemically less evolved rock. In an incompletely mixed reservoir, with increasing distance downward, away from the upper, enclosing roof rock interface, the amount of incorporated wallrock, and therefore contamination, is predictably less. Progressive, top-down magma extraction from a reservoir so contaminated yields eruptions of progressively more evolved compositions. Reversed compositional variation preserved by the rhyolite lavas in the moat of the Turkey Creek caldera suggests that the upper parts of their source reservoir were progressively less evolved as a consequence of having incorporated relatively greater amounts of roof rock. To identify other geochemical processes by which the observed reversed geochemical zonation preserved in the four rhyolite moat lava units could have developed is difficult.

REE abundance variations (fig. 10*C*) between the biotite rhyolite and unit 1 lava imply that wallrock contaminant unmixing was not the sole control on the compositional evolution depicted by these rocks. The biotite rhyolite has slightly lower REE abundances, has a slightly less well developed negative Eu anomaly, and is characterized by a REE pattern slightly less steeply negatively sloped than that of unit 1 lava. In order for unit 1 lava to have evolved from the biotite rhyolite, overall REE enrichment, which requires removal of material with REE abundances lower than those of the biotite rhyolite, must have occurred. However, the biotite rhyolite REE composition could not have evolved to that of unit 1 lava by unmixing of a lithologic contaminant, because all of the lithologies plausibly present within the intracaldera environment have overall REE abundances greater than those of the biotite rhyolite (fig 10*A*); their separation from the biotite rhyolite would have caused REE depletion in unit 1 lava relative to the biotite rhyolite. Fractionation of phenocrysts characteristic of the biotite rhyolite, sanidine and biotite, could have caused REE abundances to evolve to those of unit 1 lava. As described in the second paragraph of this section, REE mineral-melt distribution coefficients for sanidine are such that sanidine fractionation causes counterclockwise REE pattern rotation, results in negative europium anomaly development, and increases overall REE abundances in the residual liquid. Similarly, REE K_D's for biotite (0.23–0.44) are uniformly low, so that biotite fractionation causes REE enrichment (Hanson, 1980). Consequently, fractionation of sanidine and biotite phenocrysts from the biotite rhyolite could have caused the residual liquid, represented by unit 1 lava, to become REE enriched, to have a more well developed negative Eu anomaly, and to cause slight counterclockwise REE pattern rotation.

Compositional evolution from unit 1 lava to unit 2 lava and from unit 2 lava to unit 3 lava was quite different than the evolution from the biotite rhyolite to unit 1 lava. In particular, REE abundances in units 2 and 3 lavas are successively lower, negative Eu anomalies are of constant magnitude, and chondrite-normalized REE patterns are slightly counterclockwise rotated relative to that for unit 1 lava. This type of REE depletion requires removal of material with REE abundances greater than that of unit 1 lava. Because unit 1 lava has REE abundances between 100 and 10 times chondrite values, phenocryst fractionation seems improbable because very few common minerals contain sufficiently elevated REE abundances. Alternatively, addition of material, possibly including xenocrysts, with REE abundances less than that of unit 1 lava may have caused the observed REE abundance variations. However, the aphyric character of these rocks indicates that crystals were not added. As described in the previous paragraph, all of the lithologies plausibly present within the intracaldera environment are inappropriate contaminant additions, because they have REE abundances equal to or greater than those of unit 1 lava (fig. 10*A*); their addition to unit 1 lava would have caused REE enrichment in units 2 and 3 lavas relative to unit 1 lava. In contrast, removal of one of these lithologic contaminants could have caused the observed, systematic REE depletion.

Constraints on the rock unit(s) responsible for the hypothesized contamination of the moat rhyolite reservoir include the following:

1. The near contemporaneity of Turkey Creek caldera formation with eruption of the moat rhyolites,
2. The intracaldera-scale structural and lithologic configuration that prevailed immediately following Turkey Creek caldera formation, and
3. The compositions of rocks that may have been involved in the hypothesized contamination.

The fact that the Rhyolite Canyon Tuff and the moat rhyolite lavas are of essentially the same age (du Bray and Pallister, 1991) indicates that the rocks that contaminated the moat rhyolite reservoir must have been present in the intracaldera environment immediately following caldera formation. Structural relations immediately following caldera formation (du Bray and Pallister, 1991) indicate that major amounts of intracaldera Rhyolite Canyon Tuff and dacite porphyry dominated the shallow crust in the environs of the moat rhyolite reservoir. Other rocks that may have enclosed and hosted the caldera, and therefore may have been available as possible constituents of the shallow crustal roof for the moat rhyolite reservoir, include Tertiary volcanic rocks erupted before development of the Turkey Creek caldera. Volumetrically dominant among these are the intermediate composition lava flows (Tim) that are presumed to have been erupted from a set of coalescing stratovolcanoes and onto which younger, more evolved outflow ash-flow tuffs and lava were subsequently erupted.

The fact that negative Eu anomalies characteristic of rhyolite lavas of units 1, 2, and 3 are of constant magnitude indicates that the material being removed was characterized by, at most, a very small negative Eu anomaly; removal of material with a significant negative europium anomaly would have caused progressively less contaminated moat rhyolite to

have a progressively smaller negative anomaly. Of the rocks present in the central Chiricahua Mountains, only the upper member of the tuff of Horseshoe Canyon, the dacite porphyry of the Turkey Creek caldera, and the intermediate-composition lava flows at the base of the Tertiary volcanic section have small negative Eu anomalies (fig. 10). Geologic relations suggest that the upper member of the tuff of Horseshoe Canyon is not present in significant volumes, if at all, in the subsurface of the intracaldera environment; it is therefore an unlikely candidate for the unmixing lithologic contaminant. In contrast, geologic relations suggest that both the dacite porphyry and the intermediate lava flows were plausibly significant constituents of the intracaldera environment and therefore are likely candidates for the material that is inferred to have variably contaminated the rhyolite moat lava reservoir; top-down tapping of this variably but systematically contaminated reservoir could have produced the observed reversed compositional zonation.

Consideration of broader geochemical systematics is consistent with the dacite porphyry and the intermediate lava flows as plausible contaminant lithologies. Mixing considerations require that for moat lava compositional variation to be a consequence of variable contamination involving magma and an exotic constituent, the trace-element compositions of the contaminated products (the biotite rhyolite, unit 1 lava, and unit 2 lava) must be intermediate between those of the two parental components (uncontaminated rhyolite, represented by unit 3 lava and a combination of contaminants, represented by the dacite porphyry and the intermediate lava flows). An examination of compositional data for these six lithologies (table 1) indicates that, in general, the compositions of the biotite rhyolite and rhyolite lavas of units 1 and 2 are in fact intermediate between those of unit 3 lava and the inferred contaminants. However, these relations are not perfectly well developed. For example, zirconium abundances among these six units indicate that other processes, perhaps including minor fractionation, contributed to and modified compositional relations that seem largely to derive from variable magma contamination. In summary, compositional considerations indicate that the reversed compositional zonation depicted by the moat rhyolite lavas is consistent with the rhyolite reservoir's having being progressively roofward contaminated through entrainment and assimilation of dacite porphyry and intermediate-composition lava flow inclusions. Additional consideration of REE data suggests that evolution of the most contaminated moat rhyolite (the biotite rhyolite) to unit 1 lava also involved selective phenocryst fractionation.

Geochronology

Most of the samples whose ages were determined are among those used in the volcanic rock stratigraphic/composition investigation, a principal focus of this study. However, several samples (referred to as the miscellaneous units) of other igneous rocks in the study area were collected and dated by the $^{40}Ar/^{39}Ar$ method in order to augment the existing time-stratigraphic framework for this region. These samples and the map units that they represent, from oldest to youngest, are identified; and new geochronologic data are presented. Subsequently, geochronologic data and interpretations are presented for the principal volcanic rocks, from oldest to youngest. $^{40}Ar/^{39}Ar$ results are presented as age spectra (fig. 11); ages are summarized in table 2; analytical data are in table 3.

Miscellaneous Units

Sample DY91-77 (fig. 1, locality V) represents a hypabyssal dacite intrusion, about 16 km south of the Turkey Creek caldera; the sample site is within the dacitic rocks of Halfmoon Valley mapped by Drewes and Brooks (1988). The age spectrum for biotite from this sample (fig. 11*A*) is complicated, does not include a plateau, and shows the contrasting effects of both excess argon and apparent argon loss in the low-temperature steps. The isochron age for 80 percent of released ^{39}Ar, representing the least disturbed part of the age spectrum, is 74.6±0.6 Ma with $(^{40}Ar/^{36}Ar)_I = 276±19$. Although disturbed, the age spectrum for this sample confirms the presence of Cretaceous-age igneous rocks in the central Chiricahua Mountains; igneous rocks of this age have not been previously identified in this area.

Samples P650A and 202064 (fig. 1, localities P and S) were analyzed in order to establish the age of tuff and lavas that constitute the pyroclastic rocks of Rucker Canyon (du Bray and others, 1997), which are correlative, in part, with the welded tuff of Rucker Canyon (Drewes and Brooks, 1988). Although volumetrically significant, the petrographic and compositional characteristics of these rocks have not been included in the present study, because these rocks, largely composed of many separate pyroclastic flows, are lithologically heterogeneous and contain large amounts of exotic lithic fragments that would render definition of their petrography and composition somewhat meaningless. The age spectrum for biotite from sample P650A (fig. 11*B*), a rhyolite lava interbedded in the pyroclastic flows, shows the effects of a minor amount of excess argon in the low-temperature steps but yields a plateau age of 33.32±0.07 Ma. The age spectra for biotite and sanidine from a sample (fig. 11*C* and *D*, respectively) of the pyroclastic flows (202064) also show the effects of excess argon in the low-temperature steps, but both yield relatively undisturbed results. The biotite gives a plateau age of 33.21±0.09 Ma. The sanidine gives a weighted mean age of 33.04±0.04 Ma and an identical isochron age with $(^{40}Ar/^{36}Ar)_I = 310±7$, reflecting the relatively minor amount of excess ^{40}Ar in this sample. The similarity of ages for the biotite separates from the pyroclastic flow and lava samples suggests that emplacement of pyroclastic flows and lava flows was approximately simultaneous. The best age estimate for these rocks, based on the three available analyses, is 33.27±0.08

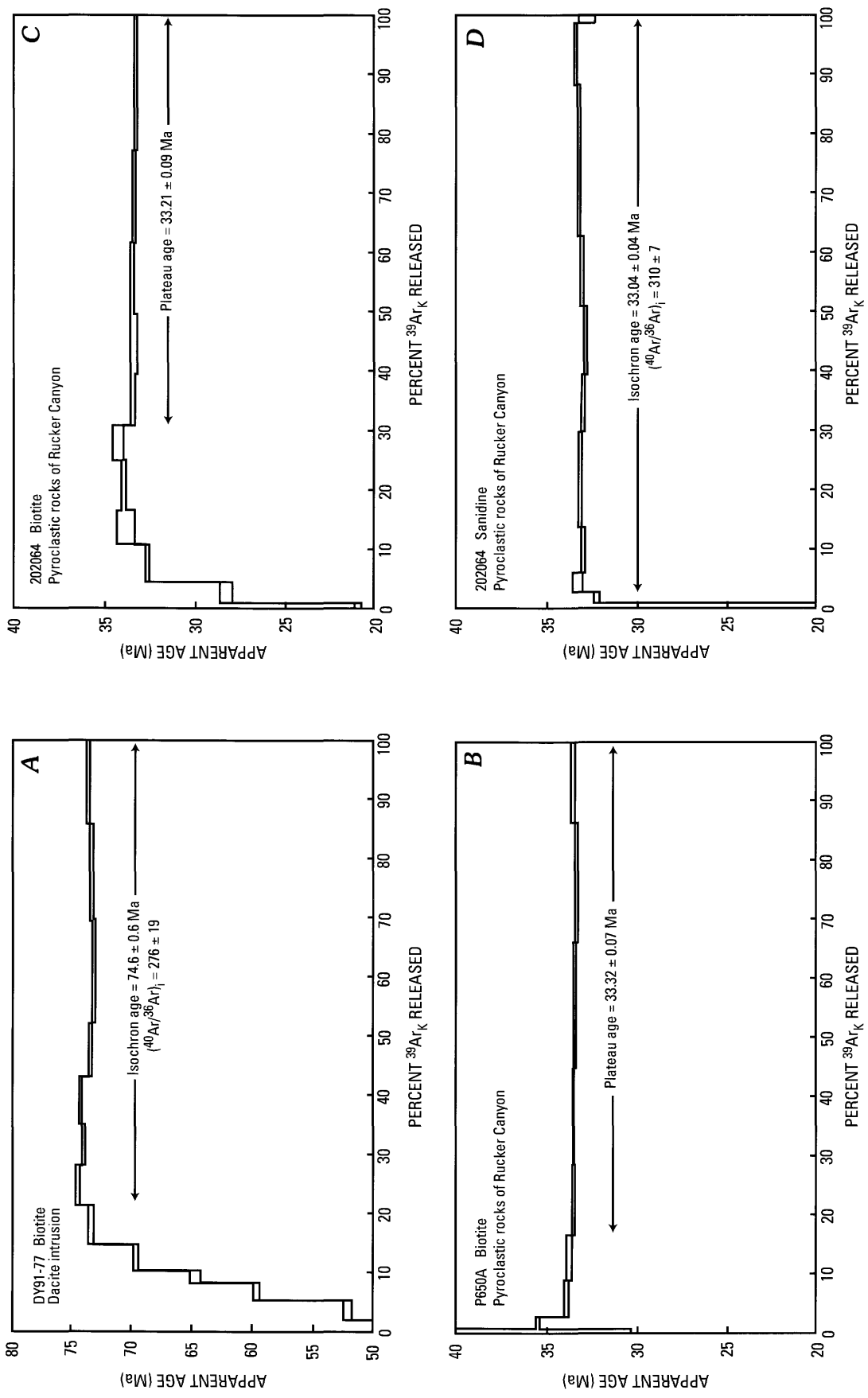
A
DY91-77 Biotite
Dacite intrusion
Isochron age = 74.6 ± 0.6 Ma
$(^{40}Ar/^{36}Ar)_i$ = 276 ± 19
B
P650A Biotite
Pyroclastic rocks of Rucker Canyon
Plateau age = 33.32 ± 0.07 Ma
C
202064 Biotite
Pyroclastic rocks of Rucker Canyon
Plateau age = 33.21 ± 0.09 Ma
D
202064 Sanidine
Pyroclastic rocks of Rucker Canyon
Isochron age = 33.04 ± 0.04 Ma
$(^{40}Ar/^{36}Ar)_i$ = 310 ± 7
APPARENT AGE (Ma)
PERCENT $^{39}Ar_K$ RELEASED

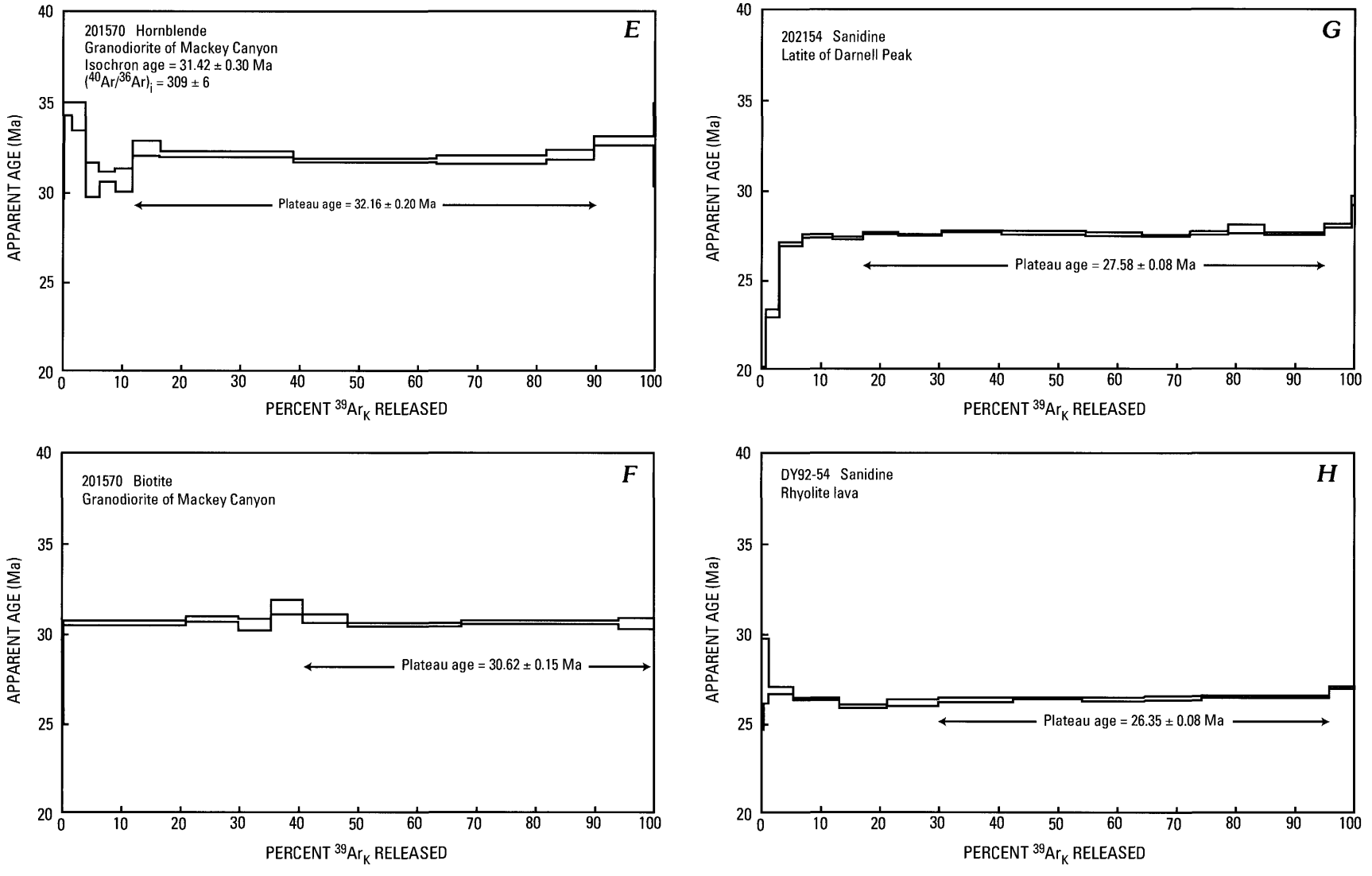

Figure 11 (above and following pages). $^{40}Ar/^{39}Ar$ age spectra for volcanic rocks of the central Chiricahua Mountains, Ariz. View letters *A* through *DD* correspond to the identifier in upper left of each view and also are the link to discussion in text.

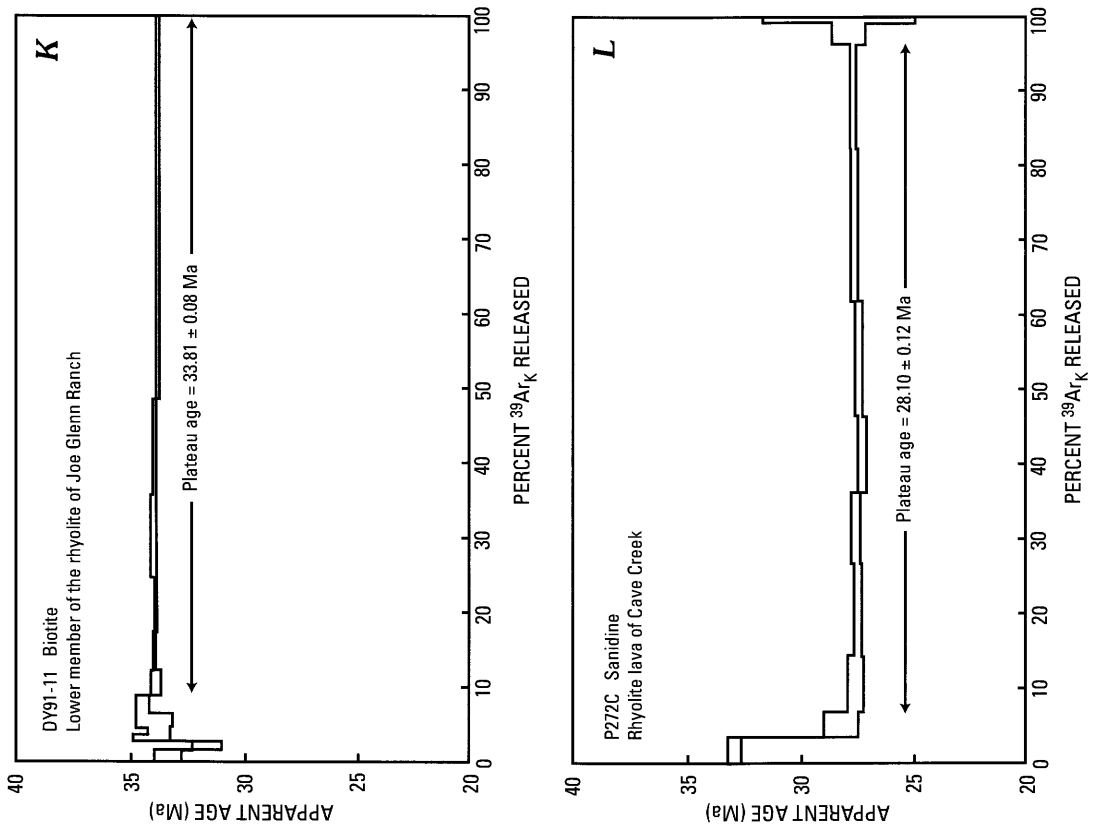
K
DY91-11 Biotite
Lower member of the rhyolite of Joe Glenn Ranch
Plateau age = 33.81 ± 0.08 Ma
L
P272C Sanidine
Rhyolite lava of Cave Creek
Plateau age = 28.10 ± 0.12 Ma
APPARENT AGE (Ma)
PERCENT $^{39}Ar_K$ RELEASED

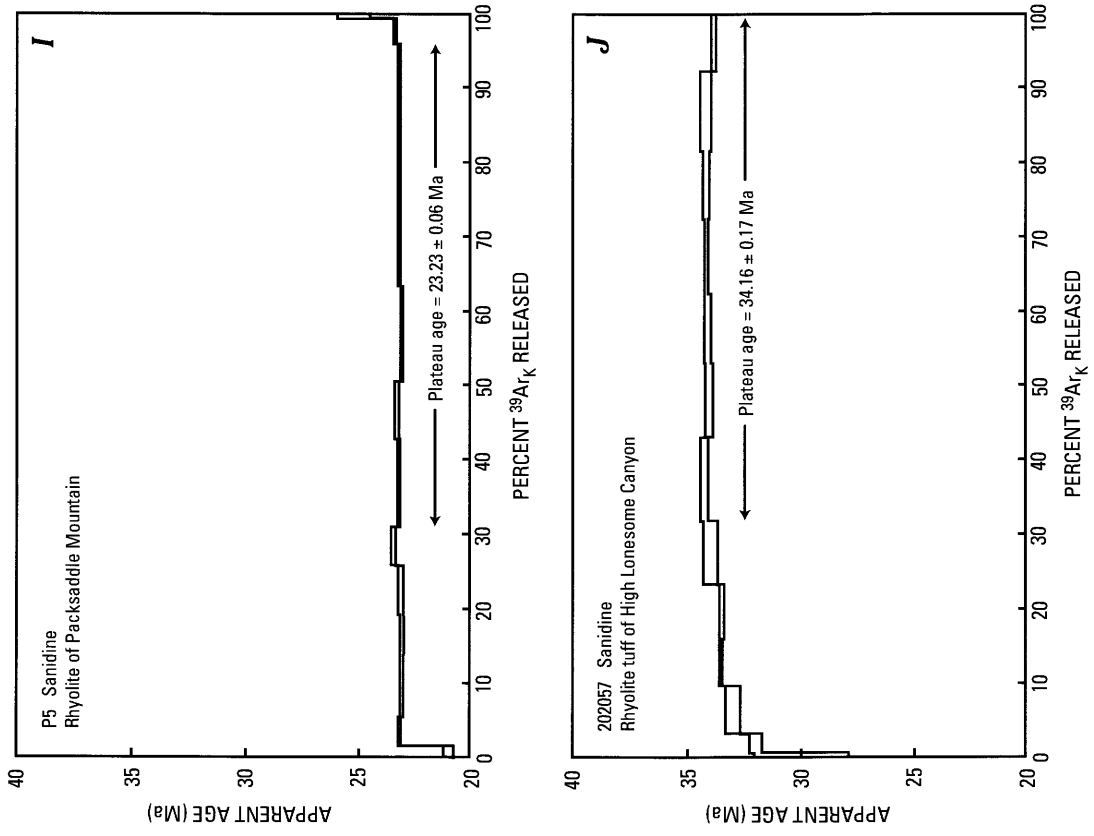
I
P5 Sanidine
Rhyolite of Packsaddle Mountain
Plateau age = 23.23 ± 0.06 Ma
J
202057 Sanidine
Rhyolite tuff of High Lonesome Canyon
Plateau age = 34.16 ± 0.17 Ma
APPARENT AGE (Ma)
PERCENT $^{39}Ar_K$ RELEASED

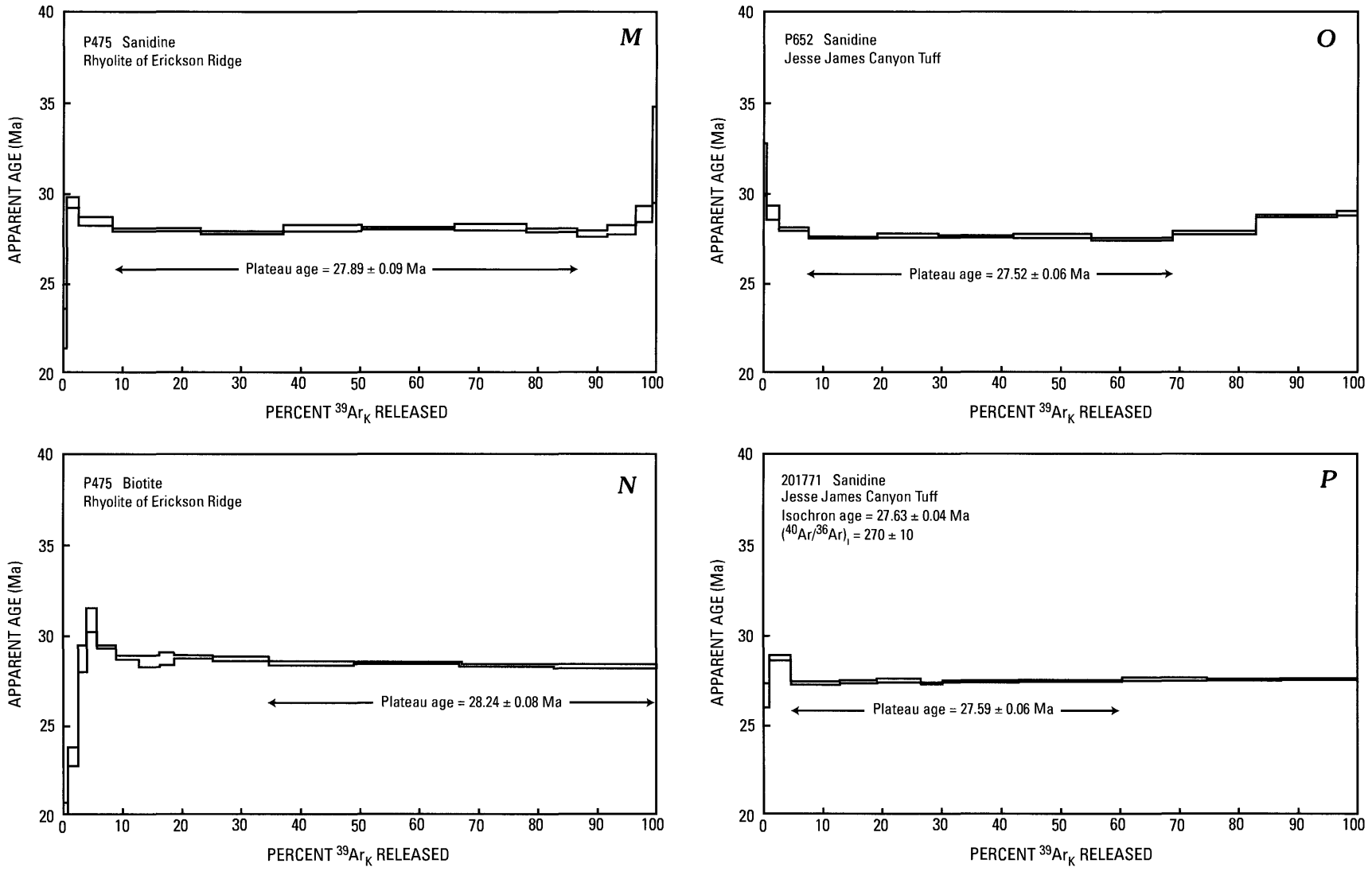

Figure 11—Continued. $^{40}Ar/^{39}Ar$ age spectra for volcanic rocks of the central Chiricahua Mountains, Ariz. View letters *A* through *DD* correspond to the identifier in upper left of each view and also are the link to discussion in text.

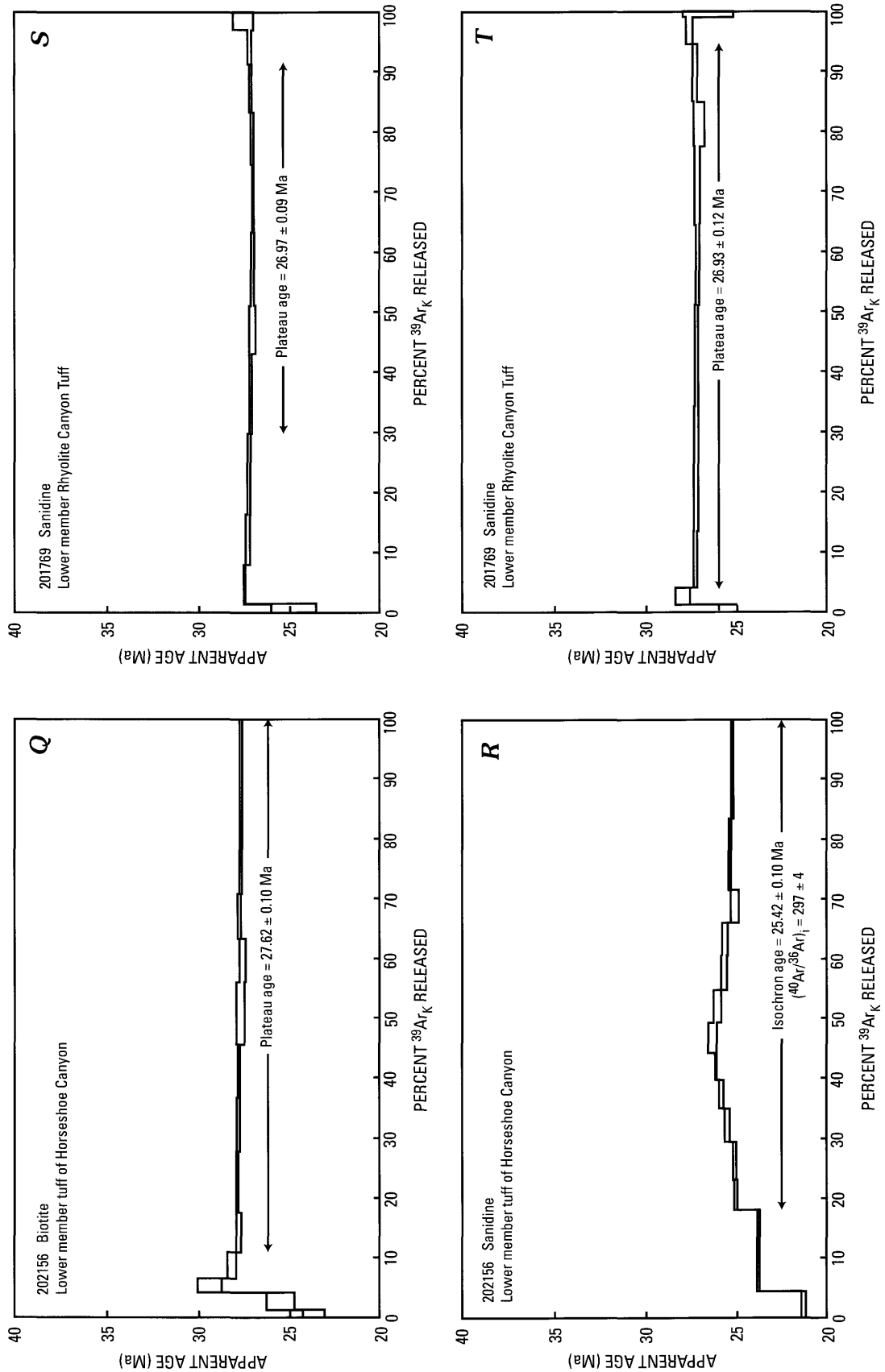
S
201769 Sanidine
Lower member Rhyolite Canyon Tuff
Plateau age = 26.97 ± 0.09 Ma
T
201769 Sanidine
Lower member Rhyolite Canyon Tuff
Plateau age = 26.93 ± 0.12 Ma
Q
202156 Biotite
Lower member tuff of Horseshoe Canyon
Plateau age = 27.62 ± 0.10 Ma
R
202156 Sanidine
Lower member tuff of Horseshoe Canyon
Isochron age = 25.42 ± 0.10 Ma
($^{40}Ar/^{36}Ar_i$) = 297 ± 4
APPARENT AGE (Ma)
PERCENT $^{39}Ar_K$ RELEASED

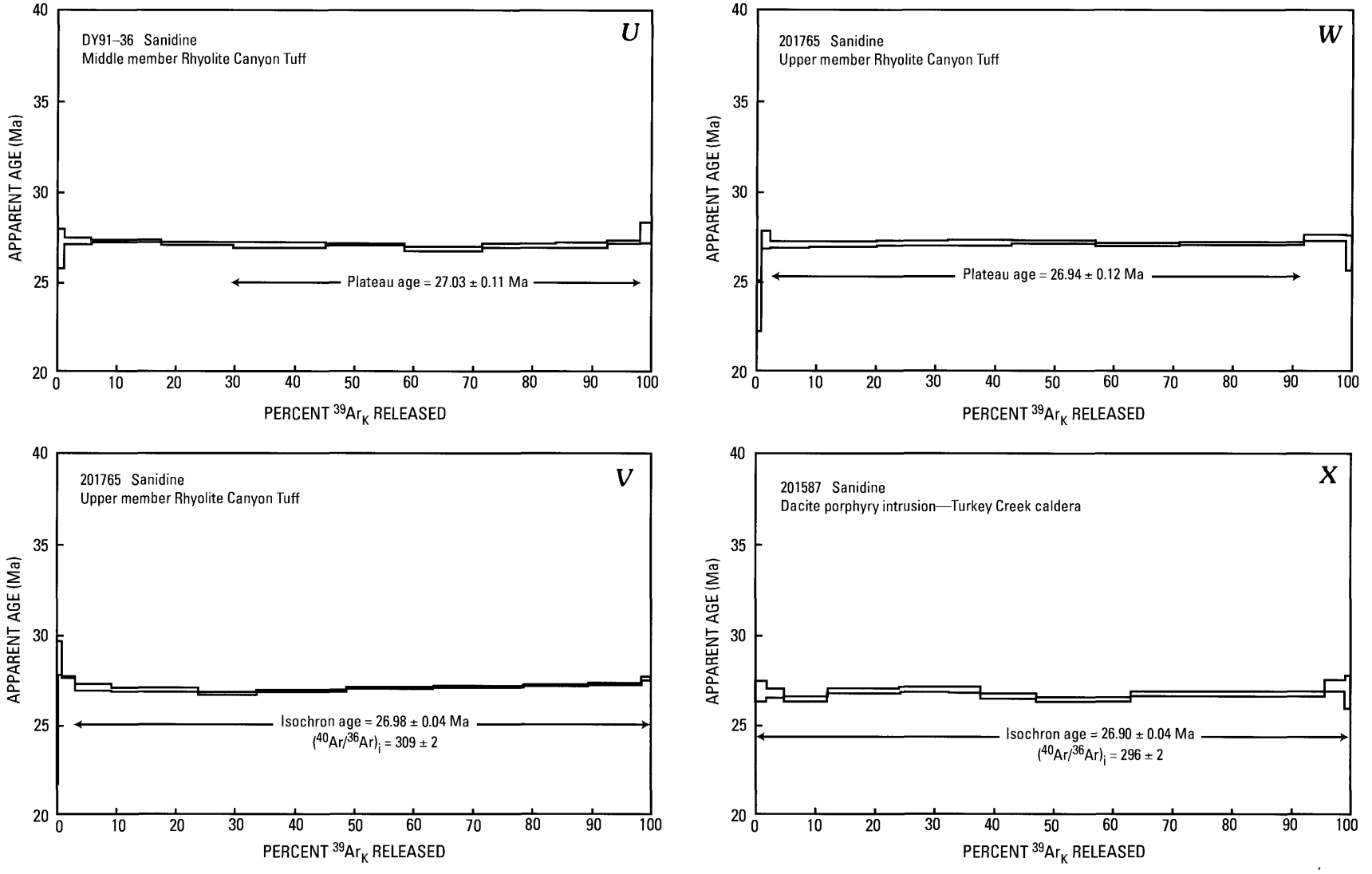

Figure 11—Continued. $^{40}Ar/^{39}Ar$ age spectra for volcanic rocks of the central Chiricahua Mountains, Ariz. View letters *A* through *DD* correspond to the identifier in upper left of each view and also are the link to discussion in text.

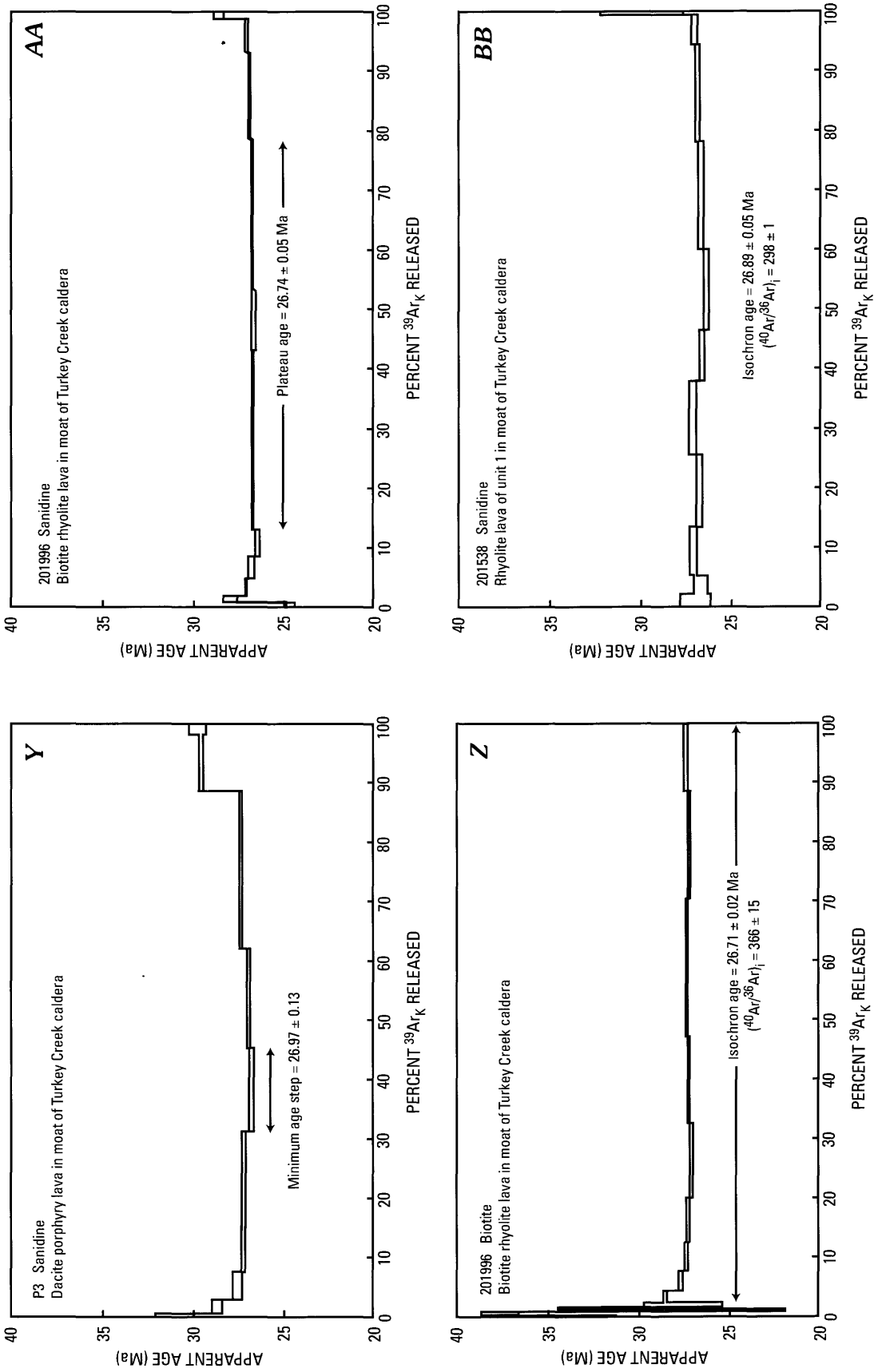
AA
201996 Sanidine
Biotite rhyolite lava in moat of Turkey Creek caldera
Plateau age = 26.74 ± 0.05 Ma
APPARENT AGE (Ma)
PERCENT $^{39}Ar_K$ RELEASED
BB
201538 Sanidine
Rhyolite lava of unit 1 in moat of Turkey Creek caldera
Isochron age = 26.89 ± 0.05 Ma
$(^{40}Ar/^{36}Ar)_i$ = 298 ± 1
APPARENT AGE (Ma)
PERCENT $^{39}Ar_K$ RELEASED
Y
P3 Sanidine
Dacite porphyry lava in moat of Turkey Creek caldera
Minimum age step = 26.97 ± 0.13
APPARENT AGE (Ma)
PERCENT $^{39}Ar_K$ RELEASED
Z
201996 Biotite
Biotite rhyolite lava in moat of Turkey Creek caldera
Isochron age = 26.71 ± 0.02 Ma
$(^{40}Ar/^{36}Ar)_i$ = 366 ± 15
APPARENT AGE (Ma)
PERCENT $^{39}Ar_K$ RELEASED

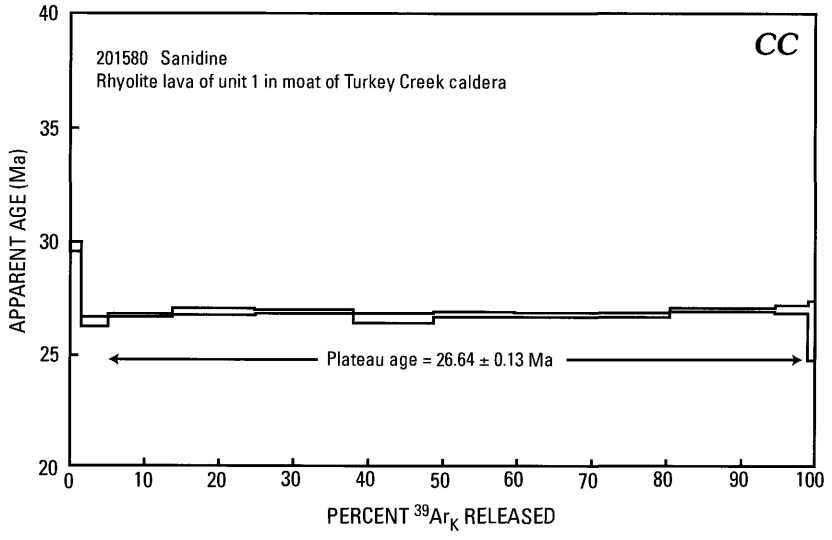

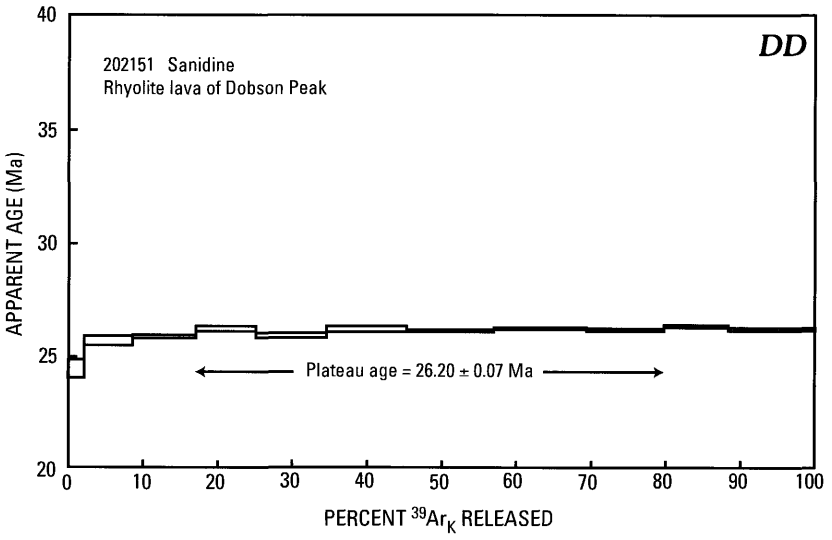

Figure 11—Continued. $^{40}Ar/^{39}Ar$ age spectra for volcanic rocks of the central Chiricahua Mountains, Ariz. View letters *A* through *DD* correspond to the identifier in upper left of each view and also are the link to discussion in text.

Ma, the average of the two biotite ages. In the study area, the pyroclastic rocks of Rucker Canyon represent the last manifestation of a short pulse of volcanic activity that began with eruption of the tuff of High Lonesome Canyon. This magmatic pulse ended at about 33.3 Ma and was followed by a 5.2 m.y. eruptive hiatus, which ended with eruption of the rhyolite lava of Cave Creek.

Sample 201570 (fig. 1, locality E) is from the granodiorite of Mackey Canyon (Pallister and others, 1994), also known as the granodiorite of Jhus stock (Drewes and others, 1995). The granodiorite is medium to coarse grained and contains subequal amounts of biotite and hornblende, which together constitute about 10 percent of the rock. Previous K-Ar analyses yielded ages of 30.9±1.2 Ma (Marvin and others, 1978, no. 100) and 29.59±0.90 Ma (Shafiqullah and others, 1978, no. 20). The age spectrum for hornblende from sample 201570 (fig. 11*E*) shows evidence of excess argon in the low- and high-temperature steps but gives a plateau age of 32.16±0.20 Ma and an isochron age 31.42±0.30 Ma with $(^{40}Ar/^{36}Ar)_I = 309\pm6$. Considering the effect of excess argon on the plateau age, we interpret the isochron age as more likely reflecting the crystallization age of the hornblende. The age spectrum for biotite from this sample (fig. 11*F*) is slightly disturbed but gives a plateau age of 30.62±0.15 Ma. Given the magnitude of uncertainties characteristic of K-Ar analyses and argon retention problems typical of biotite, we consider that the $^{40}Ar/^{39}Ar$ hornblende age for sample 201570 represents the best approximation of the age of this intrusion and the biotite age may reflect a brief period of cooling to the argon-in-biotite retention temperature. The presence of coarsely holocrystalline rocks, such as the granodiorite of Mackey Canyon, nearly adjacent to volcanic rocks as little as 5 m.y. younger implies rapid uplift, perhaps involving faulting, and unroofing of the terrane that includes the granodiorite prior to the onset of volcanism in this area at about 28 Ma.

Sample 202154 (fig. 1, locality M) represents the latite of Darnell Peak (Bryan, 1988), which forms a sill that intruded between the upper and lower members of the tuff of Horseshoe Canyon. The sill, which according to the nomenclature of Le Bas and others (1986) is composed of trachyte (11 percent Na_2O+K_2O at 68.6 percent SiO_2), is crystal rich and contains distinctive feldspar and biotite phenocrysts. The age spectrum (fig. 11*G*) for sanidine from this sample is simple, although slight effects of argon loss are evident in the low-temperature steps and excess argon in the two highest temperature steps. It gives a plateau age of 27.58±0.08 Ma. The age of the sill is indistinguishable from that of the lower member of the tuff of Horseshoe Canyon, which indicates that the sill was emplaced immediately after tuff emplacement. Bryan (1988) suggested that the considerable thickness of tuff of Horseshoe Canyon, southeast of the Turkey Creek caldera, forms an intracaldera accumulation within what he called the Portal caldera. In this context, the sill might represent resurgent magmatism within the Portal caldera and emplacement of less evolved magma up into the thick intracaldera tuff accumulation from lower within a zoned magma reservoir whose eruption created the Portal caldera. The stratigraphic and compositional relations between the sill and the tuff indicate that the reservoir from which these products were erupted was strongly and discontinuously zoned, a feature that is known to have prevailed in the adjacent and 0.5 m.y.-younger Turkey Creek caldera as well.

Sample DY92-54 represents an isolated rhyolite lava that overlies outflow facies Rhyolite Canyon Tuff about 13 km southwest of the Turkey Creek caldera (fig. 1, locality R). The age spectrum for sanidine from this sample (fig. 11*H*) yields a plateau with an apparent age of 26.35±0.08 Ma. The age for this sample indicates that the underlying Rhyolite Canyon Tuff here is at least 26.35 Ma. The age and stratigraphic position of this rhyolite are similar to those of the rhyolite of Dobson Peak, exposed about 16 km to the east. The rhyolite represented by DY92-54 could be correlative with the rhyolite of Dobson Peak. If such a correlation were substantiated, then the lava dome field represented by rhyolite of Dobson Peak must have been considerably more extensive than its present erosional remnants.

Sample P5 (fig. 1, locality W) represents the rhyolite of Packsaddle Mountain (Drewes and Brooks, 1988), an isolated, small, garnet-bearing rhyolite plug about 16 km south of the Turkey Creek caldera. Drewes and Brooks (1988) presented a K-Ar age of 22.9±0.8 Ma (R.F. Marvin, H.H. Mehnert, and E.L. Brandt, written commun., 1985) on sanidine from this unit. The age spectrum for sanidine from this sample is simple (fig. 11*I*) and gives a plateau age of 23.23±0.08 Ma, which confirms that this is one of the youngest Tertiary-age igneous rocks known in the central Chiricahua Mountains.

Pre-Turkey Creek Caldera Rocks

Sample 202057 (fig. 1, locality U) represents the rhyolite tuff of High Lonesome Canyon, a regionally distributed ash-flow tuff for which no geochronologic data have been previously reported. The age spectrum for sanidine from this sample is relatively simple (fig. 11*J*), although some effects of argon loss are evident in the low-temperature steps; it gives a plateau age of 34.16±0.17 Ma, which we interpret to represent the eruption age of the tuff. The rhyolite tuff of High Lonesome Canyon is thus the oldest ash-flow tuff in the study area with a well-established age. Unfortunately, the age of the tuff does not match that of any other regionally distributed ash-flow tuff from the Boot Heel volcanic field. As such, the source, distribution, and stratigraphic correlation of this unit remain unknown.

Sample DY91-11 (fig. 1, locality T) represents the lower member of the rhyolite of Joe Glenn Ranch, another regionally distributed ash-flow tuff. A sanidine K-Ar age of 29.6±1.9 Ma has been reported for this unit, but the collection site for the analyzed sample is uncertain (Marjaniemi, 1969; Drewes, 1982). Drewes and Brooks (1988) presented a fission track (zircon) age of 30.4±3.0 Ma for this unit. The age spectrum for biotite from this sample is relatively simple (fig. 11*K*), although it shows minor disturbance in the low-temperature

steps; it gives a plateau age of 33.81±0.08 Ma. The new geochronologic data indicate that the lower member of the rhyolite of Joe Glenn Ranch was therefore erupted within about 350,000 years of the eruption of the rhyolite tuff of High Lonesome Canyon. Like the tuff of High Lonesome Canyon, the lower member of the rhyolite of Joe Glenn Ranch does not have an age correlative among units of the Boot Heel volcanic field. Consequently, the source, distribution, and stratigraphic correlation of this unit also remain unknown.

Sample P272C (fig. 1, locality I) represents the rhyolite lava of Cave Creek which forms an extensive flow dome field, possibly including the rhyolite lava of Krentz Ranch, in the eastern part of the central Chiricahua Mountains. McIntosh and Bryan (2000) reported an $^{40}Ar/^{39}Ar$ age of 27.76±0.16 Ma for this unit. The age spectrum for sanidine from this sample is relatively simple (fig. 11*L*), although some effects of excess argon are evident in both the low- and high-temperature steps; it gives a plateau age of 28.10±0.12 Ma. This age indicates that following eruption of the pyroclastic rocks of Rucker Canyon at about 33.3 Ma, no volcanic rocks were erupted in the study area until the rhyolite lava of Cave Creek was erupted about 28.1 Ma. These three rock units therefore define a magmatic hiatus of about 5.2 m.y. in the area.

Sample P475 (fig. 1, locality A) represents the rhyolite of Erickson Ridge, which forms a set of coalesced rhyolite lava domes in the western part of the central Chiricahua Mountains; Drewes (1982) reported a biotite K-Ar age of 28.7±1.0 Ma for this rhyolite. Age spectra for coexisting sanidine and biotite are relatively simple, although the effects of excess argon and argon loss are evident, especially in the low-temperature steps, in spectra for both minerals. The sanidine (fig. 11*M*) gives a plateau age of 27.89±0.09 Ma, whereas the biotite (fig. 11*N*) gives a discordant plateau age of 28.24±0.08 Ma. Harlan and others (1998) and Kellogg and others (1994) have suggested that age discordance between coexisting sanidine and biotite is common in volcanic rocks and that in some cases biotite yields $^{40}Ar/^{39}Ar$ ages older than those indicated by coexisting sanidine. We consider the sanidine age to be more representative and reliable, because sanidine is less susceptible to the diversity of geologic processes that can disturb argon systematics in biotite and the age spectrum of the biotite clearly is more affected by excess argon. Our preferred age for the rhyolite of Erickson Ridge is 27.89±0.09 Ma, which, given the analytical uncertainties, suggests that the rhyolite of Erickson Ridge is the same age as the rhyolite lava of Cave Creek. As such, the re-initiation of volcanism in the region shortly before 28 Ma and following the 5.2 m.y. hiatus is dominated by the voluminous, effusive rhyolite lava dome field development preserved in the rhyolites of Erickson Ridge, Cave Creek, and Krentz Ranch.

Samples 201771 and P652 (fig. 1, localities C and O) represent the Jesse James Canyon Tuff. The two samples were collected and their ages determined to help verify the inferred correlation of these two isolated exposures of similar ash-flow tuff. Age spectra for sanidine from both of these samples are relatively simple, although that for sample P652 shows some effects of excess argon in the low- and high-temperature steps. The spectrum for sample P652 (fig. 11*O*) gives a plateau age of 27.52±0.06 Ma, whereas that for sample 201771 (fig. 11*P*) gives a plateau age of 27.59±0.06 Ma. An isochron analysis of 201771 yields an apparent age of 27.63±0.04 Ma, which is identical to the plateau age, with $(^{40}Ar/^{36}Ar)_i = 270±10$. That these two plateau ages are statistically indistinguishable substantiates the inferred correlation between these exposures of biotite-bearing high-silica rhyolite tuff exposed immediately beneath outflow facies Rhyolite Canyon Tuff in the northern and southern parts of the central Chiricahua Mountains. These ages suggest another correlation. Biotite-bearing high-silica rhyolite tuff exposed in the eastern and southeastern parts of the study area, and immediately beneath the Rhyolite Canyon Tuff, is the tuff of Horseshoe Canyon, which, as described following, has a preferred age of 27.62±0.10 Ma. All three of these ages are statistically indistinguishable. Therefore, because the Jesse James Canyon Tuff and the lower member of the tuff of Horseshoe Canyon occupy identical stratigraphic positions and are the same age, it seems probable that the Jesse James Canyon Tuff is the eruptive correlative of part, if not all, of the lower member of the tuff of Horseshoe Canyon. The near indistinguishability of geochemical data for these two units further substantiates the inference that these two units are, at least in part, volcanologic and therefore stratigraphic correlatives.

Sample 202156 (fig. 1, locality L) represents the lower member of the tuff of Horseshoe Canyon, a regionally distributed rhyolite ash-flow tuff. Bryan (1988) summarized the scant K-Ar age data available for this unit. He documented the attempt by Marjaniemi (1969) to determine the age of the tuff by K-Ar analysis of biotite, which resulted in an age of 26.4±0.7 Ma. Given that the tuff of Horseshoe Canyon is stratigraphically beneath the Rhyolite Canyon Tuff, and that the age of the latter (see next section) is now known to be 26.9 Ma, we conclude that the earliest attempts to date the tuff of Horseshoe Canyon resulted in a slightly too young age. Using the $^{40}Ar/^{39}Ar$ method and having analyzed 17 samples of the tuff, McIntosh and Bryan (2000) established its age as 27.6 Ma. Age spectra for sanidine and coexisting biotite from sample 202156 give significantly different ages. The spectrum for the biotite separate is relatively simple (fig. 11*Q*), although it shows some evidence of excess argon and argon loss in the low-temperature steps; it gives a plateau age of 27.62±0.10 Ma. The spectrum for the sanidine separate (fig. 11*R*) is significantly disturbed and is characterized by a progressive stepping-up pattern in the low-temperature steps, and then by a more gradual stepping-down pattern in the medium- to high-temperature steps. The sanidine analysis gives an isochron age of 25.42±0.10 Ma with $(^{40}Ar/^{36}Ar)_i = 297±4$. Given the preceding comments concerning early K-Ar analyses of this unit, clearly this age is significantly too young and therefore meaningless. Consequently, our preferred age for the lower member of the tuff of Horseshoe Canyon is 27.62±0.10 Ma, which is in good agreement with the findings of McIntosh and Bryan (2000). This age is also consistent with intrusion of the

Table 3. $^{40}Ar/^{39}Ar$ data for volcanic rocks of the central Chiricahua Mountains.[1/]

Temp (° C)	$^{40}Ar_R$ [2/]	$^{39}Ar_K$ [2/]	$^{40}Ar_R/^{39}Ar_K$ [2/]	$^{39}Ar/^{37}Ar$ [2,3/]	$\%^{40}Ar_R$	$\%^{39}Ar$	Apparent age [4,5/] (Ma at ± 1σ)
Pre-Turkey Creek caldera rocks							
Sample: DY 91-77, biotite from dacite intrusion, J = 0.007306, sample wt = 62.4 mg							
Latitude: 31°38′04″N.			Longitude: 109°22′40″W.				
800	.33645	.10407	3.233	-----	30.5	2.3	42.11 ± .07
900	.56337	.14027	4.016	-----	49.0	3.1	52.17 ± .33
950	.60808	.13195	4.609	-----	53.4	2.9	59.74 ± .25
1000	.46566	.09300	5.007	-----	62.6	2.0	64.82 ± .45
1050	1.0832	.20101	5.389	-----	74.5	4.4	69.67 ± .18
1100	1.6785	.29570	5.676	-----	83.1	6.5	73.31 ± .29
1150	1.7835	.30919	5.768	-----	87.4	6.8	74.47 ± .21
1200	1.8113	.31623	5.728	-----	88.5	6.9	73.96 ± .11
1250	2.1122	.36772	5.744	-----	89.2	8.1	74.16 ± .11
1300	2.3476	.41295	5.685	-----	86.3	9.1	73.41 ± .11
1350	4.4704	.78842	5.670	-----	85.6	17.3	73.23 ± .11
1400	4.1792	.73630	5.676	-----	89.0	16.2	73.30 ± .11
1500	3.7589	.65902	5.704	-----	90.6	14.5	73.65 ± .11
No plateau; total gas age = 71.46 ± 0.15 Ma							
Isochron age (steps 7-13) = 74.6 ± 0.6 Ma; $(^{40}Ar/^{36}Ar)_I = 276 \pm 19$							
Sample: 202057, sanidine from rhyolite tuff of High Lonesome Canyon, J = 0.007288, sample wt = 40.2 mg							
Latitude: 31°43′07″N.			Longitude: 109°22′10″W.				
850	.0712	.0310	2.29	-----	36.2	.9	30. ± 2
950	.21400	.08730	2.451	-----	85.3	2.5	31.94 ± .30
1050	.56327	.22273	2.529	-----	74.7	6.4	32.95 ± .33
1100	.56931	.22136	2.572	-----	95.4	6.4	33.50 ± .07
1150	.64957	.25317	2.566	-----	96.2	7.3	33.42 ± .10
1200	.75008	.28761	2.608	-----	97.7	8.3	33.97 ± .31
1250	1.0224	.38878	2.630	-----	98.3	11.2	34.25 ± .17
1300	.89940	.34377	2.616	-----	97.8	9.9	34.07 ± .15
1350	.86144	.32854	2.622	-----	98.4	9.5	34.15 ± .16
1400	.90951	.34579	2.630	-----	98.6	10.0	34.25 ± .07
1450	.82037	.31169	2.632	-----	98.1	9.0	34.28 ± .16
1500	.99938	.37954	2.633	-----	98.2	10.9	34.29 ± .22
1600	.70223	.26936	2.607	-----	94.8	7.8	33.95 ± .09
Total gas age = 33.89 ± 0.19 Ma							
Plateau age (steps 6-13) = 34.16 ± 0.17 Ma (for 76.5 percent of the gas produced during heating)							
Sample: DY 91-11, biotite from rhyolite of Joe Glenn Ranch, J = 0.007228, sample wt = 54 mg							
Latitude: 31°43′45″N.			Longitude: 109°22′42″W.				
800	.0228	.0077	2.96	-----	35.9	.2	38. ± 5
900	.17104	.06623	2.582	-----	49.8	1.5	33.4 ± .6
1000	.12715	.05194	2.448	-----	29.6	1.1	31.6 ± .7
1050	.09694	.03672	2.640	-----	50.1	.8	34.1 ± .8
1100	.12553	.04807	2.611	-----	58.0	1.1	33.7 ± .5
1150	.22775	.08666	2.628	-----	69.3	1.9	34.0 ± .8
1200	.27804	.10413	2.670	-----	79.1	2.3	34.5 ± .3
1250	.40447	.15428	2.622	-----	83.1	3.4	33.9 ± .2
1300	.60641	.23109	2.624	-----	85.0	5.1	33.90 ± .05
1350	.86287	.32912	2.622	-----	84.1	7.3	33.87 ± .05
1400	1.3297	.50658	2.625	-----	81.4	11.2	33.91 ± .10
1450	1.5075	.57509	2.621	-----	79.1	12.7	33.86 ± .05
1500	2.1946	.83986	2.613	-----	78.1	18.6	33.75 ± .06
1550	2.1471	.82183	2.613	-----	74.8	18.2	33.75 ± .07
1650	1.7231	.65907	2.615	-----	71.2	14.6	33.77 ± .06
Total gas age =33.81 ± 0.12 Ma							
Plateau age (steps 8-15) = 33.81 ± 0.08 Ma (for 91.1 percent of the gas produced during heating)							
Sample: P650A, biotite from lava in pyroclastic rocks of Rucker Canyon, J = 0.007273, sample wt =58.3 mg							
Latitude: 31°45′17″N.			Longitude: 109°23′18″W.				
800	.0119	.0046	2.585	-----	12.0	.1	34. ± 7
900	.0606	.0220	2.749	-----	22.5	.5	36. ± 2
1000	.0131	.0043	3.023	-----	19.1	.1	39. ± 9
1100	.25449	.09350	2.722	-----	43.2	2.0	35.36 ± .10
1200	.78074	.30083	2.595	-----	79.7	6.4	33.73 ± .11
1250	.91525	.35400	2.585	-----	85.0	7.5	33.61 ± .12
1300	1.4587	.56869	2.565	-----	83.2	12.0	33.35 ± .08
1350	2.0019	.78026	2.566	-----	75.5	16.5	33.35 ± .05
1400	2.5372	.99023	2.562	-----	70.3	20.9	33.31 ± .05
1450	2.4490	.95833	2.555	-----	70.7	20.3	33.22 ± .06
1600	1.6833	.65491	2.570	-----	73.6	13.8	33.41 ± .11
Total gas age = 33.42 ± 0.10 Ma							
Plateau age (steps 7-11) = 33.32 ± 0.07 Ma (for 83.5 percent of the gas produced during heating)							

Table 3. $^{40}Ar/^{39}Ar$ data for volcanic rocks of the central Chiricahua Mountains.[1/]—Continued

Temp (° C)	$^{40}Ar_R$ [2/]	$^{39}Ar_K$ [2/]	$^{40}Ar_R/^{39}Ar_K$ [2/]	$^{39}Ar/^{37}Ar$ [2,3/]	$\%^{40}Ar_R$	$\%^{39}Ar$	Apparent age [4,5/] (Ma at ± 1σ)
Pre-Turkey Creek caldera rocks (continued)							
Sample: 202064, sanidine from pyroclastic rocks of Rucker Canyon, J = 0.007211, sample wt = 58.3 mg							
Latitude: 31°43′45″N.			Longitude: 109°23′01″W.				
850	.11280	.08128	1.388	-----	60.8	.9	17.96 ± .29
950	.39018	.15653	2.493	-----	76.0	1.8	32.14 ± .14
1050	.73384	.28528	2.572	-----	88.7	3.3	33.16 ± .29
1150	1.6880	.66193	2.550	-----	97.9	7.6	32.87 ± .09
1200	1.8456	.72179	2.557	-----	98.3	8.3	32.96 ± .06
1250	1.7673	.69141	2.556	-----	98.3	8.0	32.95 ± .07
1300	2.0964	.82207	2.550	-----	98.2	9.5	32.87 ± .06
1350	2.5270	.99487	2.540	-----	98.3	11.5	32.74 ± .05
1400	2.6241	1.0284	2.552	-----	98.6	11.8	32.89 ± .05
1450	2.8236	1.1014	2.564	-----	99.0	12.7	33.04 ± .05
1500	2.8690	1.1192	2.564	-----	98.7	12.9	33.04 ± .06
1550	2.2979	.89018	2.581	-----	98.7	10.3	33.27 ± .05
1650	.32974	.13024	2.532	-----	86.0	1.5	32.64 ± .45
No plateau; total gas age = 32.81 ± 0.08 Ma							
Weighted mean age (steps 3-12) = 33.04 ± 0.04 Ma; $(^{40}Ar/^{36}Ar)_I = 310 \pm 7$							
Sample: 202064, biotite from pyroclastic rocks of Rucker Canyon, J = 0.007291, sample wt = 36.1 mg							
Latitude: 31°43′45″N.			Longitude: 109°23′01″W.				
800	.0119	.0044	2.729	-----	13.2	.1	36. ± 5
900	.05414	.03385	1.599	-----	13.5	1.1	20.91 ± .15
1000	.21606	.09988	2.163	-----	20.7	3.4	28.23 ± .38
1100	.49025	.19608	2.500	-----	48.5	6.6	32.59 ± .05
1150	.44536	.17204	2.589	-----	61.2	5.8	33.73 ± .49
1200	.64025	.24651	2.597	-----	67.4	8.3	33.84 ± .12
1250	.44545	.16993	2.621	-----	70.4	5.7	34.15 ± .33
1300	.67533	.26433	2.555	-----	66.9	8.9	33.29 ± .07
1350	.72277	.28346	2.550	-----	64.8	9.6	33.23 ± .14
1400	.94128	.36886	2.552	-----	72.7	12.4	33.26 ± .07
1450	1.1522	.45211	2.549	-----	79.1	15.2	33.21 ± .07
1550	1.7176	.67533	2.543	-----	84.5	22.8	33.15 ± .07
Total gas age = 33.00 ± 0.14 Ma							
Plateau age (steps 8-12) = 33.21 ± 0.09 Ma (for 68.90 percent of the gas produced during heating)							
Sample: 201570, biotite from granodiorite of Mackey Canyon, J = 0.007202, sample wt = 44.7 mg							
Latitude: 31°58′21″N.			Longitude: 109°14′04″W.				
500	.0428	.0294	1.45	10.5	2.8	.4	1.9 ± 2
700	3.8412	1.61536	2.378	270	64.4	20.6	30.63 ± .10
750	1.6872	.70572	2.391	257	86.3	9.0	30.80 ± .11
800	1.0393	.43799	2.373	186	84.8	5.6	30.57 ± .25
850	.99738	.41005	2.432	86	82.3	5.2	31.33 ± .32
900	1.4464	.60469	2.392	105	88.0	7.7	30.81 ± .18
950	3.5422	1.49360	2.372	130	90.9	19.0	30.55 ± .08
1000	4.9721	2.09179	2.377	214	92.4	26.6	30.62 ± .08
1050	1.0862	.45726	2.375	59	90.1	5.8	30.60 ± .24
1150	.0158	.0064	2.45	4.41	20.1	.1	32. ± 13
1300	.0205	.0058	3.52	.68	12.7	.1	45. ± 16
Total gas age = 30.64 ± 0.14 Ma							
Plateau age (steps 6-9) = 30.62 ± 0.15Ma (for 59.1 percent of the gas produced during heating)							
Sample: 201570, hornblende from granodiorite of Mackey Canyon, J = 0.007173, sample wt = 416.4 mg							
Latitude: 31°58′21″N.			Longitude: 109°14′04″W.				
500	.0737	.0097	7.6	.27	11.9	.3	96. ± 6
600	.13673	.04461	3.065	1.01	27.9	1.2	39.23 ± .74
700	.20655	.07720	2.676	2.14	28.2	2.1	34.29 ± .79
750	.19676	.08145	2.416	1.73	55.3	2.2	30.99 ± .85
800	.23621	.09726	2.429	.97	60.0	2.7	31.16 ± .26
850	.24370	.10093	2.415	.44	55.3	2.8	30.98 ± .58
900	.44623	.17561	2.541	.13	60.1	4.8	32.59 ± .36
950	2.0647	.81976	2.519	.09	61.0	22.6	32.30 ± .15
1000	2.1878	.87670	2.496	.10	66.7	24.2	32.01 ± .09
1050	1.6697	.66814	2.499	.09	64.7	18.4	32.05 ± .21
1100	.74820	.29713	2.518	.08	70.1	8.2	32.29 ± .26
1150	.93612	.36408	2.571	.07	57.9	10.0	32.97 ± .24
1200	.04219	.01489	2.83	.08	7.4	.4	36. ± 4
1350	.0145	.0010	14.0	.09	3.5	0.0	173. ± 44
Total gas age = 32.53 ± 0.24 Ma							
Plateau age (steps 7-11) = 32.16 ± 0.20 Ma (for 78.2 percent of the gas produced during heating)							
Isochron age (steps 7-11) = 31.42 ± 0.30 Ma; $(^{40}Ar/^{36}Ar)_I = 309 \pm 6$							

Table 3. $^{40}Ar/^{39}Ar$ data for volcanic rocks of the central Chiricahua Mountains.[1/]—Continued

Temp (° C)	$^{40}Ar_R$ [2/]	$^{39}Ar_K$ [2/]	$^{40}Ar_R/^{39}Ar_K$ [2/]	$^{39}Ar/^{37}Ar$ [2,3/]	$\%^{40}Ar_R$	$\%^{39}Ar$	Apparent age [4,5/] (Ma at ± 1σ)
Pre-Turkey Creek caldera rocks (continued)							
Sample: P272C, sanidine from rhyolite lava of Cave Creek, J = 0.007213, sample wt = 64 mg							
Latitude:	31°53′26″N.		Longitude:	109°09′25″W.			
500	.48519	.19673	2.466	26.6	16.6	3.7	31.81 ± .20
600	.37072	.16771	2.211	28.0	53.4	3.1	28.54 ± .52
700	.89466	.41087	2.177	31.0	91.2	7.7	28.11 ± .25
800	1.4218	.65488	2.171	32.4	93.5	12.2	28.03 ± .13
850	1.1244	.51623	2.178	32.8	93.6	9.6	28.12 ± .15
900	1.1607	.53686	2.162	32.8	94.2	10.0	27.92 ± .14
950	1.8113	.83389	2.172	29.8	94.9	15.6	28.05 ± .11
1000	2.3568	1.07976	2.183	32.5	95.4	20.2	28.18 ± .11
1050	1.63749	.74934	2.185	29.8	94.1	14.0	28.21 ± .10
1150	.36169	.16462	2.197	16.9	74.5	3.1	28.4 ± .5
1250	.09375	.04219	2.22	18.7	38.7	.8	29. ± 2
Total gas age = 28.26 ± 0.17 Ma							
Plateau age (steps 3-9) = 28.10 ± 0.12 Ma (for 89.3 percent of the gas produced during heating)							
Sample: P475, sanidine from rhyolite of Erickson Ridge, J = 0.007303, sample wt = 62.9 mg							
Latitude:	32°00′25″N.		Longitude:	109°21′58″W.			
850	.0411	.0240	1.713	-----	33.4	.5	22.4 ± 1.0
950	.21870	.09741	2.245	-----	62.3	1.9	29.34 ± .27
1050	.65125	.30046	2.168	-----	79.9	5.8	28.33 ± .22
1150	1.6564	.77897	2.126	-----	96.1	15.1	27.80 ± .05
1200	1.5143	.71406	2.121	-----	96.5	13.8	27.72 ± .05
1250	1.4656	.68496	2.140	-----	97.1	13.2	27.97 ± .12
1300	1.7516	.81850	2.140	-----	97.4	15.8	27.98 ± .05
1350	1.3516	.63031	2.144	-----	97.1	12.2	28.03 ± .18
1400	.92589	.43440	2.131	-----	94.3	8.4	27.86 ± .09
1450	.54858	.25939	2.115	-----	88.3	5.0	27.65 ± .15
1500	.55001	.25775	2.134	-----	83.7	5.0	27.90 ± .24
1550	.32143	.14595	2.202	-----	75.8	2.8	28.78 ± .45
1600	.0533	.0217	2.46	-----	47.5	.4	32. ± 3
1700	.0281	.0058	4.86	-----	30.1	.1	63. ± 5
Total gas age = 27.99 ± 0.13 Ma							
Plateau age (steps 4-9) = 27.89 ± 0.09 Ma (for 78.5 percent of the gas produced during heating)							
Sample: P475, biotite from rhyolite of Erickson Ridge, J = 0.007249, sample wt = 58.3 mg							
Latitude:	32°00′25″N.		Longitude:	109°21′58″W.			
800	.02905	.03459	.840	-----	11.7	.8	11.0 ± .6
900	.13580	.07591	1.789	-----	20.6	1.7	23.2 ± .5
950	.14824	.06720	2.206	-----	50.9	1.5	28.6 ± .7
1000	.20741	.08754	2.369	-----	71.8	1.9	30.7 ± .6
1050	.32763	.14511	2.258	-----	77.9	3.2	29.29 ± .06
1100	.39272	.17782	2.209	-----	80.1	3.9	28.65 ± .16
1150	.35925	.16389	2.192	-----	81.3	3.6	28.44 ± .33
1200	.22424	.10199	2.199	-----	77.6	2.2	28.53 ± .31
1250	.67488	.30564	2.208	-----	83.9	6.7	28.65 ± .09
1300	.93652	.42528	2.202	-----	83.6	9.3	28.57 ± .12
1350	1.3938	.63856	2.183	-----	83.9	13.9	28.32 ± .09
1400	1.8408	.84285	2.184	-----	84.0	18.4	28.34 ± .05
1450	1.5656	.72078	2.172	-----	84.6	15.7	28.18 ± .07
1550	1.7362	.80073	2.168	-----	86.8	17.5	28.13 ± .11
Total gas age = 28.20 ± 0.14 Ma							
Plateau age (steps 11-14) = 28.24 ± 0.08 Ma (for 65.5 percent of the gas produced during heating)							
Sample: P652, sanidine from Jesse James Canyon Tuff, J = 0.007264, sample wt = 69.2 mg							
Latitude:	31°45′05″N.		Longitude:	109°23′51″W.			
850	.0105	.0037	2.86	-----	38.8	.1	37. ± 15
950	.07493	.03117	2.404	-----	89.2	.5	31.2 ± 1.4
1050	.28184	.12708	2.218	-----	54.7	2.2	28.8 ± .4
1150	.61017	.28434	2.146	-----	96.6	5.0	27.90 ± .10
1250	1.3877	.65676	2.113	-----	97.4	11.5	27.48 ± .04
1300	1.2584	.59257	2.124	-----	97.4	10.4	27.62 ± .10
1350	1.5180	.71705	2.117	-----	97.5	12.6	27.53 ± .04
1400	1.5856	.74795	2.120	-----	98.7	13.1	27.57 ± .09
1450	1.6488	.78151	2.110	-----	98.1	13.7	27.44 ± .04
1500	1.7162	.80214	2.139	-----	98.9	14.1	27.82 ± .05
1550	1.7090	.77221	2.213	-----	98.5	13.5	28.77 ± .04
1650	.41918	.18834	2.226	-----	96.6	3.3	28.93 ± .12
Total gas age = 27.85 ± 0.08 Ma							
Plateau age (steps 5-9) = 27.52 ± 0.06Ma (for 61.3 percent of the gas produced during heating)							

Table 3. $^{40}Ar/^{39}Ar$ data for volcanic rocks of the central Chiricahua Mountains.[1/]—Continued

Temp (° C)	$^{40}Ar_R$[2/]	$^{39}Ar_K$[2/]	$^{40}Ar_R/^{39}Ar_K$[2/]	$^{39}Ar/^{37}Ar$[2,3/]	$\%^{40}Ar_R$	$\%^{39}Ar$	Apparent age[4,5/] (Ma at ± 1σ)

Pre-Turkey Creek caldera rocks (continued)

Sample: 201771, sanidine from Jesse James Canyon Tuff, J = 0.007077, sample wt = 82.3 mg
Latitude: 32°00′44″N. Longitude: 109°21′43″W.

950	.11532	.0539	2.138	-----	91.1	.8	27.1 ± 1.0
1050	.53649	.23574	2.276	-----	69.7	3.7	28.82 ± .13
1150	1.1595	.53383	2.172	-----	98.1	8.3	27.52 ± .06
1200	.87493	.40236	2.174	-----	98.3	6.3	27.55 ± .08
1250	1.0288	.47172	2.181	-----	98.2	7.4	27.63 ± .10
1300	.49043	.22584	2.172	-----	95.6	3.5	27.51 ± .04
1350	1.8168	.83416	2.178	-----	98.3	13.0	27.59 ± .04
1400	2.4049	1.10278	2.181	-----	98.6	17.2	27.63 ± .04
1450	2.0050	.91537	2.190	-----	98.9	14.3	27.75 ± .08
1500	1.7793	.81286	2.189	-----	98.7	12.7	27.73 ± .05
1600	1.7859	.81488	2.192	-----	98.2	12.7	27.77 ± .04

Total gas age = 27.69 ± 0.07 Ma
Plateau age (steps 3-8) = 27.59 ± 0.06 Ma (for 55.8 percent of the gas produced during heating)
Isochron age (steps 3-11) = 27.63 ± 0.04 Ma; $(^{40}Ar/^{36}Ar)_I$ = 270 ± 10

Sample: 202156, biotite from tuff of Horseshoe Canyon, J = 0.007167, sample wt = 36.1 mg
Latitude: 31°48′41″N. Longitude: 109°07′54″W.

800	.0011	.0047	.24	-----	1.3	.1	3. ± 13
900	.0959	.0523	1.833	-----	27.9	1.3	23.6 ± .6
1000	.2390	.1209	1.976	-----	39.3	3.0	25.4 ± .8
1050	.2098	.09215	2.276	-----	74.6	2.3	29.3 ± .7
1100	.39023	.17880	2.183	-----	81.5	4.4	28.08 ± .23
1150	.56686	.26338	2.152	-----	85.4	6.6	27.69 ± .13
1200	.87541	.40572	2.158	-----	88.0	10.1	27.76 ± .05
1250	.78254	.36346	2.153	-----	89.0	9.0	27.70 ± .08
1300	.76022	.35360	2.150	-----	86.3	8.8	27.66 ± .05
1350	.89572	.41781	2.144	-----	80.9	10.4	27.58 ± .22
1400	.63020	.29524	2.134	-----	70.8	7.3	27.46 ± .15
1450	.63368	.29453	2.151	-----	63.5	7.3	27.68 ± .04
1600	2.5219	1.1780	2.141	-----	69.7	29.3	27.55 ± .04

Total gas age = 27.53 ± 0.26 Ma
Plateau age (steps 6-13) = 27.62 ± 0.10Ma (for 88.8 percent of the gas produced during heating)

Sample: 202156, sanidine from tuff of Horseshoe Canyon, J = 0.007283, sample wt = 64.1 mg
Latitude: 31°48′41″N. Longitude: 109°07′54″W.

750	.00577	.00112	5.163	-----	8.1	0.0	67. ± 13
850	.47512	.29321	1.620	-----	44.1	4.7	21.16 ± .10
950	1.5388	.85001	1.810	-----	84.9	13.6	23.63 ± .07
1000	.58965	.30905	1.908	-----	74.2	5.0	24.90 ± .08
1050	.74928	.39174	1.913	-----	87.4	6.3	24.96 ± .07
1100	.66632	.34314	1.942	-----	86.6	5.5	25.33 ± .13
1150	.58334	.29686	1.965	-----	82.3	4.8	25.64 ± .14
1200	.56378	.28303	1.992	-----	75.1	4.5	25.98 ± .05
1250	.62872	.31318	2.008	-----	67.7	5.0	26.18 ± .24
1300	.69119	.34868	1.982	-----	62.2	5.6	25.86 ± .24
1350	.71097	.36393	1.954	-----	62.6	5.8	25.49 ± .15
1400	.64823	.33239	1.950	-----	63.5	5.3	25.44 ± .16
1450	.64756	.33920	1.909	-----	63.6	5.4	24.91 ± .21
1500	1.4407	.74702	1.929	-----	64.3	12.0	25.16 ± .08
1600	1.9596	1.0212	1.919	-----	56.4	16.4	25.04 ± .05

No plateau; total gas age =24.91 ± 0.11 Ma
Isochron age (steps 4-15) = 25.42 ± 0.10 Ma; $(^{40}Ar/^{36}Ar)_I$ = 297 ± 4

Sample: 202154, sanidine from dacite sill of Darnell Peak, J = 0.00722, sample wt = 112.5 mg
Latitude: 31°48′32″N. Longitude: 109°08′09″W.

850	.02393	.04891	.489	-----	8.2	.6	6.36 ± .09
900	.33132	.18543	1.787	-----	59.2	2.2	23.12 ± .24
950	.69998	.33580	2.085	-----	91.5	4.0	26.95 ± .11
1000	.88721	.41841	2.120	-----	78.4	5.0	27.41 ± .08
1050	.91390	.43340	2.109	-----	95.5	5.1	27.26 ± .08
1100	1.0905	.51235	2.128	-----	97.3	6.1	27.51 ± .04
1150	1.3174	.61978	2.126	-----	97.6	7.3	27.48 ± .04
1200	1.8225	.85116	2.141	-----	98.5	10.1	27.68 ± .04
1250	2.5723	1.2051	2.135	-----	98.3	14.3	27.59 ± .10
1300	1.6878	.79301	2.128	-----	97.6	9.4	27.51 ± .10
1350	1.4432	.68061	2.121	-----	96.8	8.1	27.41 ± .04
1400	1.1857	.55472	2.137	-----	96.7	6.6	27.63 ± .08
1450	1.0973	.50892	2.156	-----	90.0	6.0	27.87 ± .22
1500	1.8167	.85044	2.136	-----	69.2	10.1	27.61 ± .04
1550	.86657	.39935	2.170	-----	47.4	4.7	28.04 ± .11
1650	.09555	.04191	2.280	-----	21.3	.5	29.46 ± .29

Total gas age = 27.34 ± 0.09 Ma
Plateau age (steps 6-14) = 27.58 ± 0.08 Ma (for 77.9 percent of the gas produced during heating)

Table 3. $^{40}Ar/^{39}Ar$ data for volcanic rocks of the central Chiricahua Mountains.[1/]—Continued

Temp (° C)	$^{40}Ar_R$[2/]	$^{39}Ar_K$[2/]	$^{40}Ar_R/^{39}Ar_K$[2/]	$^{39}Ar/^{37}Ar$[2,3/]	$\%^{40}Ar_R$	$\%^{39}Ar$	Apparent age[4,5/] (Ma at ± 1σ)

Rocks associated with the Turkey Creek caldera

Sample: 201769, sanidine from Rhyolite Canyon Tuff-lower member, J = 0.007129, sample wt = 70.3 mg
Latitude: 32°00′46″N. Longitude: 109°21′46″W.

500	.2131	.1072	1.99	50.6	18.0	1.1	25.4 ± .5
600	.55956	.25904	2.160	81.5	58.1	2.7	27.6 ± .3
700	1.9368	.91631	2.114	101	94.5	9.4	26.98 ± .09
800	4.2472	2.0124	2.110	100	97.8	20.7	26.94 ± .09
850	3.4981	1.6581	2.110	100	98.0	17.0	26.93 ± .08
900	2.7618	1.3112	2.106	103	97.6	13.5	26.89 ± .09
950	2.6773	1.2700	2.108	100	88.9	13.0	26.91 ± .13
1000	1.5311	.7292	2.100	89.9	92.6	7.5	26.81 ± .26
1050	1.9843	.93790	2.116	94.7	95.8	9.6	27.01 ± .11
1150	.93865	.43976	2.134	89.4	91.0	4.5	27.24 ± .15
1300	.16154	.07816	2.067	39.4	60.2	.8	26.4 ± 1.1
1375	.0330	.0158	2.09	6.37	20.5	.2	27. ± 7

Total gas age = 26.94 ± 0.13 Ma
Plateau age (steps 3-9) = 26.93 ± 0.12Ma (for 90.8 percent of the gas produced during heating)

Sample: 201769, sanidine from Rhyolite Canyon Tuff-lower member, J = 0.007172, sample wt = 55.1 mg
Latitude: 32°00′46″N. Longitude: 109°21′46″W.

850	.00011	.00249	0.04	-----	0.0	.1	0. ± 16
950	.11672	.06072	1.922	-----	61.6	1.4	24.7 ± 1.2
1050	.58507	.27485	2.129	-----	75.1	6.4	27.33 ± .04
1100	.76053	.35883	2.119	-----	97.8	8.3	27.22 ± .12
1150	1.2153	.57467	2.115	-----	99.2	13.3	27.16 ± .09
1200	1.2029	.57099	2.107	-----	98.3	13.2	27.05 ± .04
1250	.71461	.34090	2.096	-----	97.3	7.9	26.92 ± .17
1300	1.0934	.52163	2.096	-----	98.2	12.1	26.92 ± .09
1350	1.0051	.47980	2.095	-----	98.2	11.1	26.90 ± .06
1400	.78775	.37560	2.097	-----	96.8	8.7	26.93 ± .10
1450	.72266	.34272	2.109	-----	87.3	7.9	27.08 ± .08
1500	.51758	.24488	2.114	-----	89.5	5.7	27.14 ± .12
1600	.38239	.17886	2.138	-----	91.6	4.1	27.4 ± .5

Total gas age = 27.02 ± 0.56 Ma
Plateau age (steps 6-11) = 26.97 ± 0.09 Ma (for 60.8 percent of the gas produced during heating)
Isochron age (steps 3-13) = 27.09 ± 0.04 Ma; $(^{40}Ar/^{36}Ar)_I = 309 \pm 2$

Sample: DY91-36, sanidine from Rhyolite Canyon Tuff-middle member, J = 0.007115, sample wt = 64.7 mg
Latitude: 31°44′24″N. Longitude: 109°24′06″W.

850	.0069	.0023	3.07	-----	11.8	.1	39. ± 5
950	.11256	.05347	2.105	-----	82.6	1.2	26.8 ± 1.1
1050	.43294	.20245	2.139	-----	71.5	4.6	27.24 ± .18
1150	1.0974	.51373	2.136	-----	98.7	11.8	27.21 ± .07
1200	1.1427	.53753	2.126	-----	98.5	12.3	27.08 ± .06
1250	1.4135	.66592	2.123	-----	98.2	15.2	27.04 ± .10
1300	1.2435	.58527	2.125	-----	98.9	13.4	27.07 ± .04
1350	1.1975	.56797	2.108	-----	98.2	13.0	26.86 ± .15
1400	1.1498	.54152	2.123	-----	98.7	12.4	27.05 ± .14
1450	.80364	.37822	2.125	-----	97.9	8.7	27.07 ± .17
1500	.49925	.23369	2.136	-----	95.7	5.4	27.22 ± .06
1600	.18656	.08566	2.178	-----	89.9	2.0	27.7 ± .6

Total gas age = 27.09 ± 0.12 Ma
Plateau age (steps 5-10) = 27.03 ± 0.11 Ma (for 75.0 percent of the gas produced during heating)
Isochron age (steps 2-11) = 27.14 ± 0.03 Ma; $(^{40}Ar/^{36}Ar)_I = 297 \pm 2$

Sample: 201765, sanidine from Rhyolite Canyon Tuff-upper member, J = 0.007111, sample wt = 61.3 mg
Latitude: 32°00′47″N. Longitude: 109°19′23″W.

500	.11023	.05888	1.87	31.9	6.5	.7	23.9 ± 1.2
600	.25977	.12202	2.129	44.2	36.0	1.5	27.1 ± .4
700	1.1332	.53671	2.111	54.0	82.9	6.5	26.88 ± .19
800	2.0009	.94622	2.115	54.5	92.6	11.4	26.93 ± .14
850	2.0728	.97892	2.117	53.5	94.5	11.8	26.96 ± .13
900	1.9046	.89961	2.117	53.1	95.3	10.8	26.96 ± .14
950	2.4967	1.1773	2.121	53.7	95.4	14.2	27.00 ± .08
1000	2.4659	1.1679	2.111	56.0	95.6	14.1	26.88 ± .08
1050	3.6877	1.7425	2.116	57.2	96.6	21.0	26.95 ± .07
1150	1.2413	.58051	2.138	53.7	91.2	7.0	27.22 ± .15
1250	.17004	.08177	2.08	32.8	57.5	1.0	26.5 ± .8

Total gas age = 26.94 ± 0.13 Ma
Plateau age (steps 3-9) = 26.94 ± 0.12 Ma (for 89.8 percent of the gas produced during heating)

Table 3. $^{40}Ar/^{39}Ar$ data for volcanic rocks of the central Chiricahua Mountains.[1/]—Continued

Temp (° C)	$^{40}Ar_R$ [2/]	$^{39}Ar_K$ [2/]	$^{40}Ar_R/^{39}Ar_K$ [2/]	$^{39}Ar/^{37}Ar$ [2,3/]	$\%^{40}Ar_R$	$\%^{39}Ar$	Apparent age [4,5/] (Ma at ± 1σ)
Rocks associated with the Turkey Creek caldera (continued)							
Sample: 201765, sanidine from Rhyolite Canyon Tuff-upper member, J = 0.007262, sample wt = 110.8 mg							
Latitude: 32°00′47″N.			Longitude: 109°19′23″W.				
850	.0304	.0155	1.96	-----	10.7	.2	26. ± 4
950	.11556	.05246	2.203	-----	38.1	.7	28.63 ± .92
1050	.36519	.17234	2.119	-----	62.5	2.2	27.55 ± .04
1150	.99459	.47862	2.078	-----	90.7	6.1	27.02 ± .18
1200	1.0537	.51024	2.065	-----	94.1	6.5	26.85 ± .09
1250	1.3150	.63665	2.065	-----	95.0	8.1	26.86 ± .10
1300	1.5626	.76140	2.052	-----	95.8	9.7	26.69 ± .04
1350	2.4327	1.1826	2.057	-----	97.5	15.0	26.75 ± .04
1400	2.3763	1.1468	2.072	-----	98.4	14.5	26.94 ± .07
1450	2.4623	1.1872	2.074	-----	98.4	15.0	26.97 ± .06
1500	1.7665	.84937	2.080	-----	97.7	10.8	27.04 ± .05
1550	1.4424	.69194	2.085	-----	96.8	8.8	27.10 ± .04
1650	.42926	.20363	2.108	-----	86.9	2.6	27.41 ± .08
No plateau; total gas age = 26.94 ± 0.08 Ma							
Isochron age (steps 3-13) = 26.98 ± 0.04 Ma; $(^{40}Ar/^{36}Ar)_I = 309 \pm 2$							
Sample: P3, sanidine from dacite porphyry lava, J = 0.007123, sample wt = 67.1 mg							
Latitude: 31°55′31″N.			Longitude: 109°16′22″W.				
500	.10369	.04227	2.453	4.76	5.9	.5	31.2 ± .9
600	.51280	.22671	2.262	.96	40.7	2.6	28.8 ± .3
700	.87410	.40221	2.173	4.90	76.9	4.7	27.7 ± .3
800	1.38411	.64407	2.149	11.3	85.4	7.5	27.41 ± .13
850	1.57630	.73405	2.147	14.6	81.9	8.5	27.38 ± .14
900	1.39669	.65051	2.147	18.9	79.1	7.6	27.38 ± .13
950	2.53404	1.19844	2.114	21.7	72.9	13.9	26.97 ± .13
1000	3.07313	1.44533	2.126	19.4	74.9	16.8	27.12 ± .08
1050	4.92151	2.27911	2.159	23.1	78.3	26.5	27.54 ± .08
1150	1.93264	.82957	2.330	17.8	65.4	9.6	29.69 ± .12
1250	.36452	.15550	2.344	7.66	43.0	1.8	29.9 ± .5
Total gas age = 27.66 ± 0.12 Ma; no plateau							
T_{min} = 26.97 ± 0.13 Ma (950°C); isochron age = 27.44 ± 0.15 Ma; $(^{40}Ar/^{36}Ar)_I = 303 \pm 2$							
Sample: 201587, sanidine from dacite porphyry of resurgent intrusion, J = 0.00712, sample wt = 82.9 mg							
Latitude: 31°52′25″N.			Longitude: 109°22′04″W.				
500	.57035	.27009	2.112	20.2	25.1	2.2	26.9 ± .4
600	.79823	.37890	2.107	14.9	60.0	3.1	26.86 ± .15
700	1.8771	.89706	2.092	14.7	85.0	7.3	26.68 ± .10
800	3.1487	1.49111	2.112	22.4	92.6	12.1	26.92 ± .09
850	2.1960	1.03651	2.119	27.4	92.0	8.4	27.01 ± .10
900	1.33200	.62910	2.117	26.0	91.4	5.1	26.99 ± .11
950	2.4557	1.17063	2.098	20.3	87.6	9.5	26.75 ± .08
1000	4.0596	1.94263	2.090	18.0	85.8	15.7	26.64 ± .07
1050	8.4536	4.01325	2.106	19.8	88.3	32.5	26.86 ± .07
1150	.8959	.42092	2.129	8.03	78.7	3.4	27.13 ± .21
1250	.23026	.10900	2.112	5.83	63.8	.9	26.9 ± .6
No plateau; total gas age = 26.84 ± 0.09 Ma; weighted mean age (all steps) = 26.84 ± 0.17 Ma							
Isochron age (all steps) = 26.90 ± 0.04 Ma; $(^{40}Ar/^{36}Ar)_I = 296 \pm 2$							
Sample: 201996, sanidine from biotite rhyolite lava, J = 0.007278, sample wt = 121.7 mg							
Latitude: 31°56′19″N.			Longitude: 109°19′15″W.				
850	.16089	.08517	1.889	-----	20.4	.7	24.63 ± .20
950	.28121	.13080	2.150	-----	52.1	1.1	28.01 ± .41
1050	.70405	.33878	2.078	-----	75.6	3.0	27.08 ± .04
1100	.86402	.42025	2.056	-----	91.1	3.7	26.79 ± .17
1150	1.0600	.5218	2.031	-----	93.6	4.6	26.47 ± .12
1200	1.8335	.8949	2.049	-----	96.4	7.8	26.70 ± .04
1250	2.5035	1.2220	2.049	-----	96.3	10.7	26.70 ± .04
1300	2.7035	1.3184	2.051	-----	97.2	11.5	26.72 ± .04
1350	2.37204	1.1574	2.050	-----	97.0	10.1	26.71 ± .12
1400	2.9481	1.4344	2.055	-----	96.1	12.5	26.78 ± .04
1450	3.0153	1.4667	2.056	-----	96.8	12.8	26.79 ± .04
1500	3.4135	1.6531	2.065	-----	97.6	14.5	26.91 ± .04
1550	1.3569	.65337	2.077	-----	94.7	5.7	27.06 ± .05
1650	.29582	.13464	2.197	-----	73.2	1.2	28.62 ± .27
Total gas age = 26.80 ± 0.06 Ma							
Plateau age (steps 6-11) = 26.74 ± 0.05 Ma (for 65.6 percent of the gas produced during heating)							

Table 3. $^{40}Ar/^{39}Ar$ data for volcanic rocks of the central Chiricahua Mountains.[1/]—Continued

Temp (° C)	$^{40}Ar_R$ [2/]	$^{39}Ar_K$ [2/]	$^{40}Ar_R/^{39}Ar_K$ [2/]	$^{39}Ar/^{37}Ar$ [2,3/]	$\%^{40}Ar_R$	$\%^{39}Ar$	Apparent age [4,5/] (Ma at ± 1σ)
Rocks associated with the Turkey Creek caldera (continued)							
Sample: 201996, biotite from biotite rhyolite lava, J = 0.007148, sample wt = 74.4 mg							
Latitude:	31°56′19″N.		Longitude:	109°19′15″W.			
800	.0684	.0265	2.587	-----	26.1	.4	33. ± 2
900	.0999	.0340	2.935	-----	42.9	.6	37.4 ± 1.0
950	.0328	.0167	1.967	-----	13.8	.3	25. ± 3
1000	.0546	.0207	2.640	-----	20.9	.3	33.7 ± .6
1050	.0946	.04424	2.139	-----	62.2	.7	27. ± 2
1100	.27051	.12193	2.219	-----	84.3	2.0	28.38 ± .10
1150	.42437	.19741	2.150	-----	89.7	3.3	27.51 ± .13
1200	.60224	.28319	2.127	-----	92.3	4.7	27.22 ± .09
1250	.95712	.45167	2.119	-----	94.0	7.5	27.12 ± .08
1300	1.5605	.74214	2.103	-----	93.7	12.3	26.91 ± .06
1350	1.8422	.87078	2.116	13.6	91.3	14.5	27.08 ± .04
1400	2.9339	1.3834	2.121	83.3	87.8	23.0	27.14 ± .04
1450	2.2666	1.0724	2.114	33.1	85.9	17.8	27.05 ± .04
1550	1.5975	.75188	2.125	-----	91.4	12.5	27.19 ± .10
Total gas age = 27.24 ± 0.10 Ma							
Plateau age (steps 11-14) = 27.11 ± 0.06 Ma (for 67.8 percent of the gas produced during heating)							
Isochron age = 26.71 ± 0.02 Ma; $(^{40}Ar/^{36}Ar)_i = 366 \pm 15$							
Sample: 201538, sanidine from rhyolite moat lava-unit 1, J = 0.007168, sample wt = 51.6 mg							
Latitude:	31°52′24″N.		Longitude:	109°17′00″W.			
500	.33103	.15699	2.109	7.95	9.6	2.2	27.1 ± .6
600	.46422	.22179	2.093	13.5	40.6	3.1	26.9 ± .3
700	1.2383	.58556	2.115	19.1	80.1	8.2	27.14 ± .14
800	1.7972	.85737	2.096	23.3	90.2	12.1	26.90 ± .12
850	1.8730	.88533	2.116	23.0	90.8	12.4	27.15 ± .16
900	1.2565	.60105	2.090	23.7	90.8	8.5	26.83 ± .09
950	2.0174	.97148	2.077	21.6	92.1	13.7	26.66 ± .10
1000	2.6956	1.2888	2.091	23.7	95.0	18.1	26.84 ± .10
1050	2.4154	1.1484	2.103	23.3	94.0	16.1	26.99 ± .09
1150	.73347	.34740	2.111	23.6	62.6	4.9	27.10 ± .12
1300	.1081	.0477	2.266	20.9	25.0	.7	29. ± 2
No plateau, total gas age = 26.94 ± 0.13 Ma; weighted mean age (steps 1-10) = 26.93 ± 0.17 Ma							
Isochron age = 26.89 ± 0.05 Ma; $(^{40}Ar/^{36}Ar)_i = 298 \pm 1$							
Sample: 201580, sanidine from rhyolite moat lava-unit 1, J = 0.007143, sample wt = 57.3 mg							
Latitude:	31°55′20″N.		Longitude:	109°17′39″W.			
500	.27438	.11329	2.422	7.96	13.6	1.7	30.94 ± .47
600	.47682	.23254	2.050	6.49	52.9	3.4	26.23 ± .22
700	1.2090	.58283	2.074	8.11	90.6	8.6	26.53 ± .08
800	1.5634	.74834	2.089	11.0	94.3	11.1	26.72 ± .15
850	1.8546	.88798	2.089	14.0	95.8	13.2	26.71 ± .09
900	1.5144	.73336	2.065	15.8	94.9	10.9	26.41 ± .23
950	1.5239	.73312	2.079	15.2	94.2	10.9	26.59 ± .12
1000	2.9275	1.40960	2.077	16.2	96.5	20.9	26.57 ± .08
1050	2.0132	.96080	2.095	16.3	95.1	14.2	26.80 ± .09
1150	.63156	.30099	2.098	8.83	83.8	4.5	26.84 ± .18
1250	.0872	.0432	2.02	5.28	40.7	.6	26. ± 1
Total gas age = 26.69 ± 0.13 Ma							
Plateau age (steps 3-10) = 26.64 ± 0.13 Ma (for 94.2 percent of the gas produced during heating)							
Post-Turkey Creek caldera rocks							
Sample: DY92-54, sanidine from rhyolite lava, J = 0.007237, sample wt = 74.5 mg							
Latitude:	31°42′10″N.		Longitude:	109°29′50″W.			
850	.0134	.0056	2.40	-----	14.7	.1	31. ± 6
950	.13173	.06109	2.156	-----	89.0	.9	28. ± 2
1050	.57428	.27719	2.072	-----	74.8	4.2	26.85 ± .18
1150	1.0428	.51297	2.033	-----	97.6	7.8	26.35 ± .05
1200	1.0567	.52834	2.000	-----	96.8	8.0	25.92 ± .07
1250	1.1476	.56920	2.016	-----	97.7	8.6	26.13 ± .18
1300	1.6901	.83390	2.027	-----	98.5	12.7	26.27 ± .09
1350	1.5556	.76632	2.030	-----	99.0	11.6	26.31 ± .04
1400	1.3902	.68581	2.027	-----	98.8	10.4	26.27 ± .10
1450	1.2786	.62862	2.034	-----	98.9	9.6	26.36 ± .10
1500	1.4064	.68959	2.039	-----	98.9	10.5	26.43 ± .06
1550	1.4905	.73136	2.038	-----	98.2	11.1	26.41 ± .06
1650	.60600	.29152	2.079	-----	95.7	4.4	26.94 ± .06
Total gas age = 26.36 ± 0.10 Ma							
Plateau age (steps 7-12) = 26.35 ± 0.08 Ma (for 65.9 percent of the gas produced during heating)							

Table 3. $^{40}Ar/^{39}Ar$ data for volcanic rocks of the central Chiricahua Mountains.[1/]—Continued

Temp (° C)	$^{40}Ar_R$ [2/]	$^{39}Ar_K$ [2/]	$^{40}Ar_R/^{39}Ar_K$ [2/]	$^{39}Ar/^{37}Ar$ [2,3/]	$\%^{40}Ar_R$	$\%^{39}Ar$	Apparent age [4,5/] (Ma at ± 1σ)
Post-Turkey Creek caldera rocks (continued)							
Sample: 202151, sanidine from rhyolite lava of Dobson Peak, J = 0.00702, sample wt = 66.7 mg							
Latitude:	31°46′36″N.		Longitude:	109°13′51″W.			
850	.0016	.0037	.42	-----	2.8	.1	5. ± 8
950	.28556	.14540	1.964	-----	82.7	2.2	24.70 ± .36
1050	.87253	.42507	2.053	-----	77.4	6.4	25.81 ± .18
1150	1.1464	.55507	2.065	-----	97.0	8.4	25.97 ± .06
1200	1.1399	.54601	2.088	-----	97.7	8.3	26.25 ± .11
1250	1.2690	.61365	2.068	-----	97.2	9.3	26.00 ± .10
1300	1.4994	.71792	2.089	-----	98.3	10.9	26.26 ± .10
1350	1.5883	.76260	2.083	-----	98.8	11.6	26.19 ± .04
1400	1.6971	.81162	2.091	-----	99.1	12.3	26.29 ± .04
1450	1.4332	.68728	2.085	-----	98.5	10.4	26.22 ± .04
1500	1.1885	.56667	2.097	-----	98.4	8.6	26.37 ± .06
1600	1.5862	.75997	2.087	-----	95.0	11.5	26.24 ± .05
Total gas age = 26.13 ± 0.10 Ma							
Plateau age (steps 5-10) = 26.20 ± 0.07 Ma (for 62.8 percent of the gas produced during heating)							
Sample: P5, sanidine from rhyolite of Packsaddle Mountain, J = 0.006809, sample wt = 95 mg							
Latitude:	32°36′45″N.		Longitude:	109°25′20″W.			
850	.00712	.00282	2.524	5479.74	17.5	0.0	30.74 ± 19.84
850	.0071	.0028	2.52	-----	17.5	0.0	31. ± 20
950	.18435	.10729	1.718	-----	62.8	1.4	20.98 ± .22
1050	.56527	.29758	1.900	-----	69.4	4.0	23.18 ± .07
1150	1.1616	.61307	1.895	-----	95.0	8.3	23.13 ± .09
1200	.77133	.40730	1.894	-----	95.1	5.5	23.11 ± .09
1250	.91981	.48465	1.898	-----	95.6	6.5	23.16 ± .11
1300	.72999	.37911	1.926	-----	97.2	5.1	23.50 ± .10
1350	.80739	.42362	1.906	-----	97.2	5.7	23.26 ± .07
1400	.87471	.45882	1.906	-----	97.3	6.2	23.27 ± .06
1450	1.1131	.58198	1.913	-----	97.5	7.8	23.34 ± .10
1500	1.7836	.94134	1.895	-----	96.2	12.7	23.13 ± .05
1550	4.6120	2.42217	1.904	-----	96.9	32.6	23.24 ± .04
1600	.48109	.25010	1.924	-----	91.1	3.4	23.47 ± .06
1650	.12014	.05782	2.08	-----	87.6	.8	25.3 ± .7
Total gas age = 23.22 ±0.08 Ma							
Plateau age (steps 8-12) = 23.23 ± 0.06 Ma (for 65.0 percent of the gas produced during heating)							

[1/] Mineral separates were prepared after crushing, grinding, and sieving by magnetic separator, mica-table, and heavy liquid methods; grains ranged in size between 60 and 120 mesh (250-125 μm). Individual samples ranged in mass from 36 to 416 mg. For irradiation an aluminum canister was loaded with six quartz vials each of which was loaded with samples and standards. Standards were placed between every two unknowns as well as at the top and bottom of each vial. Each standard was degassed to release argon in a single 20-minute long heating step at 1,250°C. Each sample was degassed stepwise in a series of 11 to 16 individual temperature steps for 20 minutes each. All analyses were done in the Argon Laboratory, U.S. Geological Survey, Denver, Colo. Decay constants are those of Steiger and Jäger (1977). The standard for these experiments is hornblende MMhb-1 with percent K=1.555, $^{40}Ar_R$ =1.624x10^{-9} mole/g, and K-Ar age = 520.4 Ma (Samson and Alexander, 1987).

[2/] Abundances of "Radiogenic ^{40}Ar" and "K-derived ^{39}Ar" are reported in volts measured on a Mass Analyser Products 215 rare-gas mass spectrometer using the Faraday cup. Conversion to moles can be made using a sensitivity of 9.736x10^{-13} moles argon per volt of signal. Detection limit at the time of this experiment was 2x10^{-17} moles argon. Corrections were made for volume, mass fractionation, trap current, radioactive decay of ^{37}Ar and ^{39}Ar, and interfering Ar isotopes. Mass discrimination in our mass spectrometer is routinely determined by measuring the $^{40}Ar/^{36}Ar$ ratio of atmospheric argon; our measured value is generally 298.9 the accepted value is 295.5. The calculated discrimination is applied to all samples and standards equally. Production ratios measured on pure K_2SO_4 and CaF_2 salts irradiated with the samples were used to correct for irradiation-produced ^{40}Ar (from K) and ^{39}Ar (from Ca). Corrections for Cl-derived ^{36}Ar were determined using the method of Roddick (1983). Production ratios determined for samples irradiated in the 1995 TRIGA reactor experiment are: $(^{40}Ar/^{39}Ar)_K$= 7.92x10^{-3}, $(^{38}Ar/^{39}Ar)_K$ = 1.309x10^{-2}, $(^{37}Ar/^{39}Ar)_K$ =1.8x10^{-4}, $(^{36}Ar/^{37}Ar)_{Ca}$ = 2.68x10^{-4}, $(^{39}Ar/^{37}Ar)_{Ca}$ = 6.85x10^{-4}, $(^{38}Ar/^{37}Ar)_{Ca}$ = 4.4x10^{-5}. Production ratios were not directly determined for samples irradiated in 1988; ratios suggested by Dalrymple and others (1981) were used. Analytical data for "Radiogenic ^{40}Ar" and "K-derived ^{39}Ar" are calculated to five places; "$^{40}Ar_R/^{39}Ar_K$" is calculated to three decimal places. "Radiogenic ^{40}Ar", "K-derived ^{39}Ar", and "$^{40}Ar_R/^{39}Ar_K$" are rounded to significant figures using associated analytical precisions. Apparent ages and associated errors were calculated from unrounded data and then rounded using associated errors. -----, ^{37}Ar below detection; no ratio calculated.

[3/] To calculate apparent K/Ca ratios, divide $^{39}Ar/^{37}Ar$ value by 2.

[4/] Uncertainties in calculations for the apparent date of individual steps for a sample were calculated using the equations of Dalrymple and others (1981).

[5/] The reproducibility of split gas fractions from selected monitors was used to calculate imprecision in J values This imprecision is generally 0.1%, 1 sigma. J values for each sample were interpolated from adjacent standards. The uncertainty in each apparent age includes the uncertainty in the J value.

tuff by the latite of Darnell Peak (Bryan, 1988), as described previously, for which our determined age is 26.58±0.08 Ma. The age of the upper member of the tuff of Horseshoe Canyon has not been determined, although its age is bracketed between the ages of the latite of Darnell Peak (27.6 Ma), which intrudes the tuff, and that of the overlying Rhyolite Canyon Tuff (26.9 Ma).

Rocks Associated with the Turkey Creek Caldera

Several previous attempts have been made to accurately establish the age of the Rhyolite Canyon Tuff. Drewes (1982) summarized earlier K-Ar age determinations reported by Marjaniemi (1969) and Marvin and others (1978) for parts of the Rhyolite Canyon Tuff. These ages range from about 24.7 to 25.6 Ma, and are all young relative to new $^{40}Ar/^{39}Ar$ data presented herein. McIntosh and Bryan (2000) reported three $^{40}Ar/^{39}Ar$ ages for the Rhyolite Canyon Tuff and have established their preferred age as 26.8 Ma. We determined the ages of all three of the volumetrically significant members of outflow facies Rhyolite Canyon Tuff using the $^{40}Ar/^{39}Ar$ method.

Sample 201769 (fig. 1, locality B) represents the lower member of the Rhyolite Canyon Tuff. Two splits of this sanidine separate, as well as of the sanidine separate that represents the upper member (201765; fig. 1, locality D), were analyzed several years apart in order to evaluate the reproducibility of ages determined during the several years that geochronologic investigations were conducted. Both age spectra for sample 201769 are simple (fig. 11*S* and *T*) and give statistically indistinguishable plateau ages of 26.97±0.09 and 26.93±0.12 Ma, respectively. An isochron age for one yields a statistically identical age of 27.09±0.04 Ma with a slightly elevated $(^{40}Ar/^{36}Ar)_I$ of 309±2. The average of the two sanidine ages, 26.95±0.07 Ma, is our preferred age for the lower member of the Rhyolite Canyon Tuff.

Sample DY91-36 (fig. 1, locality Q) represents the middle member of the Rhyolite Canyon Tuff. The age spectrum for sanidine from this sample is simple (fig. 11*U*) and gives a plateau age of 27.03±0.11 Ma. Sample 201765 (fig. 1, locality D) represents the upper member of the Rhyolite Canyon Tuff; as just indicated, two splits of this separate were analyzed. The age spectrum for one of these splits (fig. 11*V*) shows some evidence of excess argon, particularly in the low-temperature steps, is broadly U-shaped, and does not include a plateau age; the isochron age for this split is 26.98±0.04 Ma with $(^{40}Ar/^{36}Ar)_I$ = 309±2, which reflects the presence of minor excess argon. The spectrum for the other split (fig. 11*W*) is simple and gives a plateau age of 26.94±0.12 Ma. The ages for the two splits are statistically indistinguishable, and their average, 26.96±0.06 Ma, is our preferred age for the upper member of the Rhyolite Canyon Tuff. Data for two splits each of samples 201765 and 201769 indicate that variation of analytical data acquired over several years has not adversely impacted analytical precision or accuracy. The five analyses of sanidine from Rhyolite Canyon Tuff indicate that, within analytical uncertainty, each of the principal ash-flow tuffs that constitute this unit is the same age and that they must have been erupted in rapid succession. The absence of erosional breaks or other significant discontinuities between the members further indicates rapid eruption and emplacement of these pyroclastic flows.

Samples 201587 and P3 (fig. 1, localities J and H, respectively) represent dacite porphyry that was emplaced, after eruption of the Rhyolite Canyon Tuff and caldera collapse, as a resurgent intrusion in the core of the Turkey Creek caldera (201587) and as lava flows in the caldera's evolving moat (P3). The age spectrum for sanidine for sample 201587 is slightly disturbed (fig. 11*X*) and does not yield a plateau. The weighted average age for this sample is 26.84±0.17 Ma and the isochron age is 26.90±0.04 Ma with $(^{40}Ar/^{36}Ar)_I$ = 296±2. The age spectrum for sanidine from sample P3 is also disturbed (fig. 11*Y*), shows some evidence of excess argon, and does not yield a plateau. The isochron age for this sample is 27.44±0.15 Ma with an elevated $(^{40}Ar/^{36}Ar)_I$ = 303±2. The characteristic saddle-shaped spectrum results from the presence of excess argon. Others (Lanphere and Dalrymple, 1976) have interpreted the age of the lowest age step defining the saddle to best represent a maximum age estimate. In this case, the lowest age step in the saddle is 26.97±0.13 Ma, which is indistinguishable from the age of sanidine from sample 201587. Given this assessment of the $^{40}Ar/^{39}Ar$ data for samples of the dacite porphyry, our best estimate of its age is 26.90±0.04 Ma, which is the isochron age for sample 201587. These age data indicate that dacite porphyry intrusion and extrusion followed Rhyolite Canyon Tuff eruption and caldera collapse within less than 100,000 years, which is consistent with dacite porphyry lava flows being interbedded with lava-flow-like phase intracaldera Rhyolite Canyon Tuff in exposures north and west of John Long Canyon (fig. 1) (du Bray and others, 1997).

Sample 201996 (fig. 1, locality F) represents the biotite rhyolite lava, the first of the rhyolite lavas erupted into the moat of the Turkey Creek caldera; both biotite and sanidine separates were analyzed. The age spectrum for biotite from this sample is relatively simple (fig. 11*Z*), although it shows some evidence of excess argon in the low-temperature steps. It gives a plateau age of 27.11±0.06 Ma and an isochron age of 26.71±0.02 Ma with a significantly enhanced $(^{40}Ar/^{36}Ar)_I$ of 366±15. The plateau age is implausible given the well-defined 26.9 Ma age for Rhyolite Canyon Tuff on which this rhyolite was deposited; the isochron age is more geologically reasonable. The age spectrum for sanidine from this sample is relatively simple (fig. 11*AA*), although it also shows some slight evidence of excess argon; it gives a plateau age of 26.74±0.05 Ma. This age is consistent with the 26.9 Ma age for Rhyolite Canyon Tuff and 26.9 Ma dacite porphyry on which the rhyolite was deposited.

Samples 201538 and 201580 (fig. 1, localities K and G) represent unit 1 rhyolite lava (Tmr1) in the moat of the Turkey Creek caldera; a sanidine separate from each of these

samples was analyzed. The age spectrum for sanidine from sample 201538 is relatively simple (fig. 11*BB*) but is disturbed and does not include a plateau; it gives a weighted-mean age of 26.93±0.17 Ma and an isochron age of 26.89±0.05 Ma with $(^{40}Ar/^{36}Ar)_I$ of 298±1. This apparent age is slightly too old to be consistent with the 26.7 Ma age of the biotite rhyolite on which unit 1 rhyolite was deposited. The age spectrum for sanidine from sample 201580 is relatively simple (fig. 11*CC*), although it shows some evidence of excess argon in the low-temperature steps; it gives a plateau age of 26.64±0.13 Ma. This age seems slightly too young given that this sample is from the same unit as sample 201538 (26.9 Ma). Averaging the isochron age for sample 201538 and the plateau age for sample 201580 yields a preferred age of 26.77±0.12 Ma for unit 1 lava. Given the analytical uncertainties associated with the ages determined for the biotite rhyolite (201967) and the unit 1 lava (201538 and 201580), all of these ages are statistically indistinguishable. Perhaps the best reconciliation of the $^{40}Ar/^{39}Ar$ data for the rhyolite moat sequence would result in an age estimate of 26.7 Ma for the biotite rhyolite and unit 1 lava. Because units 2 and 3 lavas—the final rhyolite lavas erupted into the moat of the Turkey Creek caldera—are so crystal poor, no mineral separates could be prepared and their ages were not determined. Consequently, the full duration of volcanism associated with the caldera cannot be closely defined. However, the lack of significant erosional/depositional break indicates that these moat lavas were erupted in a relatively short time interval, perhaps as little as 10,000 years.

Post-Turkey Creek Caldera Rocks

Sample 202151 (fig. 1, locality N) represents the rhyolite lava of Dobson Peak, which is the youngest volumetrically significant volcanic unit in the central Chiricahua Mountains. The age spectrum for sanidine from this sample is relatively simple (fig. 11*DD*) and gives a plateau age of 26.20±0.07 Ma. Because this unit overlies unit 1 lava, the youngest rocks associated with Turkey Creek caldera volcanism must be at least this old. Consequently, the full eruptive cycle associated with the Turkey Creek caldera lasted no more than 700,000 years, from 26.9 to no less than 26.2 Ma, and all middle Tertiary volcanic activity in the central Chiricahua Mountains apparently ended about 26.2 Ma.

Concluding Remarks

Geochemical and petrographic data presented here show that volcanic units of the central Chiricahua Mountains are individually distinctive. These data can be used to corroborate stratigraphic identifications made with other data; they can also be used to identify units when either available data are insufficient or stratigraphic context is absent or ambiguous. Diagnostic age, petrographic, and geochemical features for middle Tertiary volcanic rocks of the region are summarized in table 4. In many cases, macroscopically observable features of the area's volcanic rocks, including contained phenocrysts (mineral, size, and abundance), textures (degree of welding or flow features), and (or) lithic or pumice content (size, number, and composition), are sufficient to enable rapid, field-based stratigraphic identification. When these features are insufficient, other simple techniques, such as transmitted light microscopy, can in many cases be used to rapidly eliminate uncertainties. When more detailed data are required to determine or confirm stratigraphic identity, geochemical, geochronologic, or paleomagnetic data may be necessary. Of these, geochemical data, especially trace-element data obtained by energy-dispersive X-ray fluorescence analysis of rock powders, are probably the least expensive and most rapidly obtainable type of data for establishing stratigraphic identity. Trace-element data demonstrate that almost all the stratigraphic units of this area have characteristic geochemical features diagnostic of their stratigraphic identity. Combining geochemical data with macroscopically observable rock features results in virtually certain identification of the study area rocks, which enhances correlation of isolated or ambiguous occurrences of these rocks throughout the Boot Heel volcanic field.

The preponderant volume of volcanic rock preserved in the range is ash-flow tuff, although a significant volume of lava is present as well. The overwhelmingly dominant source of volcanic rocks preserved in the area is the Turkey Creek caldera. Between 500 and 1,000 km^3 of Rhyolite Canyon Tuff is present, and approximately 60 km^3 of caldera-related rhyolite lava is preserved in the caldera's moat. Middle Tertiary volcanic activity is dominated by eruption of subalkaline rhyolite, most of which is high silica and weakly peraluminous. One of the most diagnostic compositional features of these rocks is their elevated K_2O abundances. All of the area's volcanic rocks are members of either the high-potassium calc-alkaline or the shoshonitic series. Volcanic rock within-stratigraphic-unit compositions are relatively homogeneous. The principal exception to this is among the voluminous outflow facies ash-flow tuffs, in which there is considerable compositional inhomogeneity. Sections of the Rhyolite Canyon Tuff and the tuff of Horseshoe Canyon are relatively strongly zoned in ways that appear to reflect progressive, top-down tapping of normally zoned magma reservoirs. Most of the observed zonation is consistent with crystal-liquid fractionation of the phenocryst phases that are characteristic of each unit. Compositional variation within lavas is relatively minor.

Compositional variation among eruptive products of the Turkey Creek caldera reflects a contrast between magmatic processes in the reservoirs that produced the normally zoned Rhyolite Canyon Tuff and those that subsequently produced the reversely zoned moat rhyolite sequence. As described in previous sections, geochemical zonation preserved within the principal outflow facies members of the Rhyolite Canyon Tuff is consistent with systematic magma extraction from a normally zoned reservoir. Considering the geochemical characteristics of these rocks, the phenocrysts they contain,

Table 4. Diagnostic age, petrographic, and geochemical features of middle Tertiary volcanic rocks of the central Chiricahua Mountains.

[ND, not determined]

Unit	Unit symbol	Age, in Ma	Petrographic characteristics	Geochemical characteristics
Pre-Turkey Creek caldera rocks				
Intermediate-composition lava flows.	Tim	ND	Dark greenish gray. Plagioclase, hornblende and pyroxene phenocrysts. Variable crystal content.	Dacite with high FeO*, MgO, CaO, TiO_2, P_2O_5, Sr, Ba, Eu, Co, Ni, Cr, and low Rb, Nb, and Ta.
Rhyolite tuff of High Lonesome Canyon.	Thl	34.16±0.17	Quartz and sanidine phenocrysts; 5 percent crystals. Pumice and lithic poor.	Unusually low Zr and Na_2O relative to other study area rhyolite tuffs.
Lower member of the rhyolite of Joe Glenn Ranch.	Tjg	33.81±0.08	Biotite, feldspar, and quartz phenocrysts; 20-40 percent crystal.	Higher FeO*, TiO_2, and Ba and lower Nb abundances than other study area rhyolite tuffs.
Rhyolite lava of Krentz Ranch.	Tkr	ND	Aphyric. Massive to flow banded	Low Nb abundances relative to other aphyric rhyolite lavas.
Rhyolite lava of Cave Creek.	Tc	28.10±0.12	Aphyric. Massive to flow banded	Low Nb abundances relative to other aphyric rhyolite lavas.
Rhyolite of Erickson Ridge.	Tfre	27.89±0.09	Biotite and feldspar phenocrysts; 4-10 percent crystals.	Low-silica rhyolite with high FeO*, CaO, Sr, Ba and Eu and low Rb, Ta, Th, and U abundances.
Tuff of Horseshoe Canyon lower member.	Thcl	27.62±0.10	Biotite, quartz, and sanidine phenocrysts; 20-35 percent crystals.	High K_2O, Ba, and Eu and low Zr, Nb, and Th abundances relative to other study area rhyolite tuffs.
Tuff of Horseshoe Canyon upper member.	Thcu	ND	Biotite, quartz, and sanidine phenocrysts; 10-20 percent crystals.	High Al_2O_3, FeO*, TiO_2, P_2O_5, Sr, Zr, Ba, Co, Ni, Cr, Sc, Hf, and Eu and low SiO_2, Ta, U, and Th abundances relative to other study area rhyolite tuffs.
Jesse James Canyon Tuff.	Tjj	27.56±0.04	Biotite, sanidine and quartz phenocrysts; 10 percent crystals.	Low FeO*, Zr, Ta, Th, and Hf abundances relative to other rhyolite tuffs of the study area. Low abundances of K_2O, Rb, Ba, and Eu distinguish it from Thcl.
Rocks associated with the Turkey Creek caldera				
Rhyolite Canyon Tuff basal member.	Trcb	ND	Sanidine and quartz phenocrysts; 7-35 percent crystals.	High Zr, Nb, Ta, U, Th, and Hf abundances relative to all study area tuffs. High SiO_2, Rb, Nb, and Ta and low TiO_2, Zr, Ba, and La abundances relative to Trcu, Trci, and Trcf. High K_2O and Rb abundances relative to Trcl and Trcm.
Rhyolite Canyon Tuff lower member.	Trcl	26.95±0.07	Sanidine and quartz phenocrysts; 7-35 percent crystals.	High Zr, Nb, Ta, U, Th, and Hf abundances relative to all study area tuffs. High SiO_2, Rb, Nb, and Ta and low TiO_2, Zr, Ba, and La abundances relative to Trcu, Trci, and Trcf.
Rhyolite Canyon Tuff middle member.	Trcm	27.03±0.11	Sanidine and quartz phenocrysts; 7-35 percent crystals.	High Zr, Nb, Ta, U, Th, and Hf abundances relative to all study area tuffs. High SiO_2, Rb, Nb, and Ta and low TiO_2, Zr, Ba, and and La abundances relative to Trcu, Trci, and Trcf.
Rhyolite Canyon Tuff upper member.	Trcu	26.96±0.06	Sanidine and quartz phenocrysts; 7-35 percent crystals.	High Zr, Nb, Ta, U, Th, and Hf abundances relative to all study area tuffs.
Rhyolite Canyon Tuff intracaldera facies.	Trci	ND	Sanidine and quartz phenocrysts; 7-35 percent crystals. Red-brown color. Abundant lithic fragments.	High Zr, Nb, Ta, U, Th, and Hf abundances relative to all study area tuffs.
Rhyolite Canyon Tuff lava-flow-like phase.	Trcf	ND	Sanidine and quartz phenocrysts; 7-35 percent crystals. Sanidine phenocrysts 0.5 to 1 cm long. Lacks pumice and lithic fragments.	High Zr, Nb, Ta, U, Th, and Hf abundances relative to all study area tuffs. High K_2O and Rb abundances relative to Trcu and Trci.
Dacite porphyry lava.	Tdpl	26.97±0.13	Feldspar phenocrysts 5 mm to 3 cm long. Granophyric to glassy groundmass.	High FeO*, MgO, CaO, TiO_2, P_2O_5, Ba, Co, Cr, Ni, Sc, and Eu abundances.

Table 4. Diagnostic age, petrographic, and geochemical features of middle Tertiary volcanic rocks of the central Chiricahua Mountains.—Continued

[ND, not determined]

Unit	Unit symbol	Age, in Ma	Petrographic characteristics	Geochemical characteristics
Rocks associated with the Turkey Creek caldera (continued)				
Dacite porphyry intrusion.	Tdpi	26.90±0.04	Feldspar phenocrysts 5 mm to 3 cm long. Granophyric groundmass.	High FeO*, MgO, CaO, TiO_2, P_2O_5, Ba, Co, Cr, Ni, Sc, and Eu abundances.
Trachyte porphyry lava.	Ttp	ND	Sanidine crystals 2 mm to 1 cm long.	High Na_2O, Y, Zr, and Nb and low Sr and Ba abundances relative to the dacite porphyry.
Biotite rhyolite lava	Tmrb	26.74±0.05	Biotite phenocrysts; 5 to 20 percent crystals.	Low SiO_2, Rb, Nb, Ta, U, Th, and Hf, and high FeO*, MgO, CaO, TiO_2, Sr, Ba, Co, Sc, and Eu abundances. Rb-Sr ratio >1 distinct from that of Tfre.
Unit 1 lava	Tmr1	26.77±0.12	Aphyric. Flow banded	Higher Nb abundances than Tc and Tkr, lower Rb and Nb than Trdp. Lower SiO_2 Nb, Ta, Th and higher CaO, Ba, and Eu abundances than Tmr2 and Tmr3.
Unit 2 lava	Tmr2	ND	Aphyric. Flow banded	Higher Nb abundances than Tc and Tkr, lower Rb and Nb than Trdp.
Unit 3 lava	Tmr3	ND	Aphyric. Flow banded. Spherulitic.	Higher Nb abundances than Tc and Tkr, lower Rb and Nb than Trdp.
Post-Turkey Creek caldera rocks				
Pyroclastic deposits and lava flows of Swede Peak.	Ts	ND	Quartz, sanidine, albite, and biotite phenocrysts; >20 percent crystals. Abundant lithic fragments.	No diagnostic geochemical features.
Rhyolite lava of Dobson Peak.	Trdp	26.20±0.07	Nearly aphyric	Higher Rb and Nb abundances than other study area rhyolite lavas.

pertinent mineral-melt distribution coefficients, and crystal-liquid fractionation processes, the source reservoir likely had an initial composition similar to that of the geochemically least evolved (last erupted) part of the outflow sequence, and developed more evolved (first erupted) parts. Gradients within the reservoir apparently resulted from crystallization and fractionation of small amounts of clinopyroxene, sanidine, and zircon, the principal phenocrysts characteristic of the reservoir's least evolved part. In contrast, sequential evolution of the moat rhyolite lavas from initial, relatively primitive rhyolite to final, highly evolved rhyolite appears to have been principally controlled by variable contamination of a homogeneous reservoir by relatively primitive lithologic contaminants derived from the reservoir's roof and walls. In addition, evolution of the first erupted rhyolite (the biotite rhyolite) to the subsequent batch of rhyolite (unit 1 lava) requires fractionation of biotite and sanidine, the principal phenocrysts in the biotite rhyolite, to yield a composition like that of unit 1 lava. Subsequently erupted, more evolved, moat rhyolite lava (units 2 and 3 lavas) represents a composition similar to that of unit 1 lava that contains progressively less contamination derived from intermediate-composition lava flows and dacite porphyry that enclosed the source reservoir.

New $^{40}Ar/^{39}Ar$ analyses provide accurate and precise absolute ages for many volcanic rock units whose ages were previously poorly known or unknown. These new ages are useful in stratigraphic correlation both within and beyond the central Chiricahua Mountains. For example, the new age data suggest that the Jesse James Canyon Tuff and the lower member of the tuff of Horseshoe Canyon are part of the same stratigraphic unit. Geochemical data are entirely consistent with this interpretation. The precision and small uncertainties associated with the new ages also help constrain the timing and nature of the volcanologic events that controlled middle Tertiary geologic evolution in this part of the Boot Heel volcanic field. Voluminous volcanic deposits, largely composed of regionally distributed ash-flow tuffs erupted from various caldera sources, were erupted between 34.2 and 26.2 Ma. A distinctive eruptive hiatus between 33.3 and 28.1 Ma indicates that magmatic activity in this region was not continuous but was confined to at least two discrete pulses separated by an approximately 5.2 m.y. hiatus. McIntosh

and others (1992) defined a hiatus of 3.2 m.y., between 28.9 and 32.1 Ma, within volcanic rocks of the large Mogollon-Datil volcanic field, immediately north of the Boot Heel field. McIntosh and Bryan (2000) defined a hiatus of 5.1 m.y., between 27.6 and 32.7 Ma, for the Boot Heel volcanic field itself; they also indicated that the geographic evolution of the Boot Heel field was time transgressive, with magmatism sweeping from east to west across the field. Magmatism associated with the Turkey Creek caldera, the largest and best preserved volcanic system in the central Chiricahua Mountains, as well as the westernmost and youngest major component of the Boot Heel field, seems to have been confined to a narrow time window. The oldest rocks associated with this system, Rhyolite Canyon Tuff, were erupted 26.9 Ma, whereas the youngest, moat rhyolite lavas, have ages between 26.7 and 26.8 Ma. Consequently, all eruptions from the Turkey Creek caldera occurred in as little as 200,000 years. Volumetrically significant middle Tertiary volcanic activity seems to have ended about 26.2 Ma with eruption of the rhyolite lava of Dobson Peak, the stratigraphically youngest volcanic unit preserved in the study area.

The age and composition of these volcanic rocks help to define the large-scale tectonic processes that were active along the western margin of North America and that controlled the geologic evolution of the Boot Heel volcanic field during middle Tertiary time. As suggested by du Bray and Pallister (1991) and substantiated herein, the geochemical characteristics of the area's volcanic rocks indicate genesis that changes from a subduction or arc-related tectonic regime to a within-plate, extensional regime. The transitional geochemistry of these rocks, as well as the periodicity and east-to-west sweep of magmatism within the Boot Heel volcanic field during its 35 to 27 Ma history, may reflect a sequence of events that includes (1) subduction-related magmatism between 35 and 33 Ma, (2) amagmatism related to rapid, low-angle subduction (Coney and Reynolds, 1977) between 33 and 28 Ma, (3) renewed magmatism and the beginning of extensional tectonics between about 28 and 27 Ma when subduction diminished or ceased and the downgoing Farallon plate began to founder and became more steeply inclined, and (4) magmatic re-initiation in response to restoration of an asthenospheric mantle wedge beneath this region (Coney and Reynolds, 1977; Armstrong and Ward, 1991). We interpret the approximately 5 m.y. magmatic hiatus in the central Chiricahua Mountains and the Boot Heel volcanic field as resulting from a combination of shallow subduction and the regional tectonic reorganization that began along the west edge of the North American plate during this time (Atwater, 1970). The final, brief period of magmatism terminated as subduction (and therefore subduction-related magmatism) ended with the initiation of strike-slip faulting along western North America (Atwater, 1970). In the study area, magmatism ceased as the center of extension-related magmatism rapidly shifted westward to the Great Basin, where bimodal basalt-rhyolite magmatism became dominant.

References Cited

Anders, Edward, and Ebihara, Mitsuru, 1982, Solar-system abundances of the elements: Geochimica et Cosmochimica Acta, v. 46, p. 2363–2380.

Armstrong, R.L., and Ward, Peter, 1991, Evolving geographic patterns of Cenozoic magmatism in the North American Cordillera—The temporal and spatial association of magmatism and metamorphic core complexes: Journal of Geophysical Research, v. 96, p. 13201–13224.

Atwater, Tanya, 1970, Implications of plate tectonics for the Cenozoic tectonic evolution of western North America: Geological Society of America Bulletin, v. 81, p. 3513–3536.

Baedecker, P.A., and McKown, D.M., 1987, Instrumental neutron activation analysis of geochemical samples, *in* Baedecker, P.A., ed., Methods for geochemical analysis: U.S. Geological Survey Bulletin 1770, p. H1–H14.

Boden, D.R., 1989, Evidence for step-function zoning of magma and eruptive dynamics, Toquima caldera complex, Nevada: Journal of Volcanology and Geothermal Research, v. 37, p. 39–57.

Bryan, C.R., 1988, Geology and geochemistry of mid-Tertiary volcanic rocks in the eastern Chiricahua Mountains, southeastern Arizona: Albuquerque, N.Mex., University of New Mexico M.S. thesis, 137 p.

Coney, P.J., and Reynolds, S.J., 1977, Cordilleran Benioff zones: Nature, v. 270, p. 403–406.

Dalrymple, G.B., Alexander, E.C., Lanphere, M.A., and Kraker, G.P., 1981, Irradiation of samples for $^{40}Ar/^{39}Ar$ dating using the Geological Survey TRIGA reactor: U.S. Geological Survey Professional Paper 1176, 55p.

Dalrymple, G.B., and Lanphere, M.A., 1969, Potassium-argon dating: San Francisco, Freeman, 251 p.

Drewes, Harald, 1982, Geologic map of the Cochise Head quadrangle and adjacent areas, southeastern Arizona: U.S. Geological Survey Miscellaneous Investigations Series Map I–1312, scale 1:24,000.

Drewes, Harald, and Brooks, W.E., 1988, Geologic map and cross sections of the Pedregosa Mountains, Cochise County, Arizona: U.S. Geological Survey Miscellaneous Investigations Series Map I–1827, scale 1:48,000.

Drewes, Harald, du Bray, E.A., and Pallister, J.S., 1995, Geologic map of the Portal quadrangle and vicinity, Cochise County, Arizona: U.S. Geological Survey Miscellaneous Investigations Series Map I–2450, scale 1:24,000.

du Bray, E.A., 1995, Geochemistry and petrology of Oligocene and Miocene ash-flow tuffs of the southeastern Great Basin: U.S. Geological Survey Professional Paper 1559, 38 p.

du Bray, E.A., Elliott, J.E., and Stuckless, J.S., 1988, Postorogenic peraluminous granites and associated Sn-W deposits, Kingdom of Saudi Arabia, *in* Taylor, R.P., and Strong, D.F., eds., Recent advances in the geology of granite-related mineral deposits: Canadian Institute of Mining and Metallurgy Special Volume 39, p. 142–156.

du Bray, E.A., Ludington, Steve, Brooks, W.E., Gamble, B.M., Ratté, J.C., Richter, D.R., and Soria-Escalante, Eduardo, 1995, Compositional characteristics of middle to upper Tertiary volcanic rocks of the Bolivian Altiplano: U.S. Geological Survey Bulletin 2119, 30 p.

du Bray, E.A., and Pallister, J.S., 1991, An ash-flow caldera in cross section—Ongoing field and geochemical studies of the Turkey Creek Caldera, SE Arizona: Journal of Geophysical Research, v. 96, p. 13435–13457.

du Bray, E.A., and Pallister, J.S., 1994, Stanford Canyon quadrangle, Cochise County, Arizona—Analytic data and geologic sample catalog: U.S. Geological Survey Bulletin 2021–D, 15 p.

du Bray, E.A., and Pallister, J.S., 1995, Area adjacent to the Turkey Creek caldera Cochise County, Arizona—Analytic data and geologic sample catalog: U.S. Geological Survey Bulletin 2021–E, 27 p.

du Bray, E.A., Pallister, J.S., and Yager, D.B., 1997, Geologic map of the Turkey Creek caldera, Chiricahua Mountains, Cochise County, Arizona: U.S. Geological Survey Miscellaneous Investigations Series Map I–2544, scale 1:50,000.

du Bray, E.A., Yager, D.B., and Pallister, J.S., 1992a, Fife Peak quadrangle, Cochise County, Arizona—Analytic data and geologic sample catalog: U.S. Geological Survey Bulletin 2021–A, 15 p.

du Bray, E.A., Yager, D.B., and Pallister, J.S. 1992b, Rustler Park quadrangle, Cochise County, Arizona—Analytic data and geologic sample catalog: U.S. Geological Survey Bulletin 2021–B, 24 p.

du Bray, E.A., Yager, D.B., and Pallister, J.S. 1993, Chiricahua Peak quadrangle, Cochise County, Arizona—Analytic data and geologic sample catalog: U.S. Geological Survey Bulletin 2021–C, 22 p.

Duffield, W.A., and Ruiz, Joaquin, 1992, Compositional gradients in large reservoirs of silicic magma as evidenced by ignimbrites versus Taylor Creek Rhyolite lava domes: Contributions to Mineralogy and Petrology, v. 110, p. 192–210.

Elsass, F., and du Bray, E.A., 1982, Energy-dispersive X-ray fluorescence spectrometry with the Kevex 7000 system: Saudi Arabian Deputy Ministry Mineral Resources Open File Report USGS-OF-02-52, 53 p.

Enlows, H.E., 1951, The igneous geology of Chiricahua National Monument, Arizona: Tulsa Geological Society Digest, v. 19, p. 105–107.

Enlows, H.E., 1955, Welded tuffs of the Chiricahua National Monument, Arizona: Geological Society of America Bulletin, v. 66, p. 1215–1246.

Ewart, A., 1982, The mineralogy and petrology of Tertiary-Recent orogenic volcanic rocks with special reference to the andesitic-basaltic compositional range, *in* Thorpe, R.S., ed., Andesites: Chichester, UK, John Wiley, p. 25–87.

Fernandez, L.A., Jr., and Enlows, H.E., 1966, Petrography of the Faraway Ranch Formation, Chiricahua National Monument, Arizona: Geological Society of America Bulletin, v. 77, p. 1017–1030.

Fleck, R.J., Sutter, J.F., and Elliott, D.H., 1977, Interpretation of discordant $^{40}Ar/^{39}Ar$ age spectra of Mesozoic tholeiites from Antarctica: Geochimica et Cosmochimica Acta, v. 41, p. 15–32.

Fridrich, C.J., and Mahood, G.A., 1987, Compositional layers in the zoned magma chamber of the Grizzly Peak tuff: Geology, v. 15, p. 299–303.

Gill, James, 1981, Orogenic andesites and plate tectonics: New York, Springer-Verlag, 390 p.

Hanson, G.N., 1978, The application of trace elements to the petrogenesis of igneous rocks of granitic composition: Earth and Planetary Science Letters, v. 38, p. 26–43.

Hanson, G.N., 1980, Rare earth elements in petrogenetic studies of igneous systems: Annual Review of Earth and Planetary Science, v. 8, p. 371–406.

Harlan, S.S., Duebendorfer, E.M., Deibert, J.E., 1998, New $^{40}Ar/^{39}Ar$ isotopic dates from Miocene volcanic rocks in the Lake Mead area, southern Las Vegas Range, Nevada: Canadian Journal of Earth Sciences, v. 35, p.495–503.

Hildreth, Wes, 1979, The Bishop Tuff—Evidence for the origin of compositional zonation in silicic magma chambers, *in* Chapin, C.E., and Elston, W.E., eds., Ash-flow tuffs: Geological Society of America Special Paper 180, p. 43–75.

Hildreth, Wes, 1981, Gradients in silicic magma chambers—Implications for lithospheric magmatism: Journal of Geophysical Research, ser. B, v. 86, p. 10153–10192.

Hildreth, Wes, and Mahood, Gail, 1985, Correlation of ash-flow tuffs: Geological Society of America Bulletin, v. 96, p. 968–974.

Irvine, T.N., and Baragar, W.R.A., 1971, A guide to the chemical classification of the common volcanic rocks: Canadian Journal of Earth Sciences, v. 8, p. 523–548.

Kellogg, K.S., Harlan, S.S., Mehnert, H.H., Snee, L.W., Pierce, K.L., Hackett, W.R., and Rodgers, D.W., 1994, Major 10.2 Ma rhyolitic volcanism in the eastern Snake River plain, Idaho; isotopic age and stratigraphic setting of the Arbon Valley Tuff Member of the Starlight Formation: U.S. Geological Survey Bulletin 2091, 18 p.

Lanphere, M.A., and Dalrymple, G.B., 1976, Identification of excess ^{40}Ar by the $^{40}Ar/^{39}Ar$ age spectrum technique: Earth and Planetary Science Letters, v. 32, p.141–148.

Latta, J.S., 1983, Geochemistry and petrology of the ash flows of Chiricahua National Monument, Arizona, and their relation to the Turkey Creek caldera: Tucson, Ariz., University of Arizona M.S. thesis, 194 p.

Le Bas, M.J., Le Maitre, R.W., Streckeisen, A., and Zanettin, B., 1986, A chemical classification of volcanic rocks using the total alkali-silica diagram: Journal of Petrology, v. 27, p. 745–750.

Lipman, P.W., 1965, Chemical comparison of glassy and crystalline volcanic rocks: U.S. Geological Survey Bulletin 1201-D, 24 p.

Macdonald, Ray, Smith, R.L., and Thomas, J.E., 1992, Chemistry of the subalkalic silicic obsidians: U.S. Geological Survey Professional Paper 1523, 214 p.

Marjaniemi, D.K., 1969, Geologic history of an ash-flow sequence and its source area in the Basin and Range Province of southeastern Arizona: Tucson, Ariz., University of Arizona Ph. D. dissertation, 176 p., 1 plate.

Marvin, R.F., Naeser, C.W., and Mehnert, H.H., 1978, Tabulation of radiometric age—including unpublished K-Ar and fission track ages—for rocks in southeastern Arizona and southwestern New Mexico, *in* Callender, J.F., Wilt, J.C., and Clemons, R.E., eds., Land of Cochise: New Mexico Geological Society Guidebook, p. 243–252.

McIntosh, W.C., and Bryan, C., 2000, Chronology and geochemistry of the Boot Heel volcanic field, New Mexico: New Mexico Geologic Society Guidebook, 51st field conference, Southwest Passage—A trip through the Phanerozoic, 2000, v. 51, p. 157–174.

McIntosh, W.C., Chapin, C.E., Ratté, J.C., and Sutter, J.F., 1992, Time-stratigraphic framework for the Eocene-Oligocene Mogollon-Datil volcanic field, southwest New Mexico: Geological Society of America Bulletin, v. 104, p. 851–871.

Pallister, J.S., and du Bray, E.A., 1997, Interpretive map and guide to the volcanic geology of Chiricahua National Monument and vicinity, Cochise County, Arizona: U.S. Geological Survey Miscellaneous Investigations Series Map I–2541, scale 1:24,000.

Pallister, J.S., du Bray, E.A., and Latta, J.S. IV, 1994, Geologic map of the Rustler Park quadrangle, southeast Arizona: U.S. Geological Survey Geologic Quadrangle Map GQ–1696, scale 1:24,000.

Pearce, J.A., Harris, N.B.W., and Tindle, A.G., 1984, Trace element discrimination diagrams for the tectonic interpretation of granitic rocks: Journal of Petrology, v. 25, p. 956–983.

Raydon, G.T., 1952, Geology of the northeastern Chiricahua Mountains: Berkeley, Calif., University of California, M.S. thesis, 141 p.

Roddick, J.C., 1983, High precision intercalibration of $^{40}Ar/^{39}Ar$ standards: Geochimica et Cosmochimica Acta, v. 47, p. 887–898.

Samson, S.D., and Alexander, E.C., 1987, Calibration of interlaboratory $^{40}Ar/^{39}Ar$ dating standard MMhb-1: Isotope Geoscience, v.66, p. 27–34.

Sawyer, D.A., and Sargent, K.A., 1989, Petrologic evolution of divergent peralkaline magmas from the Silent Canyon caldera complex, southwestern Nevada volcanic field: Journal of Geophysical Research, v. 94, p. 6021–6040.

Shafiqullah, M., Damon, P.E., Lynch, D.J., Kuck, P.H., and Rehrig, W.A., 1978, Mid-Tertiary magmatism in southeastern Arizona, *in* Callender, J.F., Wilt, J.C., and Clemons, R.E., eds., Land of Cochise: New Mexico Geological Society Guidebook, p. 231–242.

Steiger, R.H., and Jäger, Emilie, 1977, Subcommission on geochronology—Convention on the use of decay constants in geo- and cosmochronology: Earth and Planetary Science Letters, v. 36, p. 359–362.

Taggart, J.E., Lindsay, J.R., Scott, B.A., Vivit, D.V., Bartel, A.J., and Stewart, K.C., 1987, Analysis of geologic materials by X-ray fluorescence spectrometry, *in* Baedecker, P.A., ed., Methods for geochemical analysis: U.S. Geological Survey Bulletin 1770, p. E1–E19.

Taylor, J.R., 1982, An introduction to error analysis: Mill Valley, Calif., University Science Books, 270 p.

Thompson, R.N., Morrison, M.A., Dickin, A.P., Hendry, G.L., 1983, Continental flood basalts...Arachnids rule OK?, *in* Hawkesworth, C.J., and Norrey, M.J., eds., Continental basalts and mantle xenoliths: Cheshire, England, Shiva Publishing, Ltd., p. 158–185.

Watson, E.B., and Harrison, T.M., 1983, Zircon saturation revisited—Temperature and composition effects in a variety of crustal magma types: Earth and Planetary Science Letters, v. 64, p. 295–304.

Wood, D.A., Joron, J.-L., and Treuil, M., 1979, A re-appraisal of the use of trace elements to classify and discriminate between magma series erupted in different tectonic settings: Earth and Planetary Sciences Newsletter, v. 45, p. 326–336.

Yager, D.B., and Quick, J.E., 1992, Superxap manual: U.S. Geological Survey Open-File Report 92-13, 45 p.

Manuscript approved for publication October 17, 2003
Published in the Central Region, Denver, Colorado
Graphics by authors and Springfield and Springfield
Photocomposition by Gayle M. Dumonceaux
Edited by L.M. Carter

☆ U.S. GOVERNMENT PRINTING OFFICE: 2004 — 673-053 / 30127 Region No. 8

125 years of science for America 1879–2004

ISBN 0-607-95559-7